

**Chemical and Electrical Passivation of Single Crystal Silicon
Surfaces through Covalently Bound Organic Monolayers**

Thesis by
Eric Joseph Nemanick

In Partial Fulfillment of the Requirements
for the Degree of
Doctor of Philosophy

California Institute of Technology
Pasadena, California

Defended: 2005

Acknowledgements

In my time here at Caltech, I have enjoyed the opportunity to meet and work with many truly amazing people. Whether in the Lewis group as coworkers, as friends and acquaintances in the Chemistry or the Applied Math Departments, or the wonderful staff, or of course, the Caltech Fencing club, I have truly been blessed in these years to have such people to love and support me through all the seemingly endless trials and tribulations that are part and parcel of any graduate experience. Looking back, I can finally see what the support of all these wonderful people has meant to me in every bit of assistance towards the final goal of earning my Ph.D. I know that in any list of people to whom I am indebted I will miss many important people, and I assure you it is only from fatigue, rather than from any lack of gratitude.

Of course, none of this would have been possible without Professor Nathan S. Lewis. He gave me the opportunity to join his group all those years ago as an untested G0, raw out of Carleton College, looking for a challenge. Nate has been an invaluable source of ideas and insight over the course of my work here, and no list of acknowledgements can even be started without thanking him. We have over the years good-naturedly butted heads over a number of ideas, and I feel that the dynamic between us has strengthened me as a scientist and challenged me to look at my own work with a more critical eye. The group of people that Nate has assembled here is truly a reflection of himself; the collaborative spirit both he and this group embodies is the hallmark of successful science, and the citizen-scientists he has produced stand as a credit to him and

his work here at Caltech. I would also like to thank the members of my committee, Professor Harry Gray, Professor Geoff Blake, and Professor Jacqueline Barton, all of whom are wonderful scientists and people. It has truly been a privilege to work with scientists of their caliber in my time here at Caltech. I'd also like to thank Dr. Bruce Brunschwig, Director of the Molecular Materials Research Center, for his help and advice over the time he has been here. Bruce was always there to listen to me and give advice on topics ranging from careers in science to propagation of error. I wish now that I had used Bruce as a resource more, for while he has always made time for me when I asked, I think now that I never asked often enough.

The members of the Lewis group in my time here have been at times mentors, colleagues, good natured adversaries, and friends; oftentimes all at once. Rob Rossi was my first mentor and friend in the group, and much of the work I have done since is built on the solid foundation that he instilled in me. I have always striven to emulate the drive and focus that he had, and I owe much of who I am today to his example. Lauren Webb and Dave Michalak, my partners in silicon, have been an invaluable source of assistance and technical skill over the years, in maintaining those instruments I have often times take for granted: the XPS and the rf conductivity array. But beyond simple equipment maintenance, I think that the collaborative and noncompetitive nature of the relationship between us has gone a long way to getting all of us through this with a minimum of banging our heads against the wall. Shawn Briglin and Brian Sisk have been both truly great friends as well as peers, giving good natured ribbings with equal doses of scientific criticism. I hope we can get together again and hoist a pint for old time's sake sometime, guys. Patrick Hurley, a late comer to my graduate career, has meant so much to me both

in terms of collaborative effort as well as a friend. He always had time to work on a new question and dispensed advice as well as his expertise on the IR freely. I hope I paid him back sufficiently with electrochemistry tips and brownies. Dave Knapp, Julie Biteen, and Matt Traub along with Lauren and Dave Michalak were extraordinarily helpful during our time working on soft X-Ray experiments at Brookhaven National Labs and Stanford Synchrotron Labs, and I owe an enormous debt to these people for the long nights and endless days we spend collecting data for these experiments. I would also like to thank the administrative assistants that have made all the work of the group go smoothly at every turn: Sherry Feick and Nannette Pettis, the backbone of our group. Finally, the rest of the Lewis group, past and present: Florian, Watson, Will, Libby, Agnes, Kim, Cinco, J. J., Tom, Smiley, Tony, Ting, Eric, James, Jerry, Alex, Anna, Edgardo, Jordan, Nick, and everyone else who has passed through our doors; you have all been so supportive of me and my work, I cannot thank all of you enough. I also want to thank my collaborators, Santiago Solares here in the Goddard group and Allie Chan, whom I met at Brookhaven, for all of their help. I must also thank the teachers who put me on this path in the first place: Steve Drew from Carleton, who endured the questions of an annoying undergrad and set me on this path before me, and Marion Cass, whose comps group taught me so much.

There have been many people outside of the group who have given me support that has been just as important to me as the scientific assistance of my group and my advisors. My family, which has grown over my time here, has always been a bedrock of comfort for me; in all the trying times that I've been through they have always been there for me, and I can only hope that I have been there for them as well. I owe so much to my

mother and father, two people who have made me into the man I am today and have stood behind me from day one, cheering me on in this marathon of grad school. I love you both so much, and I only hope that I've made the both of you proud. Rik and Jeff, my loving brothers, and their wonderful wives, Dawn and Jen, gave me much of my inspiration; as I have watched them build their careers and lives they have stood as shining examples to me, and I one day hope to achieve personal and professional success that they have achieved. I would also like to thank my niece Sarah, a relative newcomer into this family who never knew her crazy uncle Joe as anything other than a grad student. At times I don't even remember myself. Sarah, I have a picture of you on my desk along with a drawing you made for me that have kept me going in my time here.

Finally, I wish to thank all the wonderful friends I have made here. Without you guys I never would have made it past day one. First, my wonderful friends at Carleton, Blinn, Nick, and Elspeth, and especially Skip, who got me through Ad Lab God knows how. Randy and Chris, you two have been my closest friends here, and I will always remember Friday night gaming and pizza at your apartment as well as our times at the fencing club. You guys have kept me grounded and sane (or close enough) since we have become friends, and I just want you two to know that I could not have done this without you. I would also like to thank my friends and teammates in fencing: Coach, Cedric and Vanessa, Wheeler, Tim, Laura and Little Johnson, Yann, Charles and Duane, and everyone else. Fencing has served as an important balance in my life, and all of you have meant a lot to me. Also, I have met many wonderful people outside of fencing and work who are not only friends but are people who I will treasure always, starting way back in the day with Chip and Kev, and Fernando, Chris and Darren, Serina and Abe,

Sherry, Millie, Amy, Matt and Chad, Justin and Mike, Joe Drew and Katie Saliba, and especially Annie, who has had to endure the last six months without knowing any other kind of Joe; I would like to thank all of you for the love and companionship you've given me, and I only hope that I have returned a little of it.

Abstract

The formation of and passivation by alkyl monolayers on Si(111) and Si(100) surfaces was studied. Crystalline Si(111) and Si(100) surfaces were alkylated in a two-step chlorination/alkylation process using both straight chain alkyl groups CH₃, C₂H₅, C₄H₉, and C₈H₁₇, as well sterically bulky alkyl groups such as (CH₃)₂CH-(*iso*-propyl), (CH₃)₃C-(*tert*-butyl), and C₆H₅- (phenyl) moieties to form well defined alkyl monolayers on the surface. X-ray photoelectron spectroscopic (XPS) data in the C 1s region of such surfaces exhibited a low energy emission at 283.6 binding eV, consistent with carbon bonded to Si, demonstrating a Si-C covalent bond. The C 1s XPS data indicated that larger alkyl groups were present at lower coverages than methyl groups on both the CH₃-terminated Si(111) surfaces as well as CH₃-terminated Si(100) surfaces. Despite the lower monolayer percent coverage, no Cl was detected after alkylation on either surface. Functionalization with even the bulky alkyl groups effectively inhibited the oxidation of the Si surfaces in air and produced low ($< 100 \text{ cm s}^{-1}$) surface recombination velocities, indicating a low density of electronically active surface trap states. Transmission infrared spectroscopy indicated that the Si(111) surfaces were partially H-terminated after the functionalization reaction for groups larger than CH₃. High resolution soft X-ray photoelectron spectroscopic (SXPS) measurements of the Si 2p region of the alkylated Si(111) and Si(100) surfaces show monolayer coverage of SiCl and SiCH₃ on the Si(111) surface, with mixtures of species on H-term Si(111) as well as H-term Si(100) surfaces. Bulkier alkyl groups such as C₂H₅ and phenyl on both Si(111) and Si(100) surfaces as

well as on CH₃-terminated Si(100) show broad Si 2p peaks with binding shifts indicative of hybrid surfaces composed of both Si-R groups and SiH/SiH₂ species. To model surface packing of these alkyl groups on the Si(111) surface, molecular dynamics modeling was employed using Cerius². The energies for various packing densities and packing patterns were calculated and referenced versus the reactant energy for each surface. From this it was concluded that 100% of the Si(111) surface should be CH₃-terminated, with lower packing densities for C₂H₅ between 50-80%, 50-66.7% for C₈H₁₇, 33.3-40% for *tert*-butyl, 33.3-50% for *iso*-propyl, and 50-66.7% for phenyl. A single electron transfer (SET) mechanism for the reaction of alkyl Grignards with the Cl-terminated surface is proposed. Application of a reducing potential, -2.5 V vs. Ag⁺/Ag, to Cl-terminated Si(111) electrodes in tetrahydrofuran resulted in the complete elimination of Cl, as measured by XPS. The data are consistent with a mechanism in which the reaction of alkyl Grignard reagents with the Cl-terminated Si(111) surfaces involves electron transfer from the Grignard reagent to the Si, loss of chloride to solution, and subsequent reaction between the resultant silicon radical and alkyl radical to form a silicon-carbon bond. Sites sterically hindered by neighboring alkyl groups abstract a H atom to produce Si-H bonds on the surface.

Table of Contents

Acknowledgements

Abstract

Chapter 1 Introduction to Silicon Photoelectrochemistry and Surface Chemistry

1.1 Introduction

1.2 Interface Formation at Semiconductor/Liquid Interfaces

1.3 Charge Carrier Recombination at Surface Localized Defect States

1.4 Formation of Organic Monolayers on Silicon Surfaces

1.5 Bibliography

Chapter 2 Chemical and Electrical Passivation of Silicon(111) Surfaces Through Functionalization with Sterically Hindered Alkyl Groups

2.1 Introduction

2.2 Experimental

2.2.1 Alkylation of Silicon

2.2.2 Electrochemistry

2.2.3 X-Ray Photoelectron Spectroscopy

2.2.4 Infrared Spectroscopy

2.2.5 Surface Recombination Velocity Measurements

2.3 Results

2.3.1 XPS Data

2.3.2 Surface Recombination Velocity Measurements

2.3.3 Infrared Spectroscopy

2.3.4 Electrochemical Studies

2.4 Discussion

**2.4.1 Coverage of Alkyl Groups on Functionalized Si(111)
Surfaces**

**2.4.2 Mechanism of Alkylation of Cl-Terminated Si(111)
Surfaces by Grignard Reagents**

**2.4.3 Electrical and Chemical Passivation of the Si(111)
Surfaces by Alkylation**

2.5 Conclusions

2.6 Acknowledgements

2.7 Bibliography

**Chapter 3. Soft X-ray Photoelectron Spectroscopic Measurements of
Alkylated Si (111) Surfaces**

3.1 Introduction

3.2 Experimental

3.2.1 Alkylation of Silicon

3.2.2 Soft X-ray Photoelectron Spectroscopy

3.3 Results

3.3.1 Hydrogen-terminated Si (111) Surfaces

3.3.2 Cl-terminated Si (111) Surfaces

3.3.3 Methyl-terminated Si (111) Surfaces

3.3.4 Ethyl-terminated Si (111) Surfaces

3.3.5 Benzyl-terminated Si (111) Surfaces

3.4 Discussion

3.4.1 Hydrogen and Chlorine-terminated Si(111) Surfaces

3.4.2 Alkyl-terminated Si(111) Surfaces

3.5 Conclusions

3.6 Acknowledgements

3.7 Bibliography

Chapter 4. Molecular Dynamics Calculations of Alkyl Monolayer

Formation on Si (111) Surfaces Under Thermodynamic Control

4.1 Introduction

4.2 Experimental

4.3 Results and Discussion

4.3.1 Straight Chain Packing Energies

4.3.2 Bulky Alkyl Surface Groups

4.3.3 Comparisons

4.4	Conclusions
4.5	Acknowledgements
4.6	Bibliography
Chapter 5.	Chemical and Electrical Passivation of Single Crystal Silicon(100) Surfaces Through a Two-step Chlorination/ Alkylation Process
5.1	Introduction
5.2	Experimental
5.2.1	Alkylation of Silicon
5.2.2	X-ray Photoelectron Spectroscopy Measurements
5.2.3	Soft X-ray Photoelectron Spectroscopy
5.2.4	Charge Carrier Lifetime Measurements
5.3	Results
5.3.1	X-ray Photoelectron Spectroscopy
5.3.2	Charge Carrier Lifetime Measurements
5.3.3	Soft X-Ray Spectroscopy
5.4	Discussion
5.4.1	Surface Passivation of Si(100)
5.4.2	Soft X-ray Photoelectron Spectra
5.5	Conclusions
5.6	Acknowledgements
5.7	Bibliography

List of Figures

- Figure 1.1** Fermi level equilibration between a semiconductor and a contacting phase.
- Figure 1.2** IR absorbance spectrum for H-terminated Si(111).
- Figure 1.3** Hydrosilylation reaction for alkenes or alkynes with H-terminated Si(111).
- Figure 1.4** Two step chlorination/alkylation reaction with H-terminated Si(111).
- Figure 2.1** XPS spectra for the two step chlorination/alkylation reaction with H-terminated Si(111).
- Figure 2.2** XPS spectra of the C 1s region of C₂H₅-terminated Si(111).
- Figure 2.3** XPS spectra of the Si 2p region of H-terminated Si(111) and CH₃-terminated Si(111) showing oxidation in air over time.
- Figure 2.4** Surface oxide growth for alkylated Si(111) and H-terminated Si(111) in air.
- Figure 2.5** Surface oxide growth for CH₃- and CCH-terminated Si(111) surfaces versus charge carrier lifetimes.
- Figure 2.6** Transmission IR absorbance of the Si-H stretching region for C₂H₅- and *tert*-butyl terminated Si(111).

- Figure 2.7** Cyclic voltammogram of the reduction of surface bound Si-Cl.
- Figure 2.8** XPS spectra of the Cl-terminated surface after application of reducing potentials.
- Figure 2.9** Cyclic voltammogram of the irreversible oxidation of Grignard reagents.
- Figure 3.1** Inelastic mean free paths for Si 2p electrons in a Si matrix.
- Figure 3.2** SXPS spectrum of H-terminated Si(111).
- Figure 3.3** SXPS spectrum of Cl-terminated Si(111).
- Figure 3.4** SXPS spectrum of CH₃-terminated Si(111).
- Figure 3.5** SXPS spectrum of C₂H₅-terminated Si(111).
- Figure 3.6** SXPS spectrum of C₆H₅CH₂-terminated Si(111).
- Figure 4.1** Packing patterns for alkyl groups on Si(111).
- Figure 4.2** Packing energy for CH₃-terminated Si(111).
- Figure 4.3** Packing energy for C₂H₅-terminated Si(111).
- Figure 4.4** Packing structure for C₂H₅-terminated Si(111).
- Figure 4.5** Packing energy for C₈H₁₇-terminated Si(111).
- Figure 4.6** Packing energy for bulky alkyl-terminated Si(111).
- Figure 4.7** Packing energy for C₆H₅-terminated Si(111).
- Figure 5.1** XPS spectra for the two-step chlorination/alkylation reaction with Si(100).
- Figure 5.2** XPS spectrum of the C 1s region of CH₃-terminated

Si(100).

Figure 5.3 XPS spectra of the Si 2p region of H-terminated Si(100) and CH₃-terminated Si(100) in air.

Figure 5.4 Surface oxide growth for H-terminated Si(100) and alkyl-terminated Si(100).

Figure 5.5 Charge carrier lifetimes for CH₃-terminated Si(100) versus surface oxidation.

Figure 5.6 SXPS spectrum for H-terminated Si(100).

Figure 5.7 SXPS spectrum for Cl-terminated Si(100).

Figure 5.8 SXPS spectrum for CH₃-terminated Si(100).

List of Tables

- Table 2.1** The C_{Si}/Si XPS integrated area ratios for alkylated Si(111).
- Table 2.2** Charge carrier lifetimes for alkylated Si(111) surfaces.
- Table 3.1** SXPS data for functionalized Si(111) surfaces.
- Table 5.1** The C_{Si}/Si XPS integrated area ratios of alkylated Si(100) surfaces.
- Table 5.2** Charge carrier lifetimes and surface recombination velocities for alkylated Si(100).
- Table 5.3** Relative integrated area for peak fits of SXPS data of functionalized Si(100) surfaces.

Chapter 1

Introduction to Silicon Photoelectrochemistry and Surface Chemistry

1.1 Introduction

Energy consumption has become the driving force behind all aspects of modern civilization. Every hallmark of technological advancement has been driven by increased energy consumption. Whether transport infrastructure such as airplanes and automobiles, medical advancements such as open heart surgery and vaccinations, information technology such as telephony and the internet, or any other technology that requires moving, building, or sanitation, massive inputs of energy are required to make them possible. At present, our energy consumption needs are met primarily by non-renewable energy sources. Fossil fuels, in particular, present a problem by the pollution generated from consumption, by their finite supply, and by the more thorny social and political issues that extend beyond the scope of this work. The likelihood that fossil fuel production can keep up with the ever growing energy need driven by progress is small, and energy from other, more stable and renewable sources must fill the gap. Currently used renewable energy sources such as wind, solar, geothermal, tidal, hydroelectric, biomass, and fusion all face significant challenges before they can relieve the burden placed on fossil fuels. Before any of these technologies can enter into more widespread

use, though, they must all overcome significant technological obstacles such as material cost, efficiency, availability, and reliability. Currently, the most advanced of the renewable energy sources available is solar powered photovoltaic devices.

Solar power generation is a concept far older than humankind. The first photosynthetic life forms evolved billions of years ago to harness the power of solar radiation, trap it for future consumption, build complex structures with this energy, and become self-propagating entities. Photosynthesis in its most general form uses solar energy to convert CO_2 and H_2O to sugars and oxygen. However, this energy conversion process is fairly inefficient, with external quantum yield from photon energy to glucose (or other sugars, alcohols, and high energy organic compounds) production of only 3-5%.¹ While biomass energy production techniques seek to build off this photosynthetic pathway, more recently the development of photovoltaics² has increased the external efficiency of solid state solar cells to over 25%.³⁻⁵ These devices rely on separation of photogenerated charge carriers formed by energetic photons being absorbed by a semiconductor, chiefly silicon, and allowing these charge carriers to recombine only after running through an external circuit and doing work. These devices consist of buried junctions of two dissimilar types of silicon, n-type and p-type. The difference in Fermi levels between these two types of silicon generates an electric potential across this junction, causing the oppositely charged electrons and holes generated by photoabsorption to drift apart and become spatially as well as energetically separated.

However, photovoltaics cannot produce easily transported or stored chemical fuels like photosynthesis does, only the more infrastructure-dependent electricity. And the requirement of using single crystal, ultra-pure, ultra expensive silicon causes a high

barrier to entry for the use conventional silicon photovoltaics. Even though the material costs for polycrystalline silicon cells or biomass fuel sources are much lower, the energetic inefficiencies make solid state solar power generation the most commonly used. Due to the high cost outlay that accompanies the production of photovoltaic devices, adoption has been slow, even with the aid of government subsidies. A much less expensive option for the production of solar energy is the photoelectrochemical cell, which by the use of redox couple in solution and a metallic electrode can replace half of the high purity semiconductor needed for energy generation.^{6,7}

Photoelectrochemical cells usually have efficiencies that lay between photosynthetic and photovoltaic devices, with efficiencies exceeding 10% in recently developed systems.⁸ The photoelectrochemical cell uses a semiconductor photoelectrode for incident light absorption and generation of energetic charge carriers, but relies on the solution phase redox couple to generate a surface potential for the separation of charges. Metal oxide semiconductors with large bandgaps such as titanium dioxide (TiO_2) are generally inexpensive and are stable in contact with water or oxygen. However, the wide bandgaps for such semiconductors make them very inefficient absorbers of solar radiation, as a large fraction of photons are subbandgap in energy.⁹ Small bandgap materials such as germanium absorb a large percent of incident photons, but energy in excess of the bandgap of the photogenerated charge carriers is released as thermal energy as the charge carriers relax down to the band edge. Medium bandgap materials¹⁰ such as silicon (Si) and gallium arsenide (GaAs) provide a middle ground for absorption of solar radiation with the largest total energy absorbed. However, these semiconductors are

unstable in oxidizing solutions, causing both chemical oxidation of the surface as well as creating electrical defect states at the surface.

Passivation of these surfaces towards oxidation as well as electronic defect generation would allow for improved efficiencies and stabilities of these photoelectrochemical cells. Towards this end, this thesis discusses the chemical and electrical passivation of the Si surface by the creation of Si-C bonds through formation of alkyl monolayers on the surface through a two-step chlorination/alkylation process using alkyl Grignard reagents.

1.2 Interface Formation at Semiconductor/Liquid Interfaces

Semiconductors by definition have an electronic bandgap wherein there exists no energy states for an electron to exist. Similar to metallic substances, there is an energetic region of empty electronic states that exist within the material, and an electron within this region is free to move with minimal interference from the crystal lattice or other electrons. Abutting this region energetically in metals are filled valence orbitals, which contribute to the bonding of the material. Electrons in these orbitals are bound in place and cannot move spatially without the displacement of neighboring electrons. With the continuous nature of filled/empty electronic orbitals in a metallic solid, the highest-energy bound electrons have essentially zero energy barrier to transfer into a nearby continuum of empty orbitals, giving them freedom to move spatially. This is the source of the conductivity of metallic substances. However, unlike metals, semiconductors do not have an energetic abutment of filled and unfilled electronic states, and thus electrons

in bonding or valence orbitals must absorb significant amounts of energy to transition to unfilled electronic states. Without a significant population of free carriers in the empty orbitals (the conduction band) these substances are quite resistive. The bandgap of a semiconductor is defined as the energy difference between the two closest points energetically between the conduction and valence bands.

An electron in the valence band that absorbs energy greater than the value of this bandgap can transition energetically to the conduction band and is then free to move under the influence of an electric potential. When this electron transitions from the valence to conduction band, it leaves behind an empty electronic state. Neighboring electrons can transition to this empty state freely, leaving behind a different empty state as it fills the first state. In effect, electrons in the valence band can continue to fill these empty states, moving it spatially. Because each electron has a negative charge, as the unfilled orbital moves there is a positive charge left behind, localized on the lattice atom where the empty state is located. This positive charge moves as the empty state does and can be thought of as a particle with a charge equal and opposite to that of an electron that is free to move within the valence band. This empty state "particle" is often called a hole. As a hole is the concerted movement of electrons, it then moves in the opposite direction of electron flow. Thus, while electrons tend to thermodynamically seek the lowest energy, the hole must then move in the opposite direction and constantly move to higher energy. The conduction band can actually be thought of as containing an infinite number of holes, and electron promotion across the bandgap can be pictured as a hole transition across the bandgap as well.

For a perfect crystal of a semiconductor, there exists no energetic states within the bandgap, and at 0 K no electrons exist within the conduction band (or holes in the valence band). At all other temperatures, thermal energy has the ability to transition an electron to the conduction band. For materials such as this, called intrinsic semiconductors, their conductivity is related to their temperature, with n the free electron concentration and p the free hole concentration:

$$np = Ke^{\frac{E_g}{kT}} \quad (1.1)$$

where k is the Boltzmann constant, T is the temperature of the sample, and K is a constant related to the density of states in the conduction and valence bands. However, in real materials, defects within the semiconducting crystal create electronic states in the material that may lie within the bandgap and contain electrons (or holes). These defects are a source of charge carriers that do not need energy equal to the full band gap to become free charge carriers, but rather only sufficient energy to transition from their location in the bandgap to the appropriate band edge. A deliberate addition of defects to semiconducting crystal is called doping. Through the addition of defects, usually atom replacement with an element in an adjacent column on the periodic table, the free charge carrier population can be tailored. By careful selection of the identity of these defect species, the energy states created within the bandgap can lie very close to one of the band edges. These carriers can then use a minimum of thermal energy to transition from their original energy to the band edge and become free carriers. In this way, the resistivity of the semiconducting material may be engineered by adding an excess of one charge carrier or another. Thus, a group IV semiconductor such as Si can be doped with excess holes

through the addition of an element like boron, or with excess electrons by the addition of phosphorus.

As with any material, a semiconducting crystal has a chemical potential, or an ability to transfer charge to a contacting phase. For a semiconductor, this is related to its Fermi level, defined as the energy at which the probability of finding an electron is $1/2$. That is, a survey of states at this energy would find an electron 50% of the time. For an intrinsic semiconductor at 0 K, when all of its electrons are within the valence band, the valence energy levels are 100% populated and the conduction band has a 0% population. The Fermi level for this material is defined as the exact middle of the band gap. Following promotion of electrons to the conduction band, the population of the conduction band increases and the population of the valence band decreases. The Fermi level would remain the same, however. For doped samples, there are now charge carriers within the band gap, and the Fermi level shifts accordingly. For an n-type material 0 K, which has extra electrons in states that lie just below the conduction band edge, the Fermi level now is half way between the energy of the dopant states and the conduction band edge. The n-type material now has a higher Fermi level than either a p-type material or the intrinsic crystal. If two materials with differing Fermi levels come in contact, the material with the higher Fermi level will transfer electrons to the material with the lower Fermi level. The addition of extra electrons to the lower Fermi level material will raise its local Fermi level (because this will alter the population of electrons and the energetic location of the “half filled state”). Electron transfer will continue until the Fermi levels at the interface come into equilibrium. Figure 1.1 shows a schematic for the equilibration of

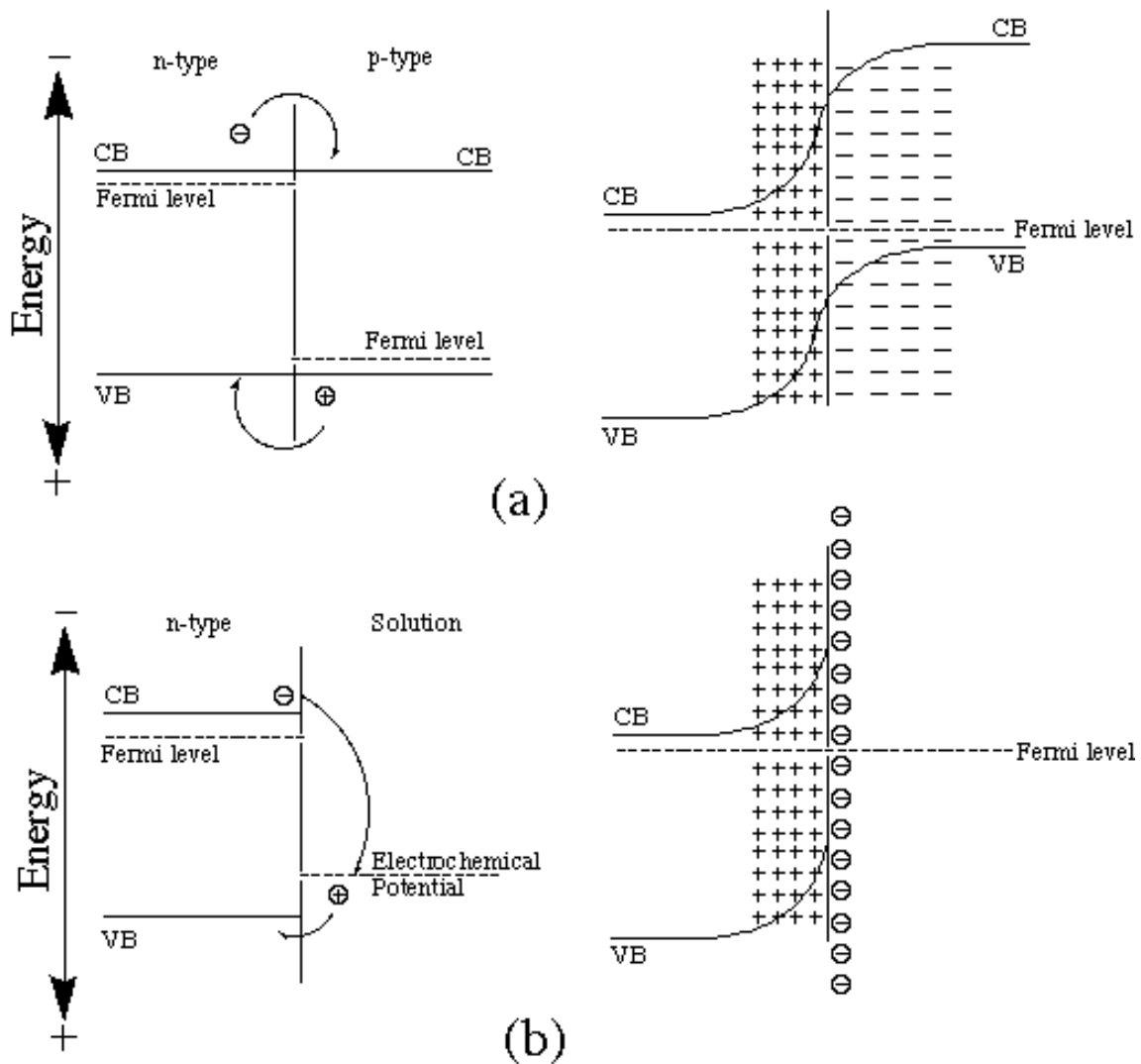


Figure 1.1: Fermi level equilibration between contacting phases for (a) n-type and p-type semiconductors, and (b) for n-type with and electrolyte solution with an electrochemical potential below the n-type's Fermi level. In (a), charges transfer from one side to the other of the interface, leaving behind charged dopant atoms, which generates a charged region near the interface. The Fermi levels equilibrate at the interface, but remain unchanged in the bulk. Charge carriers generated in the bulk that approach the interface will either be attracted to or repelled by the interface. In (b), charge transfer occurs, but the lack of fixed charges in the solution confines all the charges to a much narrower region at the interface. Electrons generated in the bulk will be repelled from the interface and holes collected at the interface, separated by the depletion region.

the Fermi levels of contacting materials. For an n-type material to transfer some of its doped electrons to another material, it must leave behind the dopant atoms from which the electrons came. These atoms also have an associated positive charge that is fixed in the atom nuclei and cannot move. By transferring electrons there now exists a region of positive charges, creating an electrostatic potential. For electrons to transfer to another material, the energy benefit they receive from moving to a lower Fermi level material must outweigh the coulombic attraction between the electrons and the positively charged nuclei left behind. The depth within a doped semiconductor to which dopant atoms are ionized is called the depletion width. For an n-type material, an electron outside of the depletion region that approaches the interface will see an equal number of positive and negative charges in front of it, and thus no net field. As soon as it enters the depletion region, there are now some positive charges behind it and thus more negative charges ahead than positive charges. The further towards the interface it progresses, the larger the electric field generated by the excess of negative charges. Therefore, for an electron in the bulk of the semiconductor outside of the depletion region, it is directed away from the interface by the electric field created by electron transfer.

This is the principle behind which lies semiconductor solar cells. Light strikes an n-type (or p-type) semiconductor, and electrons absorb the light and are promoted to the conduction band. These electrons are free to move in any direction. If this semiconductor is in contact with a material with a different Fermi level, the interface between the material will have a depletion region. As the free photoelectron approaches the depletion region, the electric field will deter it and direct it back into the bulk of the material away from the interface. The photohole created by the promotion of the

photoelectron, which moves freely as well, approaches the interface, and the electric field pulls the hole in, as it has the opposite sign of the electron. The hole is then directed through the depletion region to the interface and into the contacting material. The hole cannot return easily to the n-type material, as the depletion region is pushing it away from the interface. The photohole and photoelectron are now separated from each other by an electric field. If they were to recombine, they would release the energy from their creation but they are separated by the interface. If a conduit was created to lead from the back of the n-type material (away from the interface and the depletion region) to the back of the contacting material containing the photohole, the photoelectron could travel through this conduit and reach the photoelectron without traversing the interface potential. The flow of electrons through this conduit can be made to do work such as power a light bulb, charge a battery, or any other process that requires a flow of electricity.

The nature of the contacting phase for solid state solar cells is a semiconductor of the opposite doping type, with n-type material on one side and p-type on the other. The contacting material to create a charge separating interface can also be an electrolyte-filled solution that has a redox couple. The valence band of the contacting semiconductor is replaced with the energy level of the reduced form of the redox couple, and the conduction band is replaced by energy level the oxidized form. In making contact between the semiconductor and the electrolyte, charge transfers between the semiconductor and the electrolyte, though in the electrolyte, since all charged species are free to move, the solution does not have a depletion region in the same manner as a semiconductor (though it does have a region of increased charge at the interface, but

much thinner than a typical depletion width). There is still a depletion region within the semiconductor phase, which can effect charge separation.

The problem with semiconductor/electrolyte solar cells, called photoelectrochemical cells, is that the surface of the semiconductor is not perfect. Just as defects were added to dope the semiconductor creating filled or empty electronic states, the defects created by abruptly terminating the semiconductor also create electronic states. For an n-type material in contact with a solution with a lower electrochemical potential than its Fermi level, there will be a depletion region that directs photoelectrons away from the surface (where the holes have been collecting, awaiting rather slow electron transfer into the solution). For an empty defect state localized at the surface of an n-type semiconductor, a photoelectron can fight its way through the depletion region to fall into this empty state, and be much closer energetically to the holes. The photogenerated charges can recombine releasing the absorbed light energy as heat. For an efficient photoelectrochemical cell, the interface must be defect free and minimize the rate of recombination of photogenerated charge carriers.

1.3 Charge Carrier Recombination at Surface Localized Defect States

Shockley, Read,¹¹ and Hall,¹² fifty years ago developed the statistics for the recombination of charge carriers in semiconductors. The Shockley-Read-Hall statistics apply to all recombination processes in semiconductors; but of particular importance to this work are the equations relating to surface-based charge carrier recombination through defect-induced electronic states within the bandgap.

For an n-type semiconductor, the rate of surface recombination is given by the rate of electron capture for a surface state, $U_{n,s}$:

$$U_{n,s} = n_s N_{t,s} (1 - f_{t,s}) k_{n,s} - n_{1,s} N_{t,s} f_{t,s} k_{n,s} \quad (1.2)$$

where $N_{t,s}$ is the density of surface trap states at the surface, $f_{t,s}$ is the occupancy of surface states, and $k_{n,s}$ is the electron capture coefficient at the surface. $n_{1,s}$ is the surface electron concentration when the Fermi level is equal to the energy of the trap state, and is given by:

$$n_{1,s} = N_c e^{\left(\frac{E_{c,s} - E_{t,s}}{kT}\right)} \quad (1.3)$$

where N_c is the density of electronic states in the conduction band, $E_{c,s}$ is the energy of the conduction band edge, and $E_{t,s}$ is the energy of the surface trap states. For holes the function is similar, and the rate of hole recombination at a surface, $U_{p,s}$ is:

$$U_{p,s} = p_s N_{t,s} f_{t,s} k_{p,s} - p_{1,s} N_{t,s} (1 - f_{t,s}) k_{p,s} \quad (1.4)$$

where p_s is the hole concentration at the surface, $k_{p,s}$ is the hole capture coefficient, and $p_{1,s}$ is the surface hole concentration when the Fermi level is located at the energy of the surface trap state, given by:

$$p_{1,s} = N_v e^{\left(\frac{E_{t,s} - E_{v,s}}{kT}\right)} \quad (1.5)$$

where N_v is the density of trap states in the valence band, and $E_{v,s}$ is the energy of the valence band edge.

At steady state, the rate of electron and hole recombination are equal, as the nature of recombination requires both an electron and hole to be consumed. Setting (1.2) and (1.3) equal to each other, we get the total rate of recombination at the surface, U_s :

$$U_s = N_{t,s} \frac{k_{n,s} k_{p,s} (n_s p_s - n_{1,s} p_{1,s})}{k_{n,s} (n_s + n_{1,s}) + k_{p,s} (p_s + p_{1,s})} \quad (1.6)$$

Replacing the carrier concentrations n_s and p_s as the sum of equilibrium and excess carrier concentrations, $n_{s,0}$ and Δn_s , and $p_{s,0}$ and Δp_s , and substituting these into (1.6), gives:

$$U_s = N_{t,s} \left(\frac{k_{n,s} k_{p,s} (n_{s,0} \Delta p + p_{s,0} \Delta n_s + \Delta n_s \Delta p_s)}{k_{n,s} (n_{s,0} + \Delta n_s + n_{1,s}) + k_{p,s} (p_{s,0} + \Delta p_s + p_{1,s})} \right) \quad (1.7)$$

which represents the net charge carrier recombination through surface trap states for states at the energy $E_{t,s}$, which can be integrated over an energy distribution for surface states with varying energies.

The parameter most often used to represent charge carrier recombination through surface trap states is S , the surface recombination velocity, which has units of cm/s. For an n-type semiconductor, where the concentration of holes is rate limiting, S is defined as the recombination rate divided by the excess hole concentration at the surface, $U_s/\Delta p_s$.

Substituting this in to (1.6), gives:

$$S = N_{t,s} \left(\frac{k_{n,s} k_{p,s} \left(n_{s,0} + \left(\frac{p_{s,0} \Delta n}{\Delta p} \right)_s + \Delta n_s \right)}{k_{n,s} (n_{s,0} + \Delta n_s + n_{1,s}) + k_{p,s} (p_{s,0} + \Delta p_s + p_{1,s})} \right) \quad (1.8)$$

For a constant illumination level, potential, and temperature, measurement of S then allows the extraction of the surface trap state density.

Measured values of S range from low (1 cm/s) to extremely high (100,000 cm/s). For silicon surfaces with highly ordered thermally grown oxides used in semiconductor device manufacturing, S values as low as 3 cm/s have been observed.^{13,14} These low recombination velocities and surface trap state densities crucial for the manufacturing of

semiconductor devices, where loss of charge carriers at interfaces would cause signal loss and excess heating of the device. For a semiconductor photoelectrochemical cell, low surface recombination velocities are necessary to allow for efficient charge carrier collection and energy generation. The addition of a thermal oxide, however, at the semiconductor/liquid interface would inhibit the flow of charge carriers to and from the solution, preventing the cell from operating as a closed circuit. Investigated herein is a technique for the passivation of silicon surfaces towards charge carrier recombination through the formation of Si-C bonds to alkyl monolayers.

1.4 Formation of Organic Monolayers on Silicon Surfaces

Functionalization of atomically flat or nearly flat silicon surfaces has been accomplished through both wet-chemical as well as UHV techniques. The wet chemical functionalization of silicon begins with a chemical etch of the silicon surface, which is covered by a native oxide formed by contact with air and water. This oxide can be stripped away using various fluoride containing aqueous etches. The Si (111) surface can be prepared with atomically flat large area terraces exposing only singly H-terminated surface species by use of the anisotropic basic etch of 40% NH_4F (aq) for 20 minutes followed by rinsing in ultrapure water. Figure 1.2 shows the infrared absorbance spectra for a H-terminated Si (111) surface after etching in NH_4F showing the single sharp Si-H stretch absorbance. Shifting from p to s polarized light results in the near total disappearance of the absorbance, indicating that the Si-H bond is oriented normal to the sample surface. This perfectly H-terminated surface can be prepared with large area

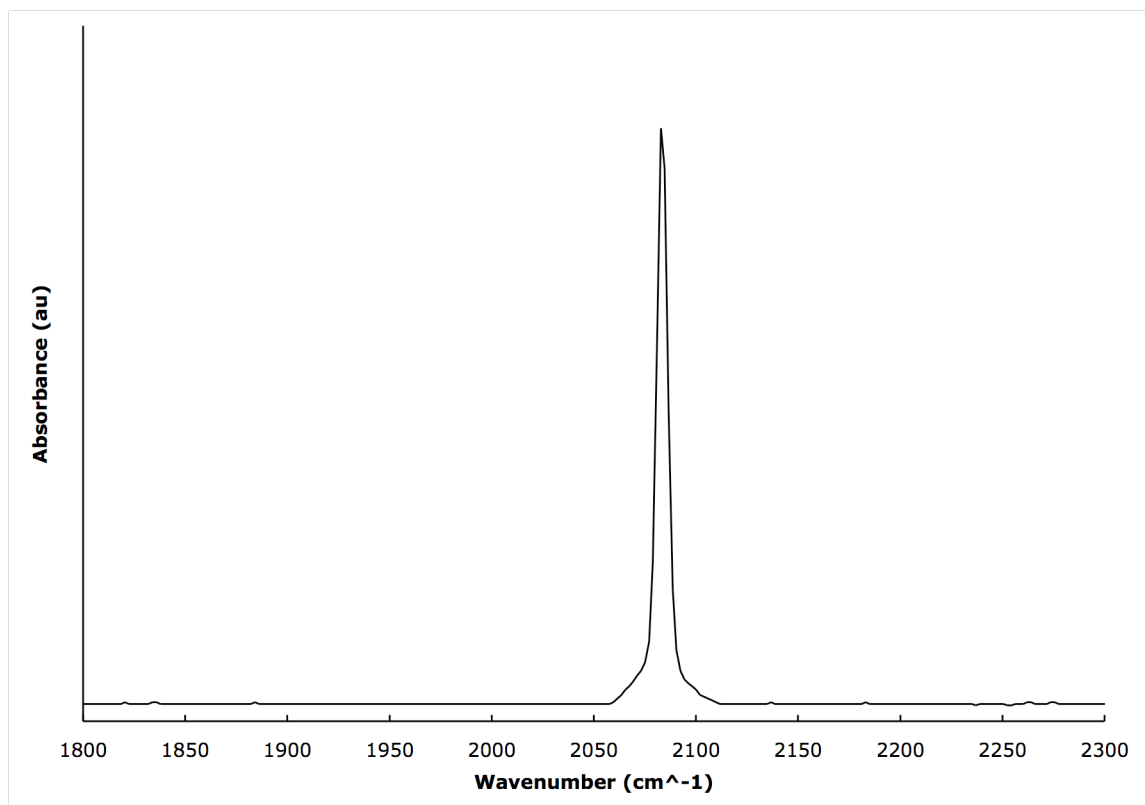


Figure 1.2: The infrared absorbance spectrum for a H-terminated Si (111) surface after etching in NH₄F showing the single sharp Si-H stretch absorbance.

atomically flat terraces, limited only by the miscut angle of the silicon wafer.¹⁵ The Si (100) surface, however, cannot be prepared with such exactitude, as there exists no anisotropic etch that reveals a perfectly flat Si (100) surface. The reason for this is that the Si (100) surface is not a low energy plane, as it has two active bonds per surface silicon, and is etched preferentially in fluoride etches, pitting the surface. While atomically flat Si (100) surfaces can be prepared in UHV by cleavage or plasma etching followed by high temperature annealing, the wet chemically prepared surface is created by a quick (< 1 minute) etch in dilute buffered (pH 4-5) HF. This surface is atomically rough and contains populations of SiH, SiH₂, and SiH₃ in concentrations that strongly depend on the etch time and pH.

The hydrogen terminated silicon surfaces are not stable in the presence of air or water, and oxidizes rapidly. The H-term Si (100) surface is far more reactive than the H-term Si (111) surface, and cannot be exposed to air without oxidation. The Si (111) surface is somewhat more stable, and can be exposed to air for very short times (< 5 minutes) before detectable levels of oxide form (*vide infra*). The Si-H bonds on the surfaces, however, are very useful as chemical handles for functionalization of the surface. A large number of methods have been published on the modification of the Si-H bond in free molecules.¹⁶ The first reactions published concerning the functionalization of the silicon surface with covalently attached organic compounds involved the reaction of the Si-H bond with octadecyl alkenes through a radical process using a diacyl peroxide initiator.^{17,18} Figure 1.3 shows the mechanism by which this reaction occurs. These surfaces formed densely packed monolayers that showed excellent oxidation stability and resistance to a variety of harsh environments. Further hydrosilylation reactions were

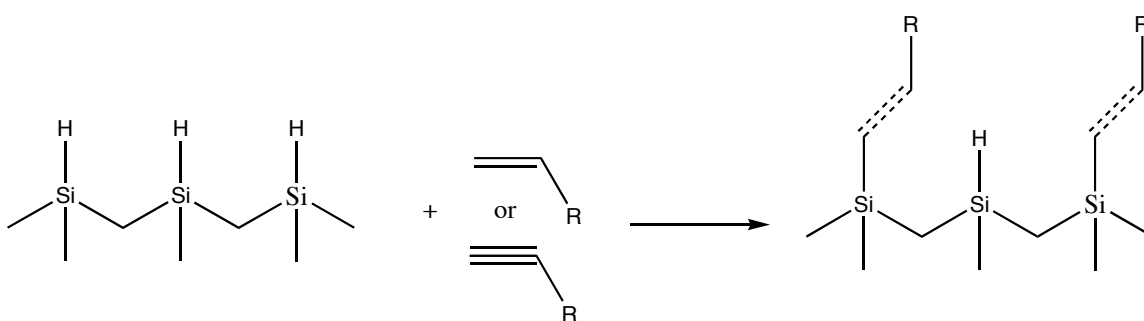


Figure 1.3: The hydrosilylation reaction mechanism, with the reaction of Si-H bonds with alkenes or alkynes after activation by either heat or light.

developed using thermal¹⁹ and photochemical^{20,21} activation of the Si-H bond for Si-C bond formation. These surfaces as well showed excellent surface oxidation resistance of both the Si (100) and Si (111) surfaces. The hydrosilylation reaction has also been performed using transition metal catalyzed^{22,23} as well as Lewis acid catalyzed reactions.^{24,25}

The formation of alkyl monolayers has also been accomplished using alkyl Grignard and alkyl lithium reagents. Originally these reagents were reacted with the Si-H surface through electrochemical grafting.²⁶ Further work using these reagents did not drive the reaction through the use of an external potential, and found that Si-C bonds could be formed from carbanionic species from the porous Si-H surface.^{27,28} Flat single crystal Si (111) surfaces were reacted with alkyl Grignards and alkyl lithium reagents in a two step process,²⁹⁻³¹ involving reaction of the Si-H surface with radical chlorine species to form an intermediate Si-Cl surface, which was then further reacted with carbanion sources to form Si-C bonded alkyl groups. Figure 1.4 shows this reaction scheme. These surfaces were shown to have exceptional stability towards surface oxidation using short (CH₃) to long chain (C₈H₁₇) alkyl Grignards and lithium reagents. These functionalized surfaces were the first shown to be electronically passivated, determined by measuring the rf absorbance of photogenerated charge carriers. These alkylated surfaces were found to have surface recombination velocities that ranged between 20-50 cm/s, showing excellent charge carrier lifetimes.

This work concerns itself with the two step chlorination/alkylation reaction developed by Lewis and co-workers, with an aim towards furthering the types of alkyl

groups bonded to the surface as well as characterization of these surfaces using a variety of spectroscopic and computational techniques.

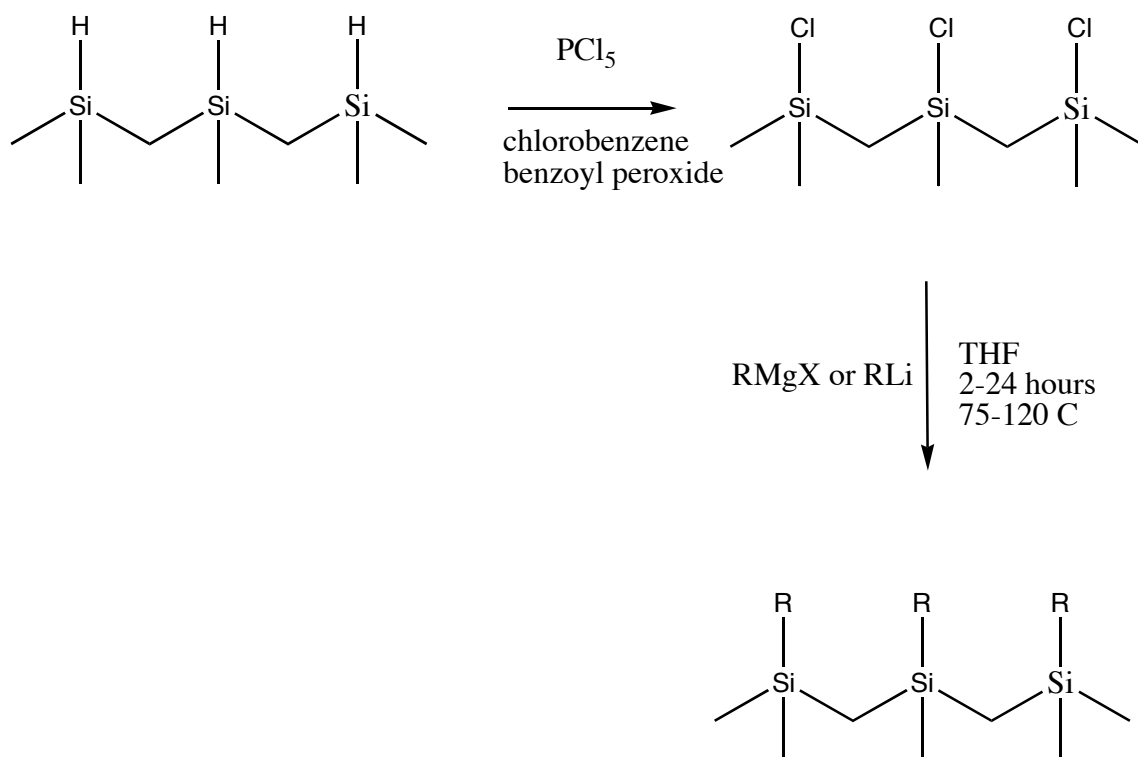


Figure 1.4: The two step chlorination/alkylation procedure for the formation of covalently bound monolayers of alkyl groups on Si (111).

1.5 Bibliography

- (1) Tan, M. X.; Laibinis, P. E.; Nguyen, S. T.; Kesselman, J. M.; Stanton, C. E.; Lewis, N. S. *Prog Inorg Chem* **1994**, *41*, 21-144.
- (2) Chapin, D. M.; Fuller, C. S.; Pearson, G. L. *J. Appl. Phys.* **1954**, *25*, 676.
- (3) Cuevas, A.; Sinton, R. A.; Midkiff, N. E.; Swanson, R. M. *IEEE Electron Device Lett.* **1990**, *11*, 6-8.
- (4) Gruenbaum, P. E.; Gan, J. Y.; Swanson, R. M. *Appl. Phys. Lett.* **1991**, *58*, 945-947.
- (5) Li, J. M.; Chong, M.; Zhu, J. C.; Li, Y. J.; Xu, J. D.; Wang, P. D.; Shang, Z. Q.; Yang, Z. K.; Zhu, R. H.; Cao, X. L. *Appl. Phys. Lett.* **1992**, *60*, 2240-2242.
- (6) Finklea, H. O. In *Semiconductor Electrodes*; Finklea, H. O., Ed.; Elsevier: New York, 1988□; Vol. 55, p 43.
- (7) Heller, A. *Acc. Chem. Res.* **1981**, *14*, 154-162.
- (8) Parkinson, B. *Acc. Chem. Res.* **1984**, *17*, 431-7.
- (9) Smestad, G.; Bignozzi, C.; Argazzi, R. *Sol Energ Mat Sol C* **1994**, *32*, 259-272.
- (10) Bradhorst, H. W., Jr. In *IEEE Photovoltaic Spec. Conf.* NASA, Lewis Research Center, Cleveland, Ohio, 1978, p 37-43.
- (11) Shockley, W.; Read, W. T. *Physical Review* **1952**, *87*, 835-42.
- (12) Hall, R. N. *Physical Review* **1952**, *87*, 387.

- (13) Yablonovitch, E.; Swanson, R. M.; Eades, W. E.; Weinberger, B. R. *Appl. Phys. Lett.* **1986**, *48*, 245.
- (14) Eades, W. D.; Swanson, R. M. *J. Appl. Phys.* **1985**, *58*, 4267.
- (15) Higashi, G. S.; Chabal, Y. J.; Trucks, G. W.; Raghavachari, K. *Appl. Phys. Lett.* **1990**, *56*, 656-658.
- (16) *The Chemistry of Organic Silicon Compounds*; John Wiley and Sons: New York, New York, 1989.
- (17) Linford, M. R.; Fenter, P.; Eisenberger, P. M.; Chidsey, C. E. D. *J. Am. Chem. Soc.* **1995**, *117*, 3145-3155.
- (18) Linford, M. R.; Chidsey, C. E. D. *J. Am. Chem. Soc.* **1993**, *115*, 12631-12632.
- (19) Sieval, A. B.; Demirel, A. L.; Nissink, J. W. M.; Linford, M. R.; van der Maas, J. H.; de Jeu, W. H.; Zuilhof, H.; Sudholter, E. J. R. *Langmuir* **1998**, *14*, 1759-1768.
- (20) Terry, J.; Linford, M. R.; Wigren, C.; Cao, R. Y.; Pianetta, P.; Chidsey, C. E. D. *Appl. Phys. Lett.* **1997**, *71*, 1056-1058.
- (21) Terry, J.; Mo, R.; Wigren, C.; Cao, R. Y.; Mount, G.; Pianetta, P.; Linford, M. R.; Chidsey, C. E. D. *Nucl. Instrum. Meth. B* **1997**, *133*, 94-101.
- (22) Zazzera, L. A.; Evans, J. F.; Deruelle, M.; Tirrell, M.; Kessel, C. R.; Mckeown, P. J. *Electrochem. Soc.* **1997**, *144*, 2184-2189.
- (23) Holland, J. M.; Stewart, M. P.; Allen, M. J.; Buriak, J. M. *J. Solid State Chem.* **1999**, *147*, 251-258.

- (24) Buriak, J. M.; Allen, M. J. *J. Am. Chem. Soc.* **1998**, *120*, 1339-1340.
- (25) Buriak, J. M.; Allen, M. J. *J. Lumin.* **1998**, *80*, 29-35.
- (26) Henry de Villeneuve, C.; Pinson, J.; Ozanam, F.; Chazalviel, J. N.; Allongue, P. In *Mat. Res. Soc. Symp. Proc.* 1997; Vol. 451, p 185-195.
- (27) Song, J. H.; Sailor, M. J. *J. Am. Chem. Soc.* **1997**, *119*, 7381-7385.
- (28) Kim, N. Y.; Laibinis, P. E. *J. Am. Chem. Soc.* **1998**, *120*, 4516-4517.
- (29) Bansal, A.; Li, X.; Lauermann, I.; Lewis, N. S.; Yi, S. I.; Weinberg, W. H. *J. Am. Chem. Soc.* **1996**, *118*, 7225-7226.
- (30) Webb, L. J.; Lewis, N. S. *J. Phys. Chem. B* **2003**, *107*, 5404-5412.
- (31) Bansal, A.; Li, X. L.; Yi, S. I.; Weinberg, W. H.; Lewis, N. S. *J. Phys. Chem. B* **2001**, *105*, 10266-10277.

Chapter 2

Chemical and Electrical Passivation of Silicon(111) Surfaces Through Functionalization with Sterically Hindered Alkyl Groups

2.1 Introduction

A variety of procedures have recently been developed to alkylate Si surfaces, in attempts to passivate crystalline Si surfaces towards oxidation and to impart other desirable properties to this widely used semiconductor. The H-terminated Si(111) surface has been immersed in terminal alkenes or alkynes to form Si-C bonds through free-radical reactions initiated thermally¹⁻⁴ or photochemically,⁵⁻⁷ and through Lewis acid catalyzed hydrosilylation^{8,9} or transition metal catalyzed¹⁰ reactions. Other alkylation strategies involve formation of surficial Si radicals with scanning tunneling microscopy,¹¹ atomic force microscopy,¹² or mechanical scribing¹³ of the surface, and subsequent reaction of these radicals with alkenes or alkynes. Several electrochemical methods have also been shown to form surface-bonded alkyl groups.¹⁴⁻¹⁶

Surfaces alkylated using a two step chlorination/alkylation process with straight chain alkyl groups (C_nH_{2n+1} , $n=1-8$) have shown excellent surface passivation both from a chemical viewpoint and from an electrical viewpoint.^{5,17-22} In this process, the H-terminated Si(111) surface is first chlorinated to make a metastable surface, and this

surface is then reacted with organo-lithium or Grignard reagents to form the desired Si-C terminated surfaces. The distance between Si atop atoms on an unreconstructed 1x1 H-terminated Si(111) surface is 3.8 Å,²³ while the Van der Waals radius of a methyl group is approximately 2.0 Å.²⁴ Hence, a methyl group can in principle react with every Si atop site on the unreconstructed Si(111) surface. Indeed, the CH₃-Si(111) surface prepared through the two-step chlorination/alkylation method has been observed using scanning tunneling microscopy methods to show a nearly complete coverage of methyl groups, in a 1x1 pattern, over wide regions of the surface.²⁵ In contrast, the Van der Waals radius of the Si-CH₂CH₂- moiety, or of any functionality with methylene groups (i.e., C_nH_{2n+1}, n≥2), is larger than 2.5 Å. Hence, on the Si(111) surface, complete functionalization of Si atop sites with methylene-containing alkyl groups would face severe steric difficulties.

Despite this steric constraint, Si(111) surfaces alkylated with straight chain alkyl groups have shown enhanced stability towards oxidation and have also shown low surface recombination velocities.^{17,18,22} Interestingly, no Cl signal is present by X-ray photoemission spectroscopy (XPS) after the alkylation process.²² Bulkier, non-straight-chain functional groups, such as *tert*-butyl or phenyl, are subject to even more severe packing limitations on the Si(111) surface. In this work, we describe the preparation of Si(111) surfaces alkylated with C_nH_{2n+1}- (n = 1, 2, and 8), (CH₃)₂CH- (*iso*-propyl), (CH₃)₃C- (*tert*-butyl), and C₆H₅- (phenyl) groups. The resulting surfaces have been characterized by X-ray photoelectron spectroscopy (XPS), surface recombination velocity (SRV) measurements, attenuated total reflectance surface infrared (ATR-IR) absorption spectrometry, and cyclic voltammetry. The alkylated Si surfaces were monitored for the rate of electron-hole recombination by SRV measurements and the rate

of oxidation by XPS. Cyclic voltammetry experiments and ATR-IR have been used to provide insight into the mechanism of the alkylation reaction in such systems.

2.2 Experimental

2.2.1 Alkylation of Silicon

The silicon samples used for SRV and XPS measurements were float-zone grown, (111)-oriented wafers that were polished on both sides (Virginia Semiconductor, Fredericksburg, VA). To minimize the bulk contribution to charge-carrier recombination, 250 μm thick, high resistivity ($> 4000 \Omega \text{ cm}$), n-type, phosphorus doped silicon was used. Prior to alkylation, samples were cut into sections $\sim 1 \text{ cm}^2$ in area. The pieces were cleaned by sonication for 5 s in a series of organic solvents (VWR Scientific Products, West Chester, PA): methanol, acetone, dichloromethane, 1,1,1-trichloroethane, dichloromethane, acetone, methanol, and then $18 \text{ M}\Omega \text{ cm}$ resistivity H_2O . To produce a hydrogen-terminated surface, the samples were then etched for 30 s in buffered HF(aq). Samples were then etched, with occasional agitation to remove bubbles forming on the edges, for 10 min in 40% NH_4F (aq) (Transene, Danvers, MA). After etching, the samples were dried under a stream of N_2 (g) and passed into a glove box for functionalization.

To chlorinate the surfaces, samples were immersed in 2 mL of anhydrous chlorobenzene (99.8% under argon, Aldrich) saturated with PCl_5 (99.995%, Strem, Newburyport, MA) for 1 hr at 95-100 $^\circ\text{C}$. Benzoyl peroxide (97%, Aldrich) was added

(<1mg) to initiate the chlorination of the surface. Care was taken to insure that the polished surfaces of the silicon samples were not touched, to prevent scratching that might influence the surface reactivity.

After chlorination, the samples were washed in anhydrous tetrahydrofuran (THF) (99.8%, inhibitor free, Aldrich) and were placed in Teflon screw-cap sealed glass reaction flasks that contained 10 mL of anhydrous THF and 10 mL of a 1 M Grignard reagent in THF. The Grignard reagents were either CH_3MgCl , $\text{CH}_3\text{CH}_2\text{MgCl}$, $\text{CH}_3(\text{CH}_2)_7\text{MgCl}$, $(\text{CH}_3)_2\text{CHMgCl}$, $(\text{CH}_3)_3\text{CMgCl}$, or $\text{C}_6\text{H}_5\text{MgCl}$. The reaction solution was heated to 110-120 °C for 21 hr in a sealed reaction vessel. After reaction, samples were rinsed in THF followed by anhydrous methanol (99.8% Aldrich), removed from the glove box, and sonicated in a 5 mL solution of methanol and glacial acetic acid (10:1) (Aldrich) for 5 min to remove any adsorbed magnesium salts. Samples were then rinsed with 18 M Ω cm resistivity H_2O and either passed directly into the ultra-high vacuum (UHV) load lock for XPS analysis or placed in scintillation vials for SRV measurements.

2.2.2 Electrochemistry

Electrodes were fashioned from 550 μm thick, double side polished, n-type (As-doped), prime grade Si(111) with a resistivity of < 0.004 Ω cm (Addison Engineering Corp, San Jose, CA). Samples were cut into 1-3 cm^2 squares and an ohmic contact was formed by the application of Ga-In (Aldrich) eutectic on an etched portion of the silicon. Silver print was used to attach a tinned Cu lead wire to the back surface of the Si. The lead wire was then encased in a glass body and sealed in epoxy.

Electrochemistry was performed in a three-electrode configuration with a Pt coil counter electrode and a Ag^+/Ag reference electrode. The electrolyte, unless otherwise noted, was 100 mM tetra(n-butyl)ammonium hexafluorophosphate (TBAPF_6 , Fluka, electrochemical grade) in THF (J. T. Baker, Phillipsburg, NJ, Ultra Low Water, BakerDry). The Ag^+/Ag reference electrode consisted of a saturated solution of silver nitrate (99.999%, Aldrich) in the THF electrolyte with a Ag wire. The reference compartment was separated from the electrochemical solution by a Vycor[®] frit. The working electrode was either Pt (0.071 cm^2 surface area) or silicon. All electrochemistry was performed under anaerobic conditions in a glove box with $< 10 \text{ ppm}$ of O_2 . Unless otherwise noted, cyclic voltammograms were taken at 150 mV s^{-1} on a Solartron 1287 potentiostat (Solartron Analytical, Farnborough, UK) with data collected using Corrware, v 2.5b (Scribner Associates). Cyclic voltammograms and potentiostatic experiments on silicon working electrodes were carried out in the dark. After electrochemical measurements, the electrodes were rinsed in THF, dried under a stream of flowing $\text{N}_2(\text{g})$, scribed below the epoxy sealant, and broken into squares for XPS measurements.

2.2.3 X-Ray Photoelectron Spectroscopy

XPS data were collected on a UHV system that has been described previously.¹⁸ The collection chamber was maintained at $\approx 5 \times 10^{-10}$ torr when not in use, whereas due to sample outgassing the pressure rose to $\approx 2 \times 10^{-8}$ torr during data collection. Due to the relatively low resistivity of the samples, charge compensation was not needed. All measurements were taken on the center of the sample to ensure reproducibility and to

minimize the effects of scratches or contamination at the edges. The incident beam consisted of 1486.6 eV X-rays from an Al K α source, and ejected electrons were collected at 55° off of the surface normal. All energies are reported as binding energies in eV. The XPS system was periodically calibrated using the 4f peaks of a Au standard at 83 and 87 binding eV.

Data were collected using ESCA 2000 E Capture software, v. 102.04 (Service Physics). Samples were first scanned from 0 to 1000 binding eV to monitor signals for Cl as well as C and O. The Si 2p, Cl 2p and C 1s regions of 98-105, 198-204, and 282-287 binding eV, respectively, were investigated in detail. The Si 2p region was used to monitor the growth of Si oxides. Scan times of up to 4 hr were employed for data collection. The spectrometer resolution was ≈ 0.5 eV.

Oxide coverages were determined by integration of the area under the broad oxygen-shifted Si 2p peak centered around 103 binding eV, which was comprised of SiO₂ and Si suboxides. This peak area was ratioed to the area of the bulk Si 2p_{3/2} and Si 2p_{1/2} peaks. Using ESCA 2000 A Analysis, v. 102.04 integration software, the peak shapes were fitted to Voigt functions fixed at 95% Gaussian and 5% Lorentzian lineshapes. The position of the Si 2p_{1/2} peak was fixed at 0.6 binding eV higher than the 2p_{3/2} peak and the FWHM was constrained to be identical to that of the Si 2p_{3/2} peak, with the total integrated area ratio of the 2p_{1/2}/2p_{3/2} peaks fixed at 0.51.¹⁷

The fractional monolayer coverage of oxide species on the surface was determined using the substrate-overlayer model:²⁶

$$\frac{d_o}{d_1} = \lambda_o \sin \theta \left\{ \ln \left[1 + \left(\frac{I_{Si}^o}{I_o^o} \right) \left(\frac{I_o}{I_{Si}} \right) \right] \right\} \quad (2.1)$$

where d_o is the overlayer thickness, d_1 is the thickness of one monolayer of oxide, (3.5 Å), and λ_o is the attenuation factor of the oxide layer (26 Å). θ is the take-off angle for the measurement (90°-55°, i.e., 35°), I_{Si}^o/I_o^o is a normalizing factor for the particular instrument used (1.3 for this instrument¹⁷), and I_o/I_{Si} is the ratio of the peak area of the oxide-shifted silicon to the area of the unshifted silicon peak.

Data from the carbon 1s emission region were fitted to three peaks, representing silicon-bonded carbon at 283.9 eV, carbon-bonded carbon at 285.0 eV, and oxygen-bonded carbon at 286.8 eV. Peaks were fitted to Voigt functions having 70% Gaussian and 30% Lorentzian character. The peak centers were allowed to float, though the center to center distances were fixed at 1.1 eV between the silicon-bonded carbon and the carbon-bonded carbon emissions, and at 1.8 eV between the oxygen-bonded carbon and the carbon-bonded carbon emissions. The integrated area under each carbon peak was ratioed to the integrated area under the silicon 2p peaks for that sample, normalized for scan time. The ratio of the silicon-bonded carbon to the normalized area for the Si 2p peak (C_{Si}/Si) was then compared between alkylated surfaces. The methyl-terminated Si(111) surface was used as a reference surface for the other alkylated Si surfaces, so surface coverages for each alkyl group are reported as $(C_{Si}/Si)_{alkyl}/(C_{Si}/Si)_{methyl}$.

2.2.4 Infrared Spectroscopy

For IR spectroscopy, n-type, phosphorous doped, float-zone, single-crystal, 505 ±25 μm thick Si(111) wafers (Silicon Valley Microelectronics Inc., Santa Clara, CA) with a resistivity of >30 Ω cm were cut into 2.1 x 3 cm segments. Samples were cleaned

with an RCA etch, before a final etch in degassed 40% $\text{NH}_4\text{F}(\text{aq})$ for 20 min. Surfaces were chlorinated and alkylated as described above, with samples sealed under N_2 for transport to the FT-IR. Samples were unsealed and placed in a GATR mount (Herrick Scientific Products Inc., Pleasantville, NY) for grazing angle (65°) ATR spectroscopy. The GATR mount was placed in a Vertex 70 FT-IR spectrometer (Bruker Optics Inc., Billerica, MA) for measurements. 512 scans for each sample were taken in air, with background scans of air subtracted from the spectra.

2.2.5 Surface Recombination Velocity Measurements

Surface recombination velocity measurements were collected using a contactless rf conductivity apparatus.¹⁹ Samples were excited with 10 ns pulses at 1064 nm from a Nd:YAG laser operating at 10 Hz. The photogenerated electron-hole pairs diffused to either surface of the sample to recombine through surface-localized electronic states within the Si bandgap. The bulk charge-carrier lifetimes as reported by the manufacturer (~ 6 ms) were much longer than the observed lifetimes, indicating that charge-carrier recombination effectively only occurred at the silicon surfaces. Charge-carrier concentrations were monitored by measuring the reflected signal from a 450 MHz rf coil. The absorbed rf signal was recorded by averaging 128 traces and the data were fitted to a single exponential decay:

$$A = y_0 + ae^{-t/\tau} \quad (2.2)$$

where τ is the observed charge-carrier lifetime. The surface recombination velocity, S , is obtained from τ through:

$$\frac{1}{\tau} = \frac{1}{\tau_b} + \frac{2S}{d} \quad (2.3)$$

where τ_b is the bulk lifetime, and d is the sample thickness. For all measurements, $\tau_b \gg \tau$, so $S \approx d/2\tau$.

All τ values are reported after the first 24 hr following alkylation. Initial measurements of τ for an individual sample showed a slight increase in charge-carrier lifetime over the first day, but stabilized thereafter. To monitor the stability of the alkylated surface towards oxidation, samples were stored in scintillation vials under laboratory air and normal laboratory illumination conditions for up to 71 days, and τ values were monitored periodically during this time interval.

2.3 Results

2.3.1 XPS Data

Figure 2.1 shows representative XPS for the two-step chlorination/alkylation of Si(111) surfaces. H-terminated surfaces exhibited peaks for elemental silicon 2s (150 eV) and 2p (100 eV) emissions as well as the silicon phonon emission bands at 17 eV and 36 eV above the 2s and 2p peaks, respectively. Trace amounts of C and O were observed at 284 and 532 eV, respectively. The Cl 2s and 2p peaks, at 201 and 271 eV, respectively, appeared after the chlorination step. After alkylation, no Cl peaks were observed, and the C 1s peak increased in amplitude. No oxidized silicon was detected in detailed scans of the Si 2p region, indicating that the oxygen present was bonded to

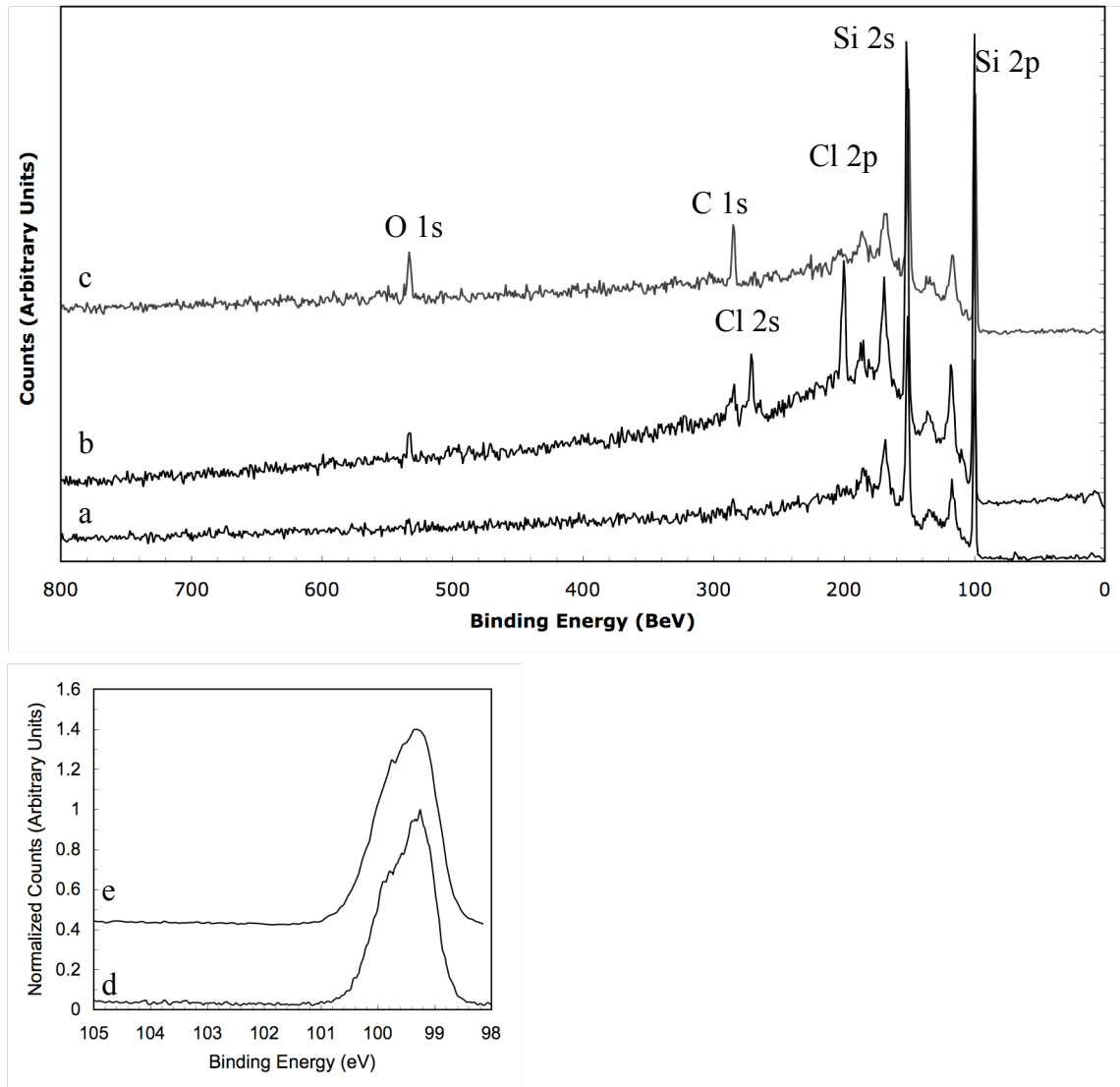


Figure 2.1: XPS spectra of a) H-terminated Si (111), b) Cl-terminated Si (111), c) CH₃-terminated Si (111), d) the silicon 2p region for H-Si, and e) the Si 2p region of CH₃-Si surfaces.

adventitious C sources resulting from the alkylation process and not from oxidation of the Si surface.

Figure 2.2 shows a high resolution XPS scan of the C 1s region of an ethylated surface. Two main peaks were observed at 283.9 and 285.0 eV, with a third, small signal at 286.8 eV. The peaks at 285.0 and 286.8 eV were common to alkylated and H-terminated silicon surfaces, whereas the low binding energy peak at 283.9 eV was unique to alkylated Si surfaces. Hence, the peak at 283.9 eV can be assigned to emission from core level electrons of carbon atoms covalently bonded to the relatively electropositive silicon.^{5,27} The higher energy peak at 285.0 can be ascribed to carbon in a non-polar bond with either hydrogen or another carbon atom. This carbon peak was the sum of C 1s electrons from adventitious carbon sources as well as alkylating carbons that do not participate in the Si-C bond. The appearance of a third C 1s peak shifted to higher binding energy at 286.8 eV is ascribed to adventitious carbon bonded to oxygen.

The assignment of the emission at 283.9 eV to the C 1s peak of silicon-bonded carbon (C_{Si}) enabled a quantitative measurement of the relative coverage of surficial Si-C bonds on the various alkylated surfaces. Table 2.1 presents the peak area ratio of the silicon-shifted carbon signal to the Si 2p signal (C_{Si}/Si) for each alkyl group, relative to the C_{Si}/Si peak ratio for the methylated surface. Methylation has been shown by various methods to provide a nearly complete monolayer on the Si(111) surface.^{25,27-29} Ethylated surfaces showed a C_{Si}/Si peak ratio of $90 \pm 20\%$ relative to that of CH_3 -terminated Si surfaces, indicating that ethyl groups can be packed at a very high density by this two-step alkylation method. Octyl and phenyl produced $60 \pm 10\%$ and $50 \pm 20\%$,

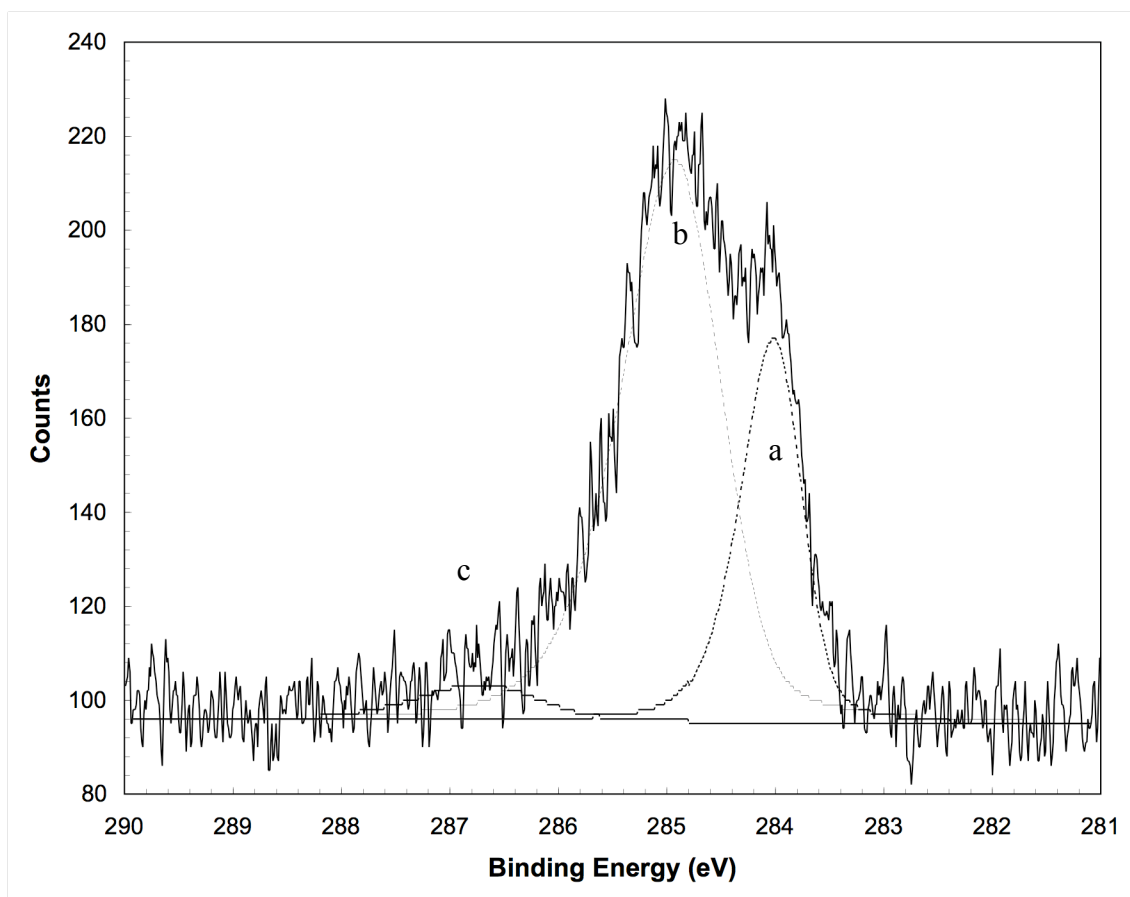


Figure 2.2: XPS spectrum of the carbon 1s region of C_2H_5 -terminated Si (111) surface with peaks fits (dashed lines) for a) carbon bonded to silicon, b) carbon bonded to carbon (and hydrogen), and c) carbon bonded to oxygen.

	ratio C _{Si} /Si	% of methyl coverage
methyl	0.16 ± 0.02	--
ethyl	0.14 ± 0.02	(9 ± 2) x 10 ¹
<i>iso-propyl</i>	0.06 ± 0.02	(4 ± 2) x 10 ¹
<i>tert-butyl</i>	0.061 ± 0.008	(4 ± 2) x 10 ¹
phenyl	0.08 ± 0.02	(5 ± 2) x 10 ¹
octyl	0.092 ± 0.008	(6 ± 1) x 10 ¹

Table 2.1: The C_{Si}/Si XPS integrated area ratios for alkylated surfaces showing the relative amount of carbon bonded to silicon for each alkyl surface. Standard deviations are over four samples. Surface coverages are reported relative to the methylated surface.

respectively, of the methyl coverage, while alkylation with *tert*-butyl and *iso*-propyl groups produced $40 \pm 20\%$ and $40 \pm 20\%$ of the C_{Si}/Si ratio of methyl-terminated Si.

Figure 2.3 shows the evolution of the XPS spectra of alkylated Si surfaces as a function of time exposed to ambient air. Oxidation of the Si surface was monitored by the growth of the broad Si^{x+} peak between 101 and 105 BeV. Relative to H-terminated Si, CH_3 -terminated Si surfaces exposed to air in the dark over a period of more than two months showed greatly reduced surface oxidation. The surface oxidation for other alkylated Si surfaces is shown in Figure 2.4. All alkylated surfaces showed similar oxidation rates, with no discernible differences correlating to alkyl coverage or size of the alkyl group.

2.3.2 Surface Recombination Velocity Measurements

Table 2.2 shows the charge-carrier lifetimes for the alkylated and H-terminated surfaces exposed to air averaged over a 24 day interval. Lifetimes for air-exposed (oxidized) H-terminated Si(111) surfaces were less than $10 \mu s$, the lower limit for the measurement technique, indicating that all charge carriers recombined upon reaching the surface, with the observed lifetime dominated by diffusion of charge carriers to the electrically active surface regions. For all alkylated surfaces, the charge-carrier lifetimes were extremely long. Charge-carrier lifetimes for these samples were still significantly less than the manufacturer's reported bulk lifetimes (~ 6 ms), implying that recombination even for the alkylated surfaces still occurred almost exclusively at the surface.

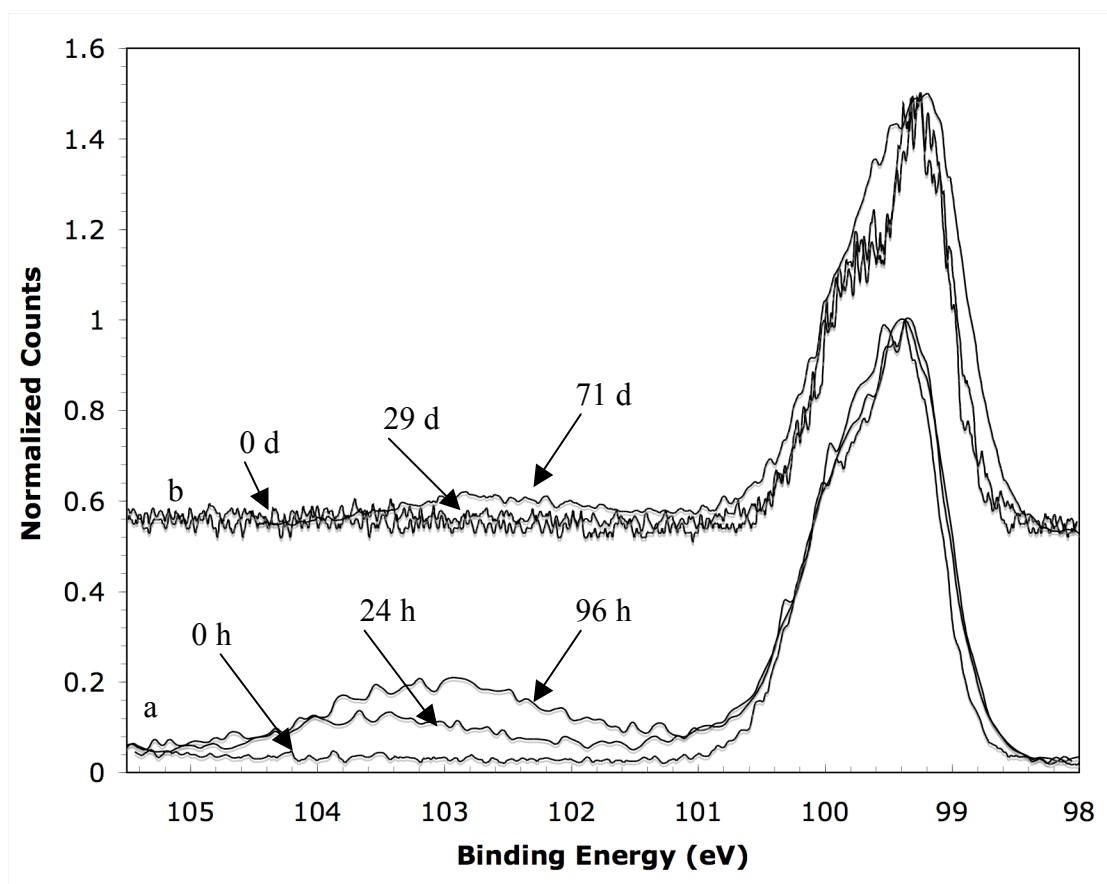


Figure 2.3: XPS spectra of the oxidation of the Si (111) 2p region for a) H-terminated Si(111) at 0, 24, and 96 h in air, and b) CH₃-terminated Si(111) at 0, 29, and 71 days in air.

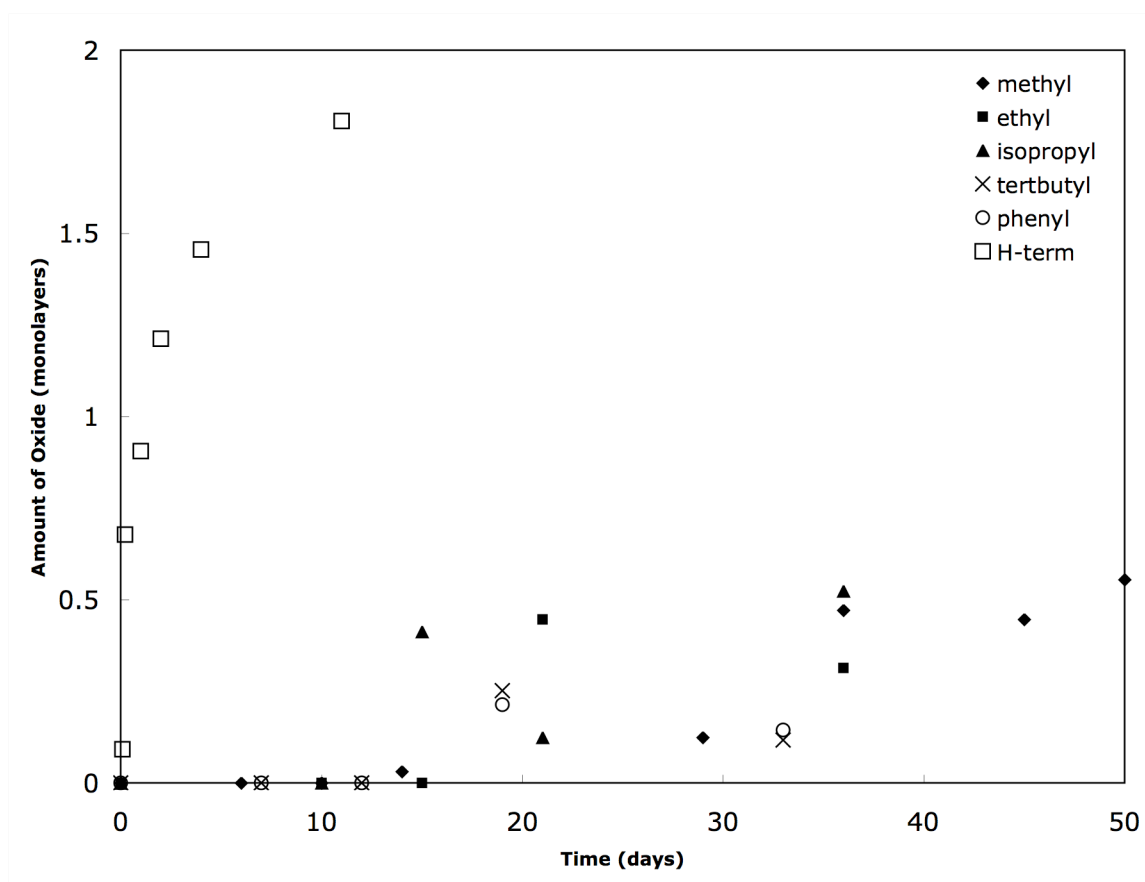


Figure 2.4: Surface oxide growth for H-terminated and alkylated Si(111) surfaces vs. time in air, showing the rapid oxidation of the H-Si(111) surface as compared to alkylated Si(111) surfaces.

	Charge Carrier Lifetime τ (ms)	Surface Recombination Velocity S (cm s ⁻¹)
methyl	$2.3 \pm 0.4 \times 10^2$	44 ± 9
ethyl	$1.8 \pm 0.5 \times 10^2$	$(6 \pm 2) \times 10^1$
<i>iso</i> -propyl	$2.0 \pm 0.5 \times 10^2$	$(6 \pm 2) \times 10^1$
<i>tert</i> -butyl	$1.6 \pm 0.6 \times 10^2$	$(8 \pm 4) \times 10^1$
phenyl	$2.0 \pm 0.9 \times 10^2$	$(6 \pm 2) \times 10^1$
H-terminated	<10	$> 1 \times 10^3$

Table 2.2: Charge carrier lifetimes for alkylated surfaces after 24 days in air. H-terminated Si(111) samples prepared had charge carrier lifetimes shorter than could be measured by the rf conductivity apparatus.

All of the alkylated surfaces exhibited substantially slower surface recombination velocities ($<100 \text{ cm s}^{-1}$) relative to air oxidized H-terminated Si(111) surfaces ($>1000 \text{ cm s}^{-1}$; Table 2.2). No clear trend was observed with respect to alkyl chain length or bulk, and all values are within experimental error, separated only from H-Si(111) at $< 10 \mu\text{s}$. Over the course of measurement, the charge carrier lifetimes initially increased and then declined over time. The decline in τ may result from introduction of surface-based recombination sites by either slow oxidation of the surface or due to sample handling. Figure 2.5 shows the progression of the charge carrier lifetimes for methylated and *tert*-butylated surfaces, superimposed on the surface oxidation of the samples as measured by XPS. The measured lifetimes of the alkylated samples remained extremely high ($> 200 \mu\text{s}$) even at significant levels of oxidation, indicating that samples which have an equivalent monolayer of oxidized silicon at the surface do not exhibit significant increases in surface recombination velocities.

2.3.3 Infrared Spectroscopy

Figure 2.6 shows ATR infrared absorbance spectra of the (111)-oriented Si surfaces alkylated with ethyl and *tert*-butyl groups. The well known Si-H stretch at $\approx 2100 \text{ cm}^{-1}$ disappeared completely after chlorination and was not apparent after alkylation with methyl groups.³⁰ However, the Si-H stretch was observed after functionalization with the larger groups *tert*-butyl and ethyl.

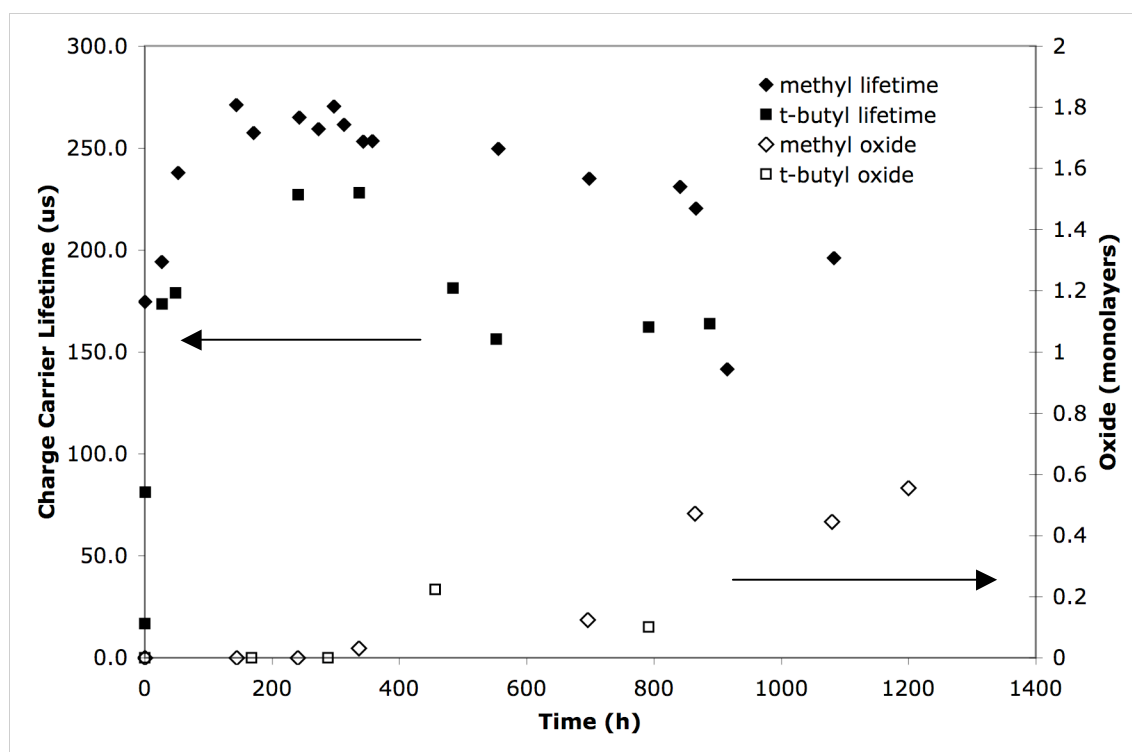


Figure 2.5: Charge-carrier lifetimes for CH_3 - and $(\text{CH}_3)_3\text{C}$ -terminated Si(111) surfaces vs. surface oxide growth. Alkylated surfaces often exhibited an increase in charge carrier lifetime over the first day, and a gradual decline over time. Samples did not show a significant loss in their charge-carrier lifetime as the surface oxidized.

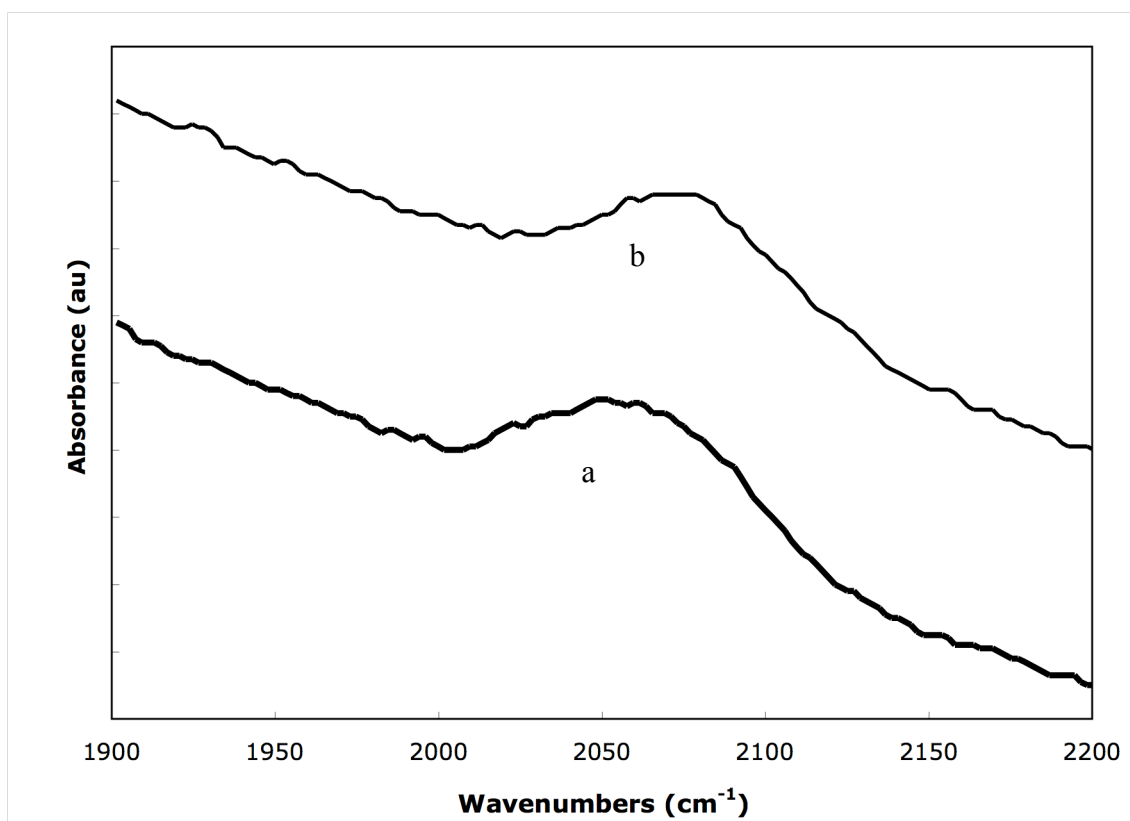


Figure 2.6: IR absorbance in arbitrary units showing the Si-H stretch for a) C₂H₅-terminated Si(111) surfaces and for b) *tert*-butyl-terminated Si(111) surfaces.

2.3.4 Electrochemical Studies

The reactivity of Cl-terminated Si(111) surfaces was investigated to elucidate the mechanism of the reaction between the Grignard alkylating reagents and the surficial Si-Cl bonds. The surficial Si-Cl bonds form a monolayer coverage for surfaces that have been chlorinated with PCl_5 .²⁸

Figure 2.7 compares the cyclic voltammetry of a chlorinated Si(111) surface with that of a Pt electrode in THF. The chlorinated silicon electrode showed an irreversible reductive peak at -2.5 V vs. Ag^+/Ag . This peak decreased in size with successive sweeps indicating that the reducible species was in finite supply at the electrode. Taking the surface density of a full monolayer of chlorinated atoms as the density of Si atop sites on an unreconstructed Si(111) (1x1) surface (7.8×10^{14} atoms per cm^2), integration of the areas under the successive reductive peaks yielded 0.8 ± 0.3 electrons per surface site. This indicates that the reduction current results from the one-electron reduction of the Si-Cl species.

Figure 2.8 displays the XPS spectra of a Cl-Si(111) electrode surface after the potentiostatic application of either -1.0 V or -2.5 V vs Ag^+/Ag for 10 min in THF. The electrode exposed to -1.0 V showed significant Cl 2s and 2p signals, while the surface exposed to -2.0 V showed no residual Cl wide-scan XPS signals. Detailed scans of the Cl 2p region (Figure 2.8 inset) showed the complete removal of the Cl 2p spin-orbit doublet.

The Grignard reagents used for alkylation are strongly reducing compounds, and show broad, irreversible oxidative waves in their cyclic voltammograms between -2.5 and

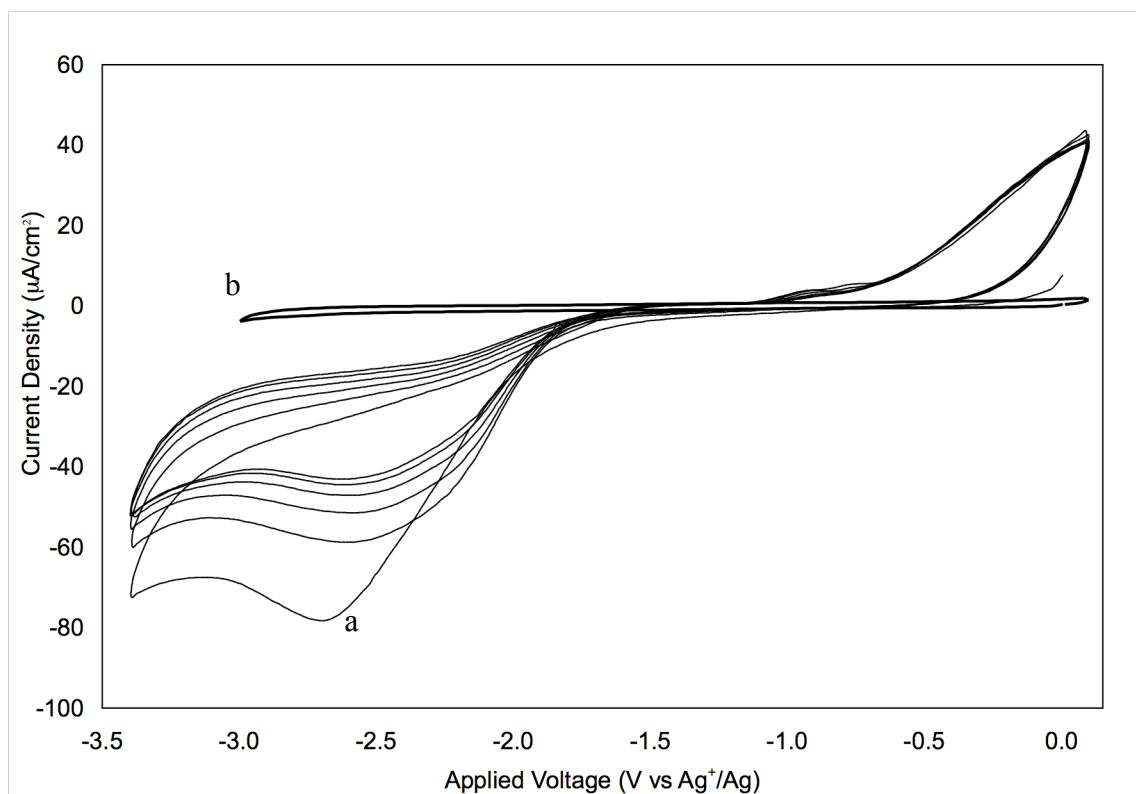


Figure 2.7: Cyclic voltammetry of a) a Cl-terminated Si(111) electrode showing a strong irreversible reductive peak at ~ -2.5 V and b) a Pt working electrode in the same solution. The area under the reductive peaks for Si-Cl electrodes was $0.8 \pm 3 e^-$ per surface site.

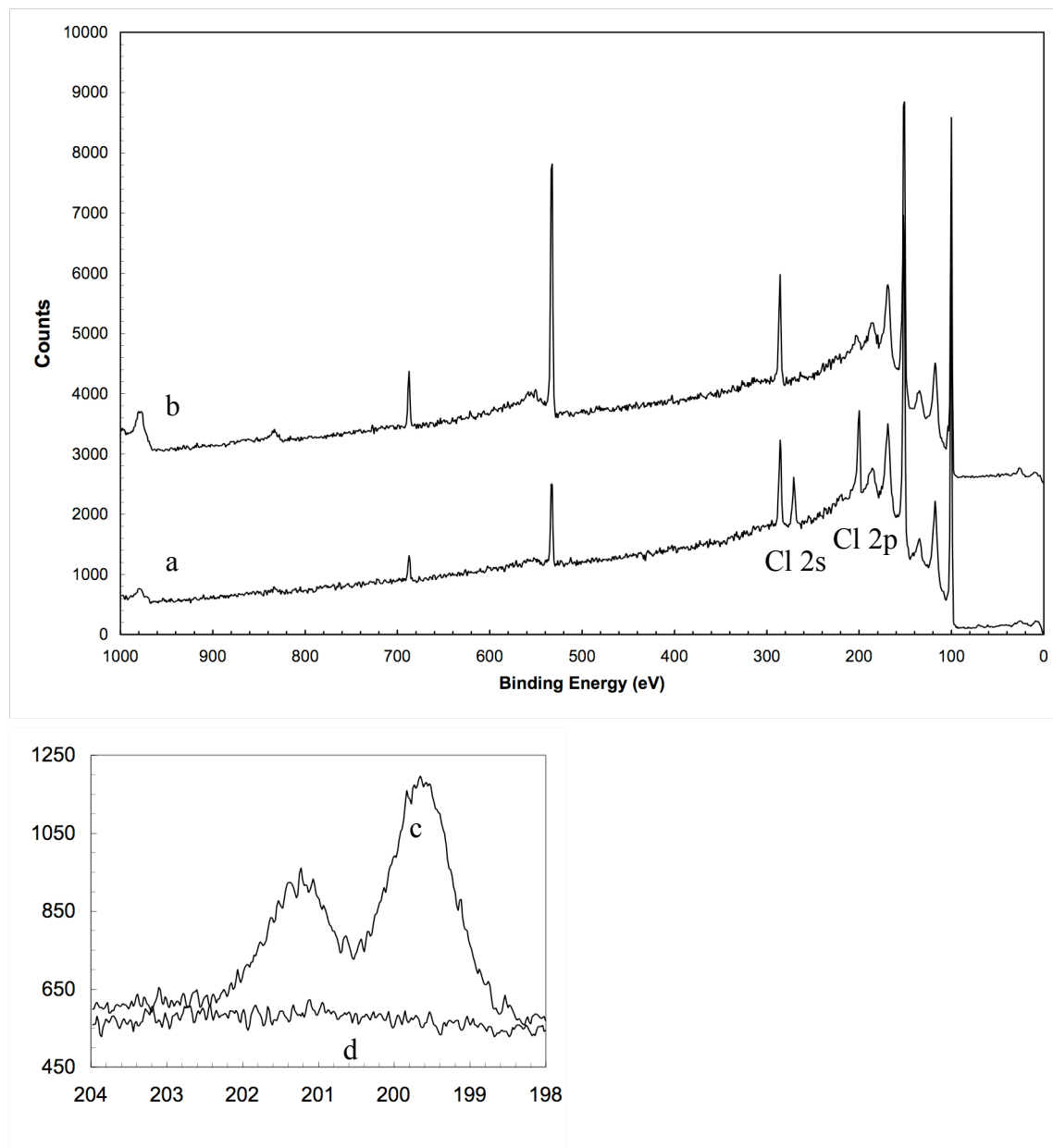


Figure 2.8: XPS spectra of a) a Cl-terminated Si(111) electrode subjected to -1 V vs. Ag^+/Ag for 10 min. in THF with 100 mM TBAPF₆, b) a Cl-terminated Si(111) electrode held at -2.5 V in the same solution, c) the chlorine 2p region for the electrode in a), and d) the Cl 2p region for the electrode in b). These spectra show the total removal of surficial chlorine only after sufficient reducing potential. The small peak visible in b) at ~201 binding eV is due to a phonon absorption band present in bulk silicon.

-1.5 V vs. Ag^+/Ag (Figure 2.9). The overlap of these oxidative waves with the reductive wave observed for the Cl-terminated Si(111) surface indicates that the Grignard reagents have a sufficiently reducing electrochemical potential to reduce the chlorine bonds on the Cl-Si(111) surface.

2.4 Discussion

2.4.1 Coverage of Alkyl Groups on Functionalized Si(111) Surfaces

The C 1s XPS signals on alkylated Si(111) surfaces reflect both alkyl carbons bonded to Si and adventitious C physisorbed on the surface. Resolution of the various carbon signals is possible because the C binding energy shifts with the nature of the atom(s) bound to the carbon center. These shifts result from differences in the effective charge on the C. Because Si-C bonds are appreciably more polar than C-C or C-H bonds (Pauling electronegativities for carbon, hydrogen, and silicon are 2.55, 2.2, and 1.90, respectively³¹) a C bound to Si is relatively more negative than a C bound to C or H. Thus a lowered binding energy is observed for C bound to Si than for to C bound to C or H. The low binding energy peak observed for alkylated Si surfaces in the C 1s region was therefore identified with a C bonded to Si and this signal was used to estimate the packing density of the alkyl groups on the functionalized silicon surface.

As expected, the bulky alkyl groups were present at a lower surface coverage than methyl groups on CH_3 -terminated Si(111) surfaces. Functionalization with C_2H_5 -groups produced a coverage of silicon-bonded carbon which was $90 \pm 20\%$ of that observed for

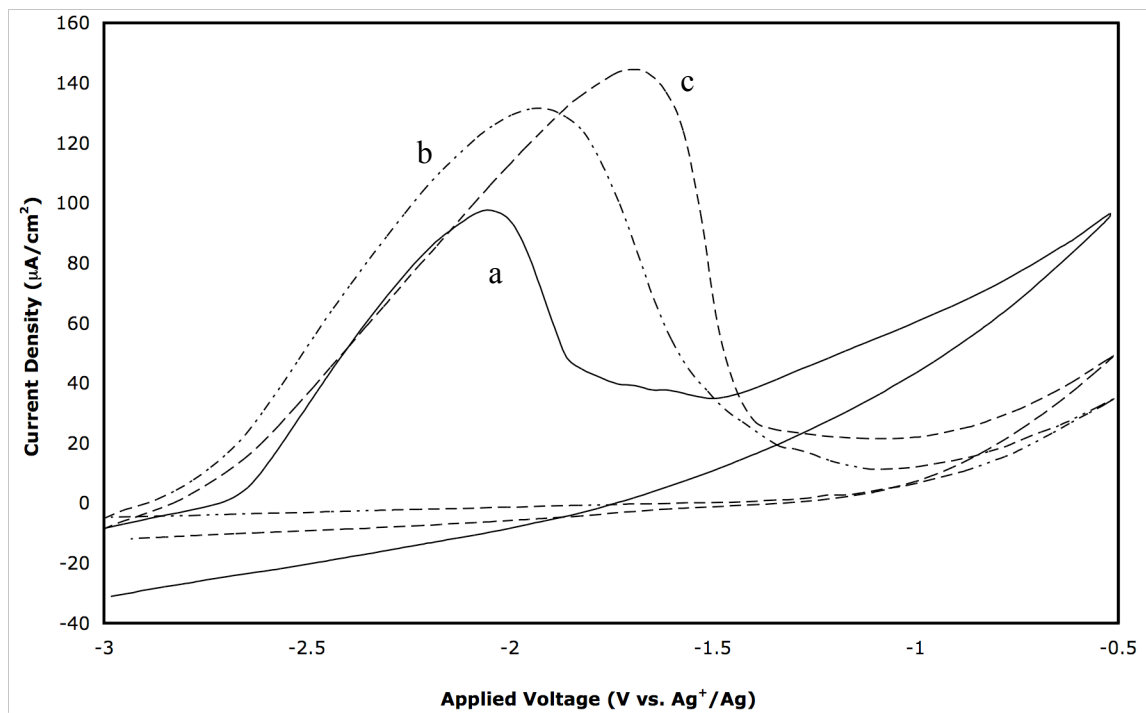


Figure 2.9: The irreversible oxidation at a Pt working electrode of a) 1 M CH_3MgCl , b) 1 M *n*-hexyl MgCl , and c) 1 M phenyl MgCl in THF, with 100 mM LiBr.

CH₃-terminated Si(111) surfaces. These data contrast with simplistic models for functionalized Si(111) surfaces, which suggest that steric restrictions imposed by the bent Si-C-C bonds will limit the surface packing for ethyl to approximately 50% of surface sites.^{1,32} Although octyl and ethyl groups should have similar footprints on the Si surface, as determined by the tetrahedral bonding at the terminal silicon-bound carbon, the surface coverage for octyl was significantly less: $60 \pm 10\%$ of that for CH₃-Si(111). Steric interactions between the long tails of the bound octyl groups will increase with each successive octyl group. Because these steric interactions increase with tail length, fewer octyl groups than ethyl groups are expected to bind to the surface. The *iso*-propyl moiety was observed to bond to even fewer of the surface sites ($40 \pm 20\%$ relative to CH₃-Si(111)) than octyl, even though both ethyl and *iso*-propyl have only a CH₃- tail. The addition of another CH₃- group bound to the silicon-bonded carbon atom, however, forces the *iso*-propyl group to bind to the surface with its two CH₃- groups projecting more laterally over the surface. This larger footprint relative to -C₂H₅ restricts binding to adjacent silicon atoms, resulting in a relatively low coverage of *iso*-propyl groups on Si atop sites. Thus, surface alkylation can be inhibited both by tail-tail interactions as the alkyl groups get longer, and by overlap of neighboring silicon atoms on branched alkyl groups.

2.4.2 Mechanism of Alkylation of Cl-Terminated Si(111) Surfaces by Grignard

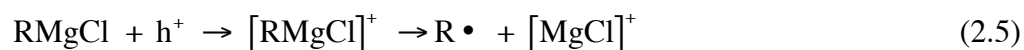
Reagents

For the two-step alkylation reaction, functionalization of the silicon surface with alkyl groups proceeds through the Cl-terminated Si(111) surface. The alkylation of the chlorinated surface results in the complete removal of Cl by XPS regardless of the size of the alkyl group.

Cl-terminated Si(111) surfaces were observed to be robust in sealed reaction vessels towards hot (120 °C) THF, and showed by XPS no significant loss of Cl after 21 hr. The first step of the reaction between the Grignard reagents and the Cl-terminated Si(111) surface therefore can not be abstraction of chlorine by solvent molecules, or a pure S_N1 -type reaction. Nor could abstraction of Cl proceed through the direct attack by the alkyl Grignard reagent on a Cl atom, because a large alkyl group, such as octyl, would be unable to reach every surface chlorine atom after partial surface alkylation had occurred. Hence, steric constraints argue against the reaction of the Cl-Si(111) surface with the Grignard reagent occurring by an S_N2 -type mechanism through a 5-coordinate intermediate on the front side of the Si. Additionally, the Grignard reagent has no access to the back of the Si-Cl bond due to the presence of the bulk crystal.

A mechanism consistent with the data involves electron transfer to the silicon surface followed by chemical reaction of a reduced surficial Si-Cl. As shown in Figure 9, the Grignard alkylating reagents have sufficiently negative reduction potentials to reduce the Cl-terminated Si(111) surface. Electrochemical reduction at these potentials clearly results in removal of all of the surface Cl atoms (Figure 8). Due to the conductive nature of the doped silicon, electron transfer could occur at locations removed from the Si-Cl bond that is ultimately reduced, providing a mechanism to explain the observed reactivity of all of the Cl-terminated sites with the hindered alkyl Grignard reagents.

A mechanism consistent with the observations presented herein is thus:



Steps (2.4) and (2.5) would be (nearly) simultaneous, with reduction of the Si-Cl bond by the Grignard reagent leading to the removal of Cl from the surface, as well as creating alkyl radicals for subsequent reaction. This type of single electron transfer reaction (SET) for Grignard reagents is well known, and produces alkyl radicals.³³⁻³⁶ Step (2.6) yields the expected alkylated surface. For silicon sites that cannot be accessed by the larger alkyl radicals, the silicon radical would abstract a hydrogen from either the solvent or neighboring surface bonded alkyl groups which could eventually abstract hydrogen from the solvent. This mechanism explains why the Cl signal is eliminated even for reagents that can not sterically form Si-C bonds to every surficial site on the Si(111) surface.

This reaction mechanism is similar to one proposed recently by Fella et al. for the reaction of H-Si(111) surfaces with alkyl Grignards.³⁷ In that mechanism, alkyl halide impurities in the Grignard solution were proposed to be reduced to form alkyl radicals, which attacked the H-terminated surface or halogenated the surface as an intermediate step before reaction with the alkyl Grignard. Although the work was performed on a different surface process than the one considered herein, the mechanistic proposal nevertheless lends support to the notion that the electron-transfer processes, followed by single electron transfer reactions, provide a viable mechanism for the reactivity of Cl-terminated Si(111) surfaces under the conditions evaluated herein.

2.4.3 Electrical and Chemical Passivation of the Si(111) Surfaces by Alkylation

The bulky alkyl groups used herein clearly cannot bond to all Si atop sites on an unreconstructed Si(111) surface. The IR studies described above, as well as electrochemical measurements and related IR studies,^{30,38} indicate that a majority of the nonalkylated Si sites form Si-H bonds after the two-step chlorination/alkylation process.

The presence of H-termination of unalkylated Si atop sites offers an explanation for the low initial surface recombination velocities observed for such systems. Unoxidized H-terminated Si(111) surfaces and CH₃-terminated Si(111) surfaces both have low surface recombination velocities. Scanning tunneling spectroscopic studies³⁹ as well as UHV-based photoemission studies²⁷ have shown that CH₃-Si(111) surfaces have essentially no band bending and no detectable electronic states within the band gap. Additionally, the bond strength of Si-H and Si-C bonds is similar in small molecule models,⁴⁰⁻⁴² and valence band photoelectron spectroscopic data indicates that the emission energies of CH₃-terminated Si(111) surfaces are similar to those of H-terminated Si(111) surfaces.²⁷ Thus, even surfaces with mixed Si-C and Si-H functionality would be expected to have relatively few mid-gap states, in accord with the present observations.

The relatively slow oxidation in air of the Si-H sites on Si(111) surfaces alkylated with groups other than CH₃- has been discussed in detail for C₂H₅-terminated surfaces.²⁸ For the bulky alkyl groups investigated herein, at least partial inhibition of the rate of surface oxidation might be expected due to steric crowding of surficial Si-H bonds by

neighboring alkyl groups. This crowding should inhibit the oxidation of the initially unreacted site as well as the oxidation of adjacent surface silicon atoms, because oxygen or water would need to intercalate into the alkyl surface covering, or through previously oxidized sites to attack the surface. A modest degree of oxidative protection has been observed by forming self-assembled monolayers with very long chain alkylthiols on Cu.⁴³ The stark contrast in air oxidation rates of alkylated versus H-terminated Si surfaces indicates that the reaction mechanism involves neighboring Si-H sites or initial oxidation on step edges.²⁸ Thus even modest alkyl coverages on the terraces and step edges of functionalized Si(111) surfaces are sufficient to significantly reduce the observed rate of oxidation.

2.5 Conclusions

Alkylation of Si(111) surfaces through a two-step chlorination/alkylation procedure provides both chemical and electrical passivation of Si surfaces even when bulky alkyl groups are used as alkylating reagents. The intensity of a low binding energy C 1s XPS peak, ascribable to carbon bonded to Si, provided a quantitative estimate of the coverage of alkyls on such surfaces relative to the coverage of methyl groups on CH₃-terminated Si(111) surfaces. Ethyl groups yielded coverages as high as 80% of a monolayer, whereas bulkier groups produced lower coverages, as expected. Even *tert*-butyl groups, which were measured by XPS to bond to only 38% of the surface sites on an unreconstructed Si(111) surface, showed excellent surface passivation, with less than half a monolayer of Si oxide formed on the surface after three weeks exposure to air, and

surface recombination velocities $<100 \text{ cm s}^{-1}$ after that same time period. All of the Cl was removed by reaction even with very bulky alkyl Grignard reagents, and infrared spectroscopy indicated that Si-H bonds were formed on sites that had not been alkylated by the bulky alkyl groups. A viable mechanism for reaction of the Cl-terminated Si(111) surface with alkyl Grignard reagents involves electron transfer between the Grignard reagent and the Cl-terminated Si surface, producing a loss of Cl^- and producing Si radicals that can then react either with alkyls, alkyl Grignards, or abstract H from solvent to form Si-C bonds or Si-H bonds.

2.6 Acknowledgements

We gratefully acknowledge the NSF, grant CHE-021358; the California Institute of Technology; and the Beckman Institute Molecular Materials Research Center for support of this work. IR spectra were collected in collaboration with Dr. Patrick Hurley.

2.7 Bibliography

- (1) Linford, M. R.; Fenter, P.; Eisenberger, P. M.; Chidsey, C. E. D. *J. Am. Chem. Soc.* **1995**, *117*, 3145-3155.
- (2) Sieval, A. B.; Demirel, A. L.; Nissink, J. W. M.; Linford, M. R.; van der Maas, J. H.; de Jeu, W. H.; Zuilhof, H.; Sudholter, E. J. R. *Langmuir* **1998**, *14*, 1759-1768.
- (3) Sieval, A. B.; Linke, R.; Heij, G.; Meijer, G.; Zuilhof, H.; Sudholter, E. J. R. *Langmuir* **2001**, *17*, 7554-7559.
- (4) Boukherroub, R.; Morin, S.; Wayner, D. D. M.; Lockwood, D. J. *Physica Status Solidi A-Applied Research* **2000**, *182*, 117-121.
- (5) Terry, J.; Linford, M. R.; Wigren, C.; Cao, R. Y.; Pianetta, P.; Chidsey, C. E. D. *Appl. Phys. Lett.* **1997**, *71*, 1056-1058.
- (6) Cicero, R. L.; Linford, M. R.; Chidsey, C. E. D. *Langmuir* **2000**, *16*, 5688-5695.
- (7) Effenberger, F.; Gotz, G.; Bidlingmaier, B.; Wezstein, M. *Angew. Chem. Int. Ed.* **1998**, *37*, 2462-2464.
- (8) Boukherroub, R.; Morin, S.; Bensebaa, F.; Wayner, D. D. M. *Langmuir* **1999**, *15*, 3831-3835.
- (9) Buriak, J. M.; Stewart, M. P.; Geders, T. W.; Allen, M. J.; Choi, H. C.; Smith, J.; Raftery, D.; Canham, L. T. *J. Am. Chem. Soc.* **1999**, *121*, 11491-11502.
- (10) Saghatelian, A.; Buriak, J.; Lin, V. S. Y.; Ghadiri, M. R. *Tetrahedron* **2001**, *57*, 5131-5136.

- (11) Cicero, R. L.; Chidsey, C. E. D.; Lopinski, G. P.; Wayner, D. D. M.; Wolkow, R. A. *Langmuir* **2002**, *18*, 305-307.
- (12) Wacaser, B. A.; Maughan, M. J.; Mowat, I. A.; Niederhauser, T. L.; Linford, M. R.; Davis, R. C. *Appl. Phys. Lett.* **2003**, *82*, 808-810.
- (13) Jiang, G. L.; Niederhauser, T. L.; Davis, S. D.; Lua, Y. Y.; Cannon, B. R.; Dorff, M. J.; Howell, L. L.; Magleby, S. P.; Linford, M. R. *Colloid Surface A* **2003**, *226*, 9-16.
- (14) Henry de Villeneuve, C.; Pinson, J.; Ozanam, F.; Chazalviel, J. N.; Allongue, P. In *Mat. Res. Soc. Symp. Proc.* 1997; Vol. 451, p 185-195.
- (15) Allongue, P.; de Villeneuve, C. H.; Pinson, J.; Ozanam, F.; Chazalviel, J. N.; Wallart, X. *Electrochim Acta* **1998**, *43*, 2791-2798.
- (16) Fidelis, A.; Ozanam, F.; Chazalviel, J. N. *Surf. Sci.* **2000**, *444*, L7-L10.
- (17) Webb, L. J.; Lewis, N. S. *J. Phys. Chem. B* **2003**, *107*, 5404-5412.
- (18) Bansal, A.; Li, X. L.; Yi, S. I.; Weinberg, W. H.; Lewis, N. S. *J. Phys. Chem. B* **2001**, *105*, 10266-10277.
- (19) Royea, W. J.; Juang, A.; Lewis, N. S. *Appl. Phys. Lett.* **2000**, *77*, 1988-1990.
- (20) Bansal, A.; Lewis, N. S. *J. Phys. Chem. B* **1998**, *102*, 1067-1070.
- (21) Okubo, T.; Tsuchiya, H.; Sadakata, M.; Yasuda, T.; Tanaka, K. *Appl. Surf. Sci.* **2001**, *171*, 252-256.
- (22) Bansal, A.; Li, X.; Lauermann, I.; Lewis, N. S.; Yi, S. I.; Weinberg, W. H. *J. Am. Chem. Soc.* **1996**, *118*, 7225-7226.

- (23) Dabrowski, J.; Mussig, H. J. *Silicon Surfaces and Formation of Interfaces*; World Scientific Publishing Co. Pte. Ltd.: London, 2000.
- (24) Pauling, L. *The Nature of the Chemical Bond*; Cornell University Press: New York, NY, 1960.
- (25) Yu, H. B.; Webb, L. J.; Ries, R. S.; Solares, S. D.; Goddard, W. A.; Heath, J. R.; Lewis, N. S. *J. Phys. Chem. B* **2005**, *109*, 671-674.
- (26) Seah, M. P. In *Practical Surface Analysis*; 2nd ed.; Briggs, D., Seah, M. P., Eds.; John Wiley & Sons: Chichester, 1990; Vol. 1, p 201-255.
- (27) Hunger, R.; Fritsche, R.; Jaeckel, B.; Jaegermann, W.; Webb, L. J.; Lewis, N. S. *Phys. Rev. B* **2005**, *72*.
- (28) Webb, L. J.; Nemanick, E. J.; Biteen, J. S.; Knapp, D. W.; Michalak, D. J.; Traub, M. C.; Chan, A. S. Y.; Brunschwig, B. S.; Lewis, N. S. *J. Phys. Chem. B* **2005**, *109*, 3930-3937.
- (29) Miyadera, T.; Koma, A.; Shimada, T. *Surf. Sci.* **2003**, *526*, 177-183.
- (30) Webb, L. J.; Rivillon, S.; Michalak, D. J.; Chabal, Y. J.; Lewis, N. S. *to be submitted*.
- (31) Atkins, P. W. *Physical Chemistry, Sixth Edition*; W. H. Freeman and Company: New York, New York, 1998.
- (32) Yuan, S. L.; Cai, Z. T.; Jiang, Y. S. *New J. Chem.* **2003**, *27*, 626-633.
- (33) Ashby, E. C.; Bowers, J. R. *J. Am. Chem. Soc.* **1981**, *103*, 2242-2250.
- (34) Ashby, E. C.; Bowers, J.; Depriest, R. *Tetrahedron Lett.* **1980**, *21*, 3541-3542.

- (35) Blomberg, C.; Salinger, R. M.; Mosher, H. S. *J. Org. Chem.* **1969**, *34*, 2385-&.
- (36) Blomberg, C.; Mosher, H. S. *J. Organomet. Chem.* **1968**, *13*, 519-&.
- (37) Fellah, S.; Boukherroub, R.; Ozanam, F.; Chazalviel, J. N. *Langmuir* **2004**, *20*, 6359-6364.
- (38) Hurley, P. T.; Nemanick, E. J.; Lewis, N. S. *to be submitted*.
- (39) Yu, H. B.; Webb, L. J.; Ries, R. S.; Solares, S. D.; Goddard, W. A.; Heath, J. R.; Lewis, N. S. *to be submitted*.
- (40) Wu, Y. D.; Wong, C. L. *J. Org. Chem.* **1995**, *60*, 821-828.
- (41) Kanabus-Kaminska, J. M.; Hawari, J. A.; Griller, D.; Chatgililoglu, C. *J. Am. Chem. Soc.* **1987**, *109*, 5267-5268.
- (42) Walsh, R. *Acc. Chem. Res.* **1981**, *14*, 246-252.
- (43) Laibinis, P. E.; Whitesides, G. M. *J. Am. Chem. Soc.* **1992**, *114*, 9022-9028.

Chapter 3

Soft X-ray Photoelectron Spectroscopic Measurements of Alkylated Si(111) Surfaces

3.1 Introduction

Surfaces require different spectroscopic techniques to characterize compared to bulk solid state materials, solutions, or gas phase entities. Surfaces, by definition limited to a small depth into a sample, have far fewer species to measure than bulk solids and liquids,¹⁻³ requiring more sensitive techniques for characterization. X-ray photoelectron spectroscopy (XPS) is a surface sensitive technique for the determination of surface species identities.^{4,5} The depth into a sample that XPS probes is dependent on the mean free path of electrons ejected from core levels of probed atoms. These electrons must pass through all overlayers of a sample to be collected by a detector for analysis, with scattering by intervening atoms causing the loss of signal. The inelastic mean free path of photoejected electrons is related to the number of atomic interactions that the electron experiences as well as the kinetic energy of the electron. While the X-rays used to excite samples in XPS penetrate essentially an infinite depth into a sample to be probed, exciting and ejecting photoelectrons the entire way, only those electrons with enough energy and the fewest atomic interactions will survive to exit the sample and be collected at a detector. Figure 1 shows the inelastic mean free path for electrons at varying kinetic

energies.⁶ The short exit depth for photoelectrons allows for only surface atoms to be measured by this technique. A common X-ray source used for XPS is the Al K α source, which relies on the application of an electric field on a block of aluminum. Photons ejected in this fashion have a precise energy of 1486.6 eV. When these electrons strike sample atoms, core level electrons absorb these photons and are ejected to space. The energy absorbed is used to unbind the electron, and all remaining energy is converted to kinetic energy. Because of the higher the kinetic energy, the farther an ejected electron can travel through a solid before being scattered, (Figure 3.1) an electron from the Si 2p orbital, travelling through a Si matrix, with a binding energy of 100 eV, will have 1386.6 eV of kinetic energy. This corresponds to an inelastic mean free path of ~ 20 Å. For the Si(111) surface, the lattice constant is 3.8 Å,⁷ meaning that XPS using the Al K α source on the Si (111) surface measures between 5 and 6 atomic layers of silicon, only one of which is the true surface of the sample. And since for the Si(111) surface, only half of the surface atoms point up and have terminal bonds,⁷ the fraction of the signal that consists of atoms that are bonded to surface species is 1/10 to 1/12 of the total signal. This results in the bulk signal overwhelming the true surface signals, obscuring the species of interest.

Using a lower energy of photons in the far UV or near X-ray can significantly reduce the escape depth of photoelectrons.⁸⁻¹¹ Brookhaven National Laboratories, in Brookhaven New York, has the National Synchrotron Light Source, with an X-ray and UV ring. Synchrotron radiation is caused by the acceleration of charged particles in a vacuum. By moving electrons in a circle, they are constantly being accelerated radially.

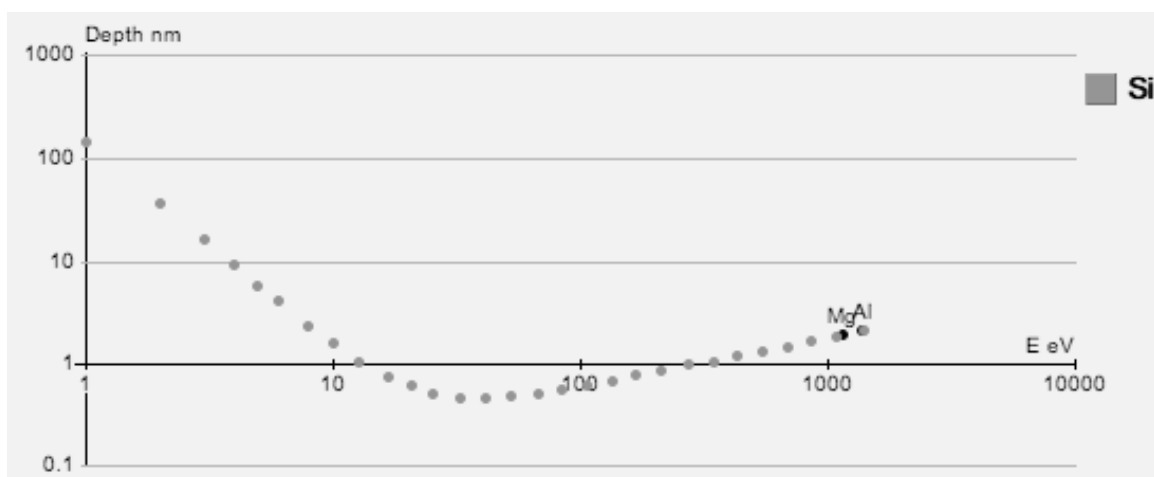


Figure 3.1: The inelastic mean free paths for Si 2p photoelectrons in a Si matrix at varying energies. Generated using La Surface IMFP Grapher, at www.lasurface.com/IMFP/imfp_cal.htm

This constant acceleration causes the release of light energy, which can be harnessed to probe samples. Depending on the speed (and thus the acceleration) of the particles, the light energy can be anywhere from UV to X-ray in energy. Selection of photons of an energy just sufficient to eject core electrons of interest, but without sufficient kinetic energy to allow for ejected electrons from deeply buried atoms to be detected probes fewer subsurface atoms.

The silicon 2p peak, studied extensively,¹²⁻¹⁴ serves as a useful tool for the determination of the nature of surface bound species on silicon surfaces. This peak is split into two segments, the Si 2p_{1/2} and Si 2p_{3/2} peak by the spin-orbit splitting of silicon. The Si 2p_{3/2} is located at 99.4 eV, while the Si 2p_{1/2} peak comes 0.6 eV higher, at 100.0 eV.¹⁵ A well studied surface is the oxidized Si surface, and the interface between bulk Si and SiO_x overlayers. In participation in a polarized bond, the electropositive silicon atoms bonded to the very electronegative oxygen atoms suffer a loss of electron density.¹⁶ By acquiring a partial positive charge in this manner, ionization of the atoms becomes more difficult, depending on the size of the positive charge. Partially oxidized silicon surfaces are a combination of silicon oxides that have between one and four bonds to oxygen. Pure SiO₂ has a Si 2p peak centered at 103.5 eV. Suboxides formed by the partial oxidation of silicon atoms have peaks that range from 103.5 to 100 eV, depending on the degree of bonding.^{17,18} This shift in the binding energy of the Si 2p peak can be measured for silicon atoms bound to any atom of sufficiently different electronegativity. Electronegative elements of Cl, C, and H all cause large to small shifts in the binding energy of the Si 2p peak.¹⁹⁻²² High resolution measurement of these peak shifts, in

addition to the relative intensities of the peaks, can allow for the determination of the relative populations of surface bonded species.

The formation of alkyl monolayers on the Si (111) surface have already been covered, as well as the passivation of these surfaces by said monolayers.²³⁻²⁵ By selection of soft X-ray photons at the National Synchrotron Light Source with an energy just above the binding energy of the Si 2p peak, in addition to a more sensitive detection scheme and a more narrow excitation beam energy, the populations and energy shifts of bond-shifted surface species can be determined, allowing for the high resolution characterization of the surface. By using photons of 140 eV, only the first 2.2 atomic layers of the silicon surface can be probed. Measurements of the H-terminated, Cl-terminated, and CH₃, C₂H₅, and C₆H₅CH₂ functionalized surfaces are reported herein.

3.2 Experimental

3.2.1 Alkylation of Silicon

The silicon samples used for SXPS measurements were float-zone grown, (111)-oriented wafers that were polished on both sides (Virginia Semiconductor, Fredericksburg, VA), and were 250 μm thick, high resistivity ($> 4000 \Omega \text{ cm}$), n-type, phosphorus doped. Prior to alkylation, samples were cut into sections $\sim 1 \text{ cm}^2$ in area. The pieces were cleaned by sonication for 5 s each in a series of organic solvents (VWR Scientific Products, West Chester, PA): methanol, acetone, dichloromethane, 1,1,1-trichloroethane, dichloromethane, acetone, methanol, and then $18 \text{ M}\Omega \text{ cm}$ resistivity

H₂O. To remove the native oxide, the samples were etched for 30 s in buffered HF(aq). Samples were then etched, with occasional agitation to remove bubbles forming on the edges, for 10 min in 40% NH₄F(aq) (Transene, Danvers, MA). After etching, the samples were dried under a stream of N₂(g) and passed into a glove box for functionalization.

To chlorinate the surfaces, samples were immersed in 2 mL of anhydrous chlorobenzene (99.8% under argon, Aldrich) saturated with PCl₅ (99.995%, Strem, Newburyport, MA) for 1 hr at 95-100 °C. Benzoyl peroxide (97%, Aldrich) was added (<1mg) to initiate the chlorination of the surface. Care was taken to insure that the polished surfaces of the silicon samples were not touched, to prevent scratching that might influence the surface reactivity.

After chlorination, the samples were washed in anhydrous tetrahydrofuran (THF) (99.8%, inhibitor free, Aldrich) and were placed in Teflon screw-cap sealed glass reaction flasks that contained 10 mL of anhydrous THF and 10 mL of a 1 M Grignard reagent in THF. The Grignard reagents were either CH₃MgCl, CH₃CH₂MgCl, or C₆H₅CH₂MgCl. The reaction solution was heated to 110-120 °C for 21 hr in a sealed reaction vessel. After reaction, samples were rinsed in THF followed by anhydrous methanol (99.8% Aldrich), removed from the glove box, and sonicated in a 5 mL solution of methanol and glacial acetic acid (10:1) (Aldrich) for 5 min to remove any adsorbed magnesium salts. Samples were then rinsed with 18 MΩ cm resistivity H₂O and attached to a sample holder for measurement. Samples were transferred to SXPS in sealed tubes, and were unsealed before insertion into a UHV load lock.

3.2.2 Soft X-ray Photoelectron Spectroscopy

High-resolution soft X-ray photoelectron spectroscopy was performed at Brookhaven National Laboratories (Brookhaven, NY) at the National Synchrotron Light Source. The sample was attached to a ring shaped sample holder, with a stainless steel retaining collar, leaving the center of the sample exposed for measurement. Only the outer edges were in contact with the holder, and for samples repeatedly mounted in the sample holder, care was taken to only measure parts of the sample that were untouched. The sample was then passed into a load lock for insertion into the SXPS. The UHV system was kept at $< 1 \times 10^{-9}$ torr when not in use. After insertion of the sample, the pressure rose to the mid 10^{-9} torr range. The beamline had a spherical grating monochromator with a resolution of 0.1 eV. Samples were exposed to 140 eV soft X-ray, hard UV photons for photoexcitation. Ejected core level photoelectrons were collected at 0° , 35° , or 70° off the sample normal by a hemispherical analyzer fixed at 45° to the incident photon beam. Beam intensity was measured and the collected spectra were normalized for photon flux.

The escape depth, d , for ejected photoelectrons can be calculated for this system by:²⁶

$$d = \sqrt{C a_{Si}^3 E_{Si}} \quad (3.1)$$

where a_{Si} is the diameter of a silicon atom, determined to be 0.272 nm;²⁷ C is 0.168 nm eV; and E_{Si} is the kinetic energy of the ejected photoelectron (40 eV). This gives an escape depth of 0.37 nm for Si 2p electrons ejected by 140 eV photons.

For data analysis, spectra were first fit to a Shirley background, which was then subtracted to allow for peak fitting. After subtracting the Shirley background, the Si 2p_{1/2} component peaks were stripped from the spectra for each surface species present to facilitate peak fitting. The Si 2p_{1/2} was removed by fixing the peak-peak energy shift at 0.6 eV, and the 2p_{3/2}/2p_{1/2} peak area at 0.51. For each Si2p_{3/2} peak, a peak 0.6 eV higher in energy and 0.51 the size was subtracted from the spectra. Residual spectra were fit to modified Voigt peaks with peak shapes that were 95% Gaussian and 5% Lorentzian. Using a substrate-overlayer model, the sum of all surface species present was assigned to one monolayer as a tool for distinguishing between equivalent local minima on the peak fitting surface. This model gives the surface monolayer coverage of a species derived from the ratio of the surface to bulk Si 2p signal. The peak area ratio for the surface and bulk species (A_s/A_b) is equal to:

$$\frac{A_s}{A_b} = \frac{MD_s}{D_b d - D_s} \quad (3.2)$$

where M is the monolayers of surface atoms; D_s is the surface density of atoms for Si(100), 6.9×10^{14} atoms cm⁻²; D_b is the bulk density for silicon, 5.0×10^{22} atoms cm⁻³; and d is the escaped depth for the photoelectrons (3.7Å).

3.3 Results

3.3.1 Hydrogen-terminated Si (111) Surfaces

Figure 3.2 shows the SXPS spectra of the Si 2p region for a H-terminated Si(111) surface. The Si 2p_{1/2} peaks have been stripped from the data after fitting a Shirley

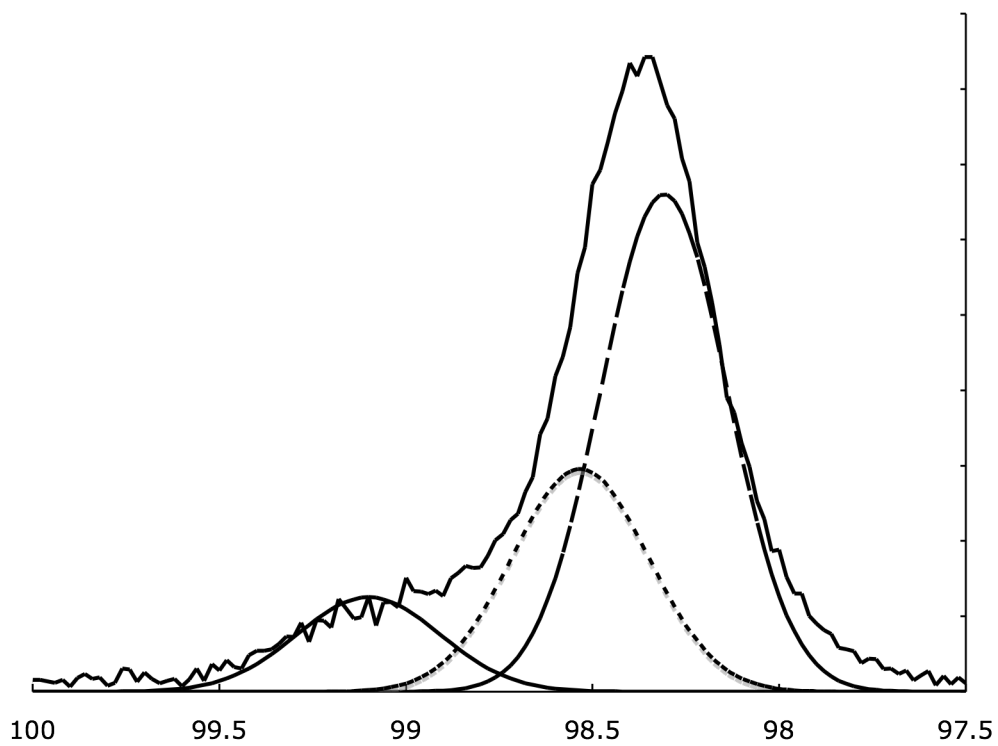


Figure 3.2: The SXPS spectrum of H-terminated Si (111) surface. Dashed line: bulk silicon. Dotted line: H-shifted silicon. Dashed/dotted line: $\text{SiH}_2/\text{SiH}_3$ silicon.

background for Figure 2. The entire Si 2p region showed no trace of oxidized silicon signal in the region from 101-104 eV, indicating the samples were prepared extremely cleanly. Figure 3.2 shows three peaks fit to the signal: a bulk Si 2p peak, a peak shifted higher in energy by 0.20 eV, and a smaller peak at 0.55 eV higher in energy than the bulk peak. The peak shifted 0.20 eV higher in energy was ascribed to silicon bonded to a H atom, with the more electronegative H atoms drawing electron density from the silicon atoms they were bonded to, thereby increasing the binding energy of core level Si 2p electrons. The small electronegativity difference between Si (1.90) and H (2.20)²⁸ is seen in this spectrum by the relatively small binding energy shift of 0.20 eV. The smaller peak shifted to 0.55 eV higher in energy can be the result of many different causes; a small amount of suboxide such as from -OH groups, the residual of SiH₂ and SiH₃ groups at step edges and defects, or coupled with the small residual signal from the low binding energy side of the bulk peak, an indication that the peak fit does not have sufficient Lorentzian character. The total amount of the surface that is contained in this peak represents a significant fraction, about 30%, and no techniques are available to separate out the nature of this peak adequately. Table 3.1 gives the integrated peak area totals for all functionalized surfaces reported for the SXPS data. The amount of the surface ascribed to SiH bonding was 0.64 monolayers, while the second peak contained 0.20 monolayers of silicon. The roughness of this surface may be due to dioxygen in the etching medium, as other high resolution measurements of the SiH surface etched in deoxygenated NH₄F showed only SiH.²⁹

3.3.2 Cl-terminated Si (111) Surfaces

Surface	% bulk	% Surface	Surface % SiX	Surface % SiX ₂	Peak Shift 1	Peak Shift 2	ML Peak 1	ML Peak 2
SiH	0.59	0.41	0.69	0.31	0.20	0.77	0.64	0.20
SiCl	0.55	0.45	0.90	0.10	0.83	1.37	0.92	0.09
SiCH ₃	0.61	0.39	1.00		0.33		0.89	
SiC ₂ H ₅	0.54	0.46	0.92	0.08	0.23	0.67	0.95	0.07
SiC ₆ H ₅ CH ₂	0.60	0.40	0.90	0.10	0.22	0.62	0.81	0.08

Table 3.1: SXPS data for functionalized Si (111) surfaces. The first two columns breakdown the relative percent of the spectra which are attributed to bulk and surface species. The next two columns show percent of the surface that each peak contributes. For SiH, the SiX₂ number refers to the population of SiH₂ and SiH₃. Peak shifts are in eV for each surface peaks.

Figure 3.3 shows the SXPS spectrum for the Cl-terminated Si (111) surface. After chlorination by a radical Cl source in an inert atmosphere, the samples were transferred in a sealed container to the SXPS to prevent oxidation. There was no trace of the higher order oxides, indicating the surface is wholly unoxidized. Figure 3.3 shows the Shirley background subtracted and stripped version of the spectrum, with three peaks fit to the data. The first and largest peak was ascribed to bulk silicon, and constituted the majority of the signal. A peak shifted to 0.83 eV higher in energy is ascribed to Cl shifted silicon, from the Si-Cl species on the surface. This peak shift was consistent with the electronegativity difference between Si (1.90) and Cl (3.16).²⁸ This peak shift is consistent with other Cl induced Si 2p peak shifts measured on similar surfaces.¹⁹⁻²¹ A peak shifted to 1.37 eV above the bulk peak was ascribed to SiCl₂ species on the surface, at twice the single Cl atom peak shift. The SiCl peak was integrated to 0.92 monolayers of surface coverage, while the SiCl₂ peak was integrated to 0.09 monolayers of surface coverage. The presence of the SiCl₂ species as 9% of the surface indicates that only some of the SiH₂ species present on the surface were converted to SiCl₂, with the bulky nature of a Cl atom hindering doubly or triply chlorination of the surface due to steric effects.

3.3.3 Methyl-terminated Si (111) Surfaces

Figure 3.4 shows the SXPS spectrum for a sample reacted with CH₃MgCl after radical chlorination. The data shows no oxidation of the surface at 101-104 eV,

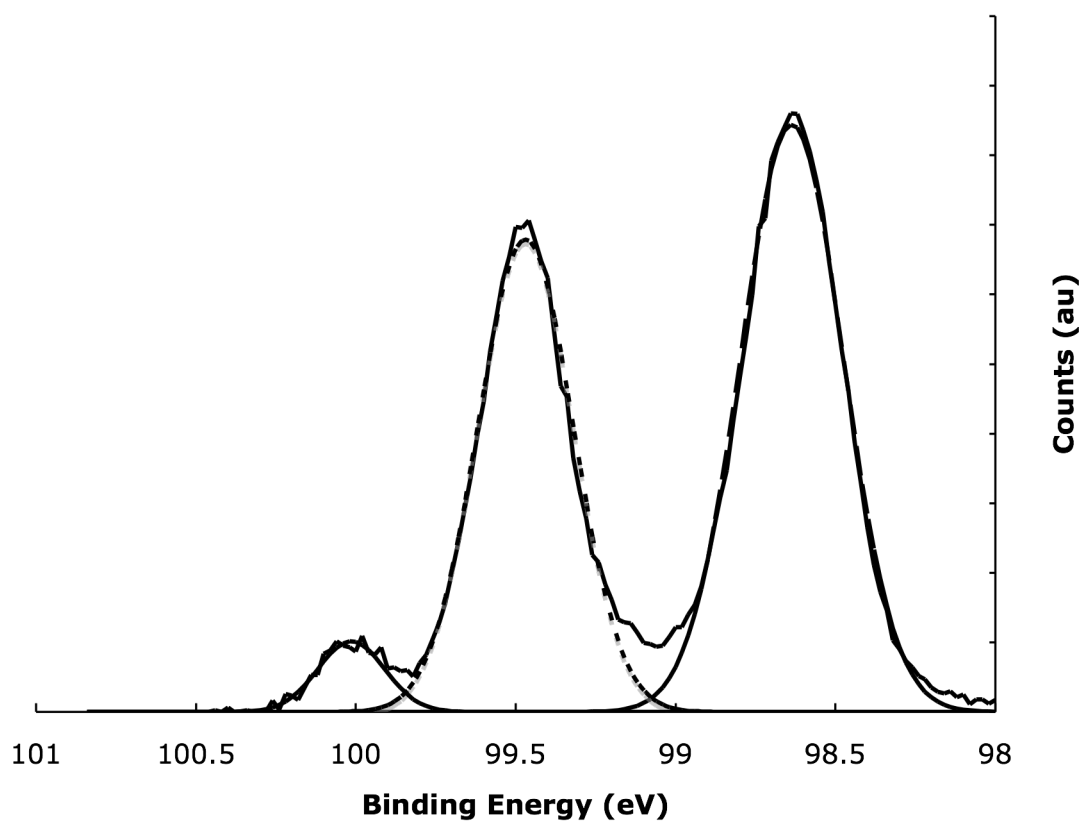


Figure 3.3: The SXPS spectrum of the Cl-terminated Si (111) surface. Dashed line: bulk silicon. Dotted line: singly chlorinated silicon. Dashed/dotted line: doubly chlorinated silicon.

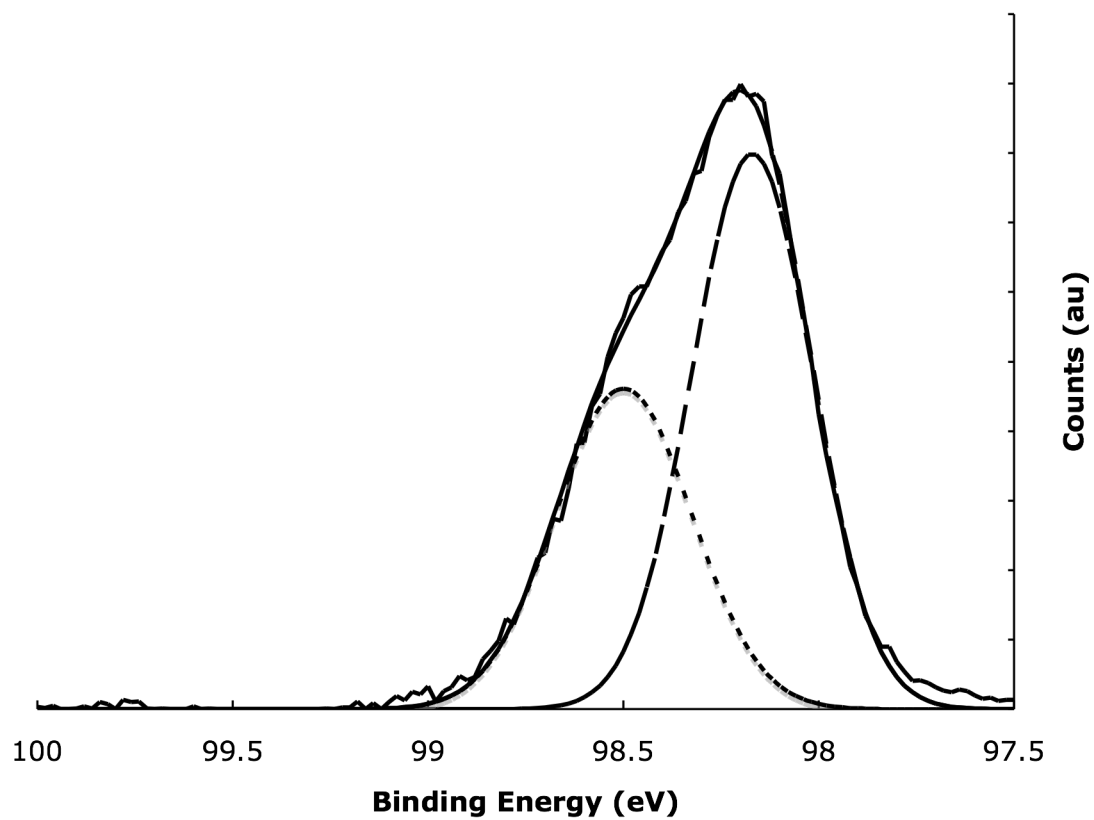


Figure 3.4: The SXPS spectrum of the CH₃-terminated Si (111) surface. Dashed line: bulk silicon. Dotted line: CH₃-shifted silicon.

indicating that the reaction was clean and the inert atmosphere was intact. After stripping of the Si 2p doublet, two peaks were fit to the spectrum, the lower of which represents the bulk Si 2p signal. At 0.33 eV higher in energy was a second peak, ascribed to Si bonded to a CH₃ group. This peak shift was consistent with the electronegativity difference between Si (1.90) and C (2.55)²⁸ on the Pauling electronegativity scale. This shift was smaller than the Cl-induced peak shift of 0.83 eV and larger than the H induced peak shift of 0.20 eV, in accordance with the relative electronegativities. The carbon-shifted peak of the methylated Si atoms was integrated to 0.89 monolayers of coverage, showing excellent coverage of the surface. The complete absence of any peaks shifted higher in energy than this peak indicate both that oxidation did not occur during alkylation, but also that there was no residual amounts of chlorine on the surface, down the detection level of this instrument. This was consistent with measurement of the surface made by XPS (*vide supra*). While no other peak was fit, it was not possible to conclusively eliminate the possibility of other peaks between the bulk Si peak and the methyl-shifted Si peak. The presence of small to moderate amounts of SiH on the surface for unfunctionalized surface sites cannot be eliminated by this technique.

3.3.4 Ethyl-terminated Si (111) Surfaces

Figure 3.5 shows the SXPS spectrum for a sample reacted with CH₃CH₂MgCl after radical chlorination. The data shows no oxidation of the surface at 101-104 eV, indicating that the reaction was clean and the inert atmosphere was intact. After stripping of the Si 2p doublet, three peaks were fit to the spectrum, the lower of which represents

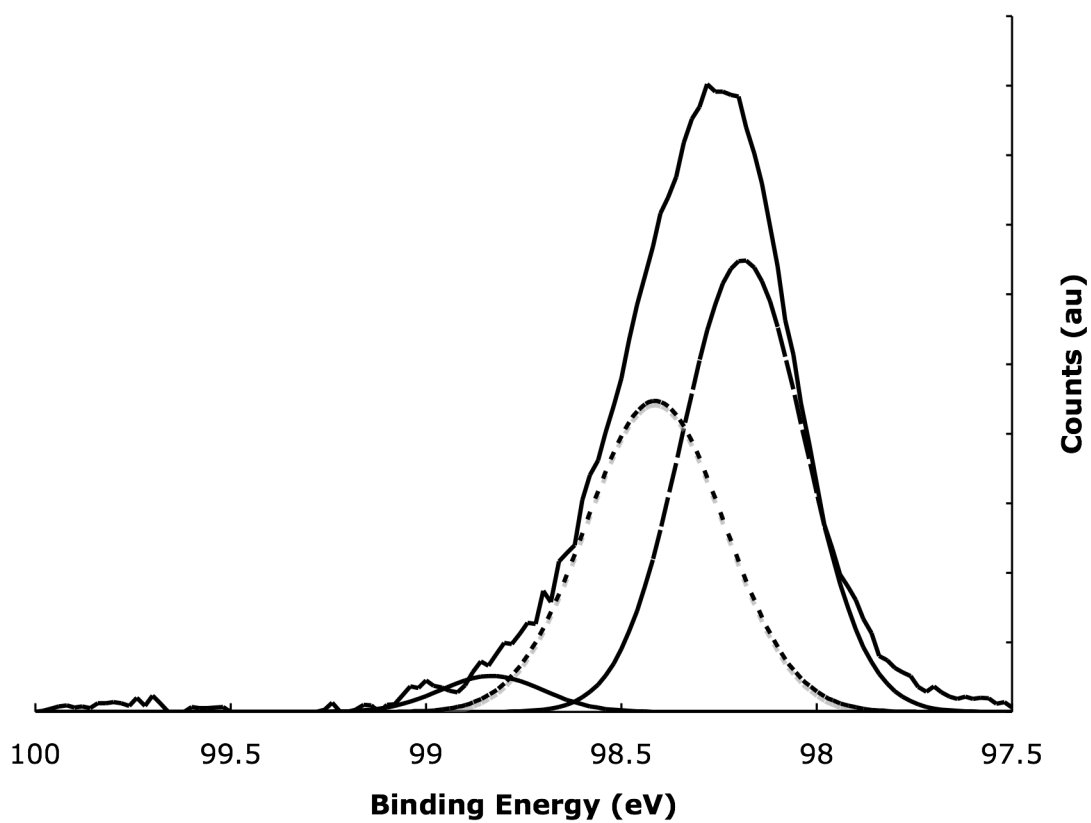


Figure 3.5: The SXPS spectrum of CH₂CH₃-terminated Si (111) surface. Dashed line: bulk silicon. Dotted line: singly ethylated silicon and SiH silicon. Dashed/dotted line: doubly ethylated silicon.

the bulk Si 2p signal. At 0.23 eV higher in energy was a second peak, ascribed to Si bonded to an ethyl group as well as silicons bound to H. This shift is a hybrid of the carbon shift and the hydrogen shift, relatively inseparable in this data by any reasonable means. This hybrid peak integrated to 0.95 monolayers. A second peak was shifted 0.67 eV higher in energy, and was attributed to double ethylated silicon atoms. This shift was to be expected for doubly bonded Si atoms, being roughly twice the 0.33 eV shift of the singly methylated silicon. This peak integrated to 0.07 monolayers on the surface. It is important to note that small amounts of singly oxidized silicon could also be in this region and contribute to the integrated area of this peak.

3.3.5 Benzyl-terminated Si (111) Surfaces

Figure 3.6 shows the SXPS spectrum for a sample reacted with $C_6H_5CH_2MgCl$ after radical chlorination. The data shows no oxidation of the surface at 101-104 eV, indicating that the reaction was clean and the inert atmosphere was intact. After stripping of the Si 2p doublet, three peaks were fit to the spectrum, the lower of which represents the bulk Si 2p signal. At 0.22 eV higher in energy was a second peak, ascribed to Si bonded to an benzyl group as well as silicons bound to H. Similar to the ethylated surface, this shift is a hybrid of the carbon shift and the hydrogen shift, relatively inseparable in this data by any reasonable means. This hybrid peak integrated to 0.81 monolayers. A second peak was shifted 0.62 eV higher in energy, and was attributed to doubly benzylated silicon atoms. This shift was similar to the 0.67 eV shift for the doubly ethylated silicon atoms, and roughly twice the 0.33 eV shift of the singly

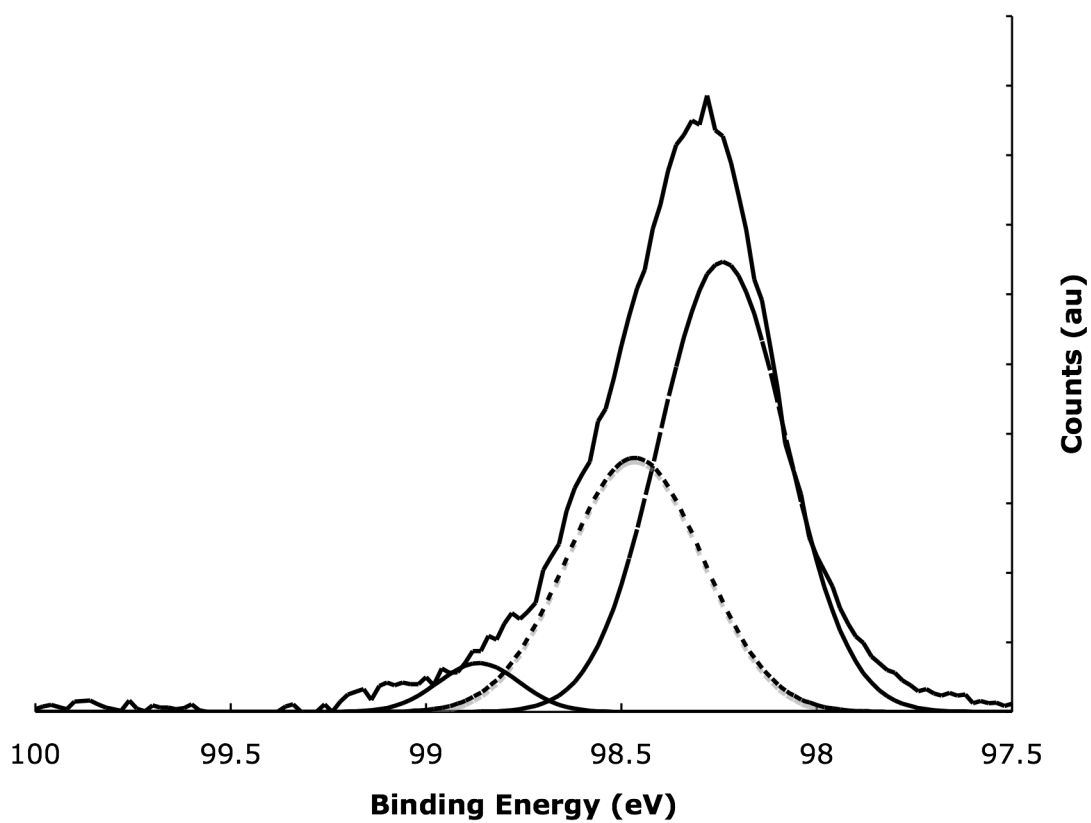


Figure 3.6: The SXPS spectrum of $C_6H_5CH_2$ -terminated Si (111) surface. Dashed line: bulk silicon. Dotted line: singly benzylated silicon and SiH silicon. Dashed/dotted line: doubly phenylated silicon.

methylated silicon. This peak integrated to 0.08 monolayers on the surface. The steric hindrance of doubly bonding a benzyl group to a single silicon atom would greatly limit the number of such groups formed, with the exception of step edges or pits.

3.4 Discussion

3.4.1 Hydrogen and Chlorine-terminated Si(111) Surfaces

The presence of both SiH and SiH₂, and perhaps traces of SiH₃ on the H-terminated Si(111) surface after basic fluoride etch indicates that the surface was not sufficiently etched during preparation. While the samples were etched in 40% NH₄F for 20 minutes, these surfaces do not show the single SiH species seen by IR in other studies.³⁰⁻³² Further measurements using this SXPS instrument indicate that sparging the etching solution with nitrogen to remove dioxygen results in SPXS spectra with only SiH species present.²⁹ However, the functionalized spectra presented herein derived from these flawed surfaces show a resulting increase in the plural species as expected. It must be acknowledged that the surfaces did not start perfectly SiH terminated, and to analyze the functionalized surfaces without this information would cause neglect of small population species on the surface such as SiR₂, HSiR, and SiCl₂ in subsequent spectra, which would be otherwise unexplained. Furthermore, the peak shift of the second shifted peak, of 0.77, indicates that this peak may contain not only SiH₃ species, but singly oxidized species as well.

For the SiCl surfaces, this was dramatically apparent, as the presence of SiCl₂ indicates that the original SiH sample was not perfectly hydrogenated, and subsequently some population of SiCl₂ was formed by this. While it is possible that the chloride functionalization was sufficiently harsh to pit the surface, it is far more likely that the surface was not originally perfectly covered by SiH, but rather with some significant population of SiH₂/SiH₃. Furthermore, the large residual between the bulk Si peak and the SiCl peak is about 0.4 eV shifted from the bulk silicon peak, and may benefit from fitting an additional small peak that could be assigned to SiH₂ species, which was observed to have a similar binding energy shift on the SiH surface.

3.4.2 Alkyl-terminated Si(111) Surfaces

It was not possible to deconvolute the first peak shifted from bulk silicon for the alkyl groups into components representing SiH groups and SiR groups (or SiH₂). Thus quantitative determination of the relative coverage of these individual species by this method remains elusive. However, qualitatively, it was clear that the CH₃-terminated surface contained a far smaller proportion of the surface as SiH, as the aggregate peak shift was 0.33, compared to ~0.23 for the other alkyl groups studied, indicating that this peak may be shifted to lower binding energy by a higher proportion of SiH species within it. However, this apparent peak shift may be due to the fact that no second shifted peak was fitted to the CH₃-terminated spectra, shifting the apparent peak center to a higher binding energy. There does not seem to be a need for this second peak in the Si-methyl spectra, as the residual in the +0.6 region was very small, compared to the residual in the

other alkylated surfaces. From this it can be seen that the methyl surface has fewer SiH groups on the surface than do the larger alkyl groups, as expected from the larger size of both the ethyl group as well as the benzyl group.

3.5 Conclusions

The spectra presented herein demonstrate the direct bonding of alkyl groups to the Si(111) surface through a covalent bond. The differing electronegativities between C and Si cause a binding energy shift of the core level electrons, which was observable through SXPS measurements. The H-terminated surfaces prepared for functionalization were not perfectly monohydrogen-terminated, due to dioxygen in the etching solution. The surfaces functionalized from these defective precursors then must have some significant populations of SiX_2 as well as HSiX . Not considering this would lead to defective fitting of the peaks, as well as unexplained peaks within the fit.

The alkylated surfaces were shown to have at least one hybrid peak with a binding energy shift corresponding to the bonding of both SiC and SiH species. The 0.33 eV shift for the methyl-terminated surface over the 0.23 and 0.22 eV shifts for the ethyl- and benzyl-terminated surfaces indicate that far more of the surface was alkylated than for either of the larger alkyl groups, as has been seen using conventional XPS (*vide supra*).

3.6 Acknowledgements

This work was performed in collaboration with Dr. Lauren Webb, and the spectra presented have been published elsewhere.^{27,29} Spectra were collected in collaboration with Dr. Webb, David Michalak, David Knapp, and Julie Bitteen. This work was carried out in part at the National Synchrotron Light Source, Brookhaven National Laboratory, which is supported by the U.S. Department of Energy, Division of Materials Sciences and Division of Chemical Sciences, under contract DE-AC02-98CH 10866.

3.7 Bibliogrphahy

- (1) Altarelli, M.; Bachelet, G.; Del Sole, R. *J. Vac. Sci. Tech.* **1979**, *16*, 1370.
- (2) Margaritondo, G.; Rowe, J. E.; Christman, S. B. *Phys. Rev. B: Condens. Matter* **1976**, *14*, 5396.
- (3) Pipino, A. C. R. *Phys. Rev. Lett.* **1999**, *83*, 3093.
- (4) McIntyre, N. S.; Sunder, S.; Shoesmith, D. W.; Stanchell, F. W. *J. Vac. Sci. Tech.* **1981**, *18*, 714.
- (5) Hoffman, S. *Surf. Interface Anal.* **1986**, *9*, 3-20.
- (6) Somerjai, G. *Chemistry in Two Dimensions: Surfaces*; Cornell University Press: Ithaca, NY, 1981.
- (7) Dabrowski, J.; Mussig, H. J. *Silicon Surfaces and Formation of Interfaces*; World Scientific Publishing Co. Pte. Ltd.: London, 2000.
- (8) Matsubayashi, N.; Shimada, H.; Tanaka, K.; Sato, T.; Yoshimura, Y.; Nishijima, A. *Rev Sci Instrum* **1992**, *63*, 1363.
- (9) Hague, C. F. *J. Phys. F* **1976**, *6*, 899.
- (10) Wassdahl, N.; Nilsson, A.; Weill, T.; Tillborg, H.; Duda, L.-C.; Gue, J. H.; Martensson, N.; Nordgren, J.; Anderson, J. N.; Nyholm, R. *Phys. Rev. Lett.* **1992**, *69*, 812.
- (11) Nordgren, J.; Cramm, S.; Nyholm, R.; Rubensson, J.-E.; Wassdahl, N. *Rev Sci Instrum* **1989**, *60*, 1690.
- (12) Lehner, A.; Steinhoff, G.; Brandt, M. S.; Eickhoff, M.; Stutzmann, M. *Journal Of Applied Physics* **2003**, *94*, 2289-2294.

- (13) Haber, J. A.; Lauermann, I.; Michalak, D.; Vaid, T. P.; Lewis, N. S. *J. Phys. Chem. B* **2000**, *104*, 9947-9950.
- (14) Barrelet, C. J.; Robinson, D. B.; Cheng, J.; Hunt, T. P.; Quate, C. F.; Chidsey, C. E. D. *Langmuir* **2001**, *17*, 3460-3465.
- (15) Himpsel, F. J.; McFeely, F. R.; Taleb-Ibrahimi, A.; Yarmoff, J. A.; Hollinger, G. *Phys. Rev. B* **1988**, *38*, 6084-6096.
- (16) Pauling, L. *The Nature of the Chemical Bond*; Cornell University Press: New York, NY, 1960.
- (17) Grunthaner, P. J.; Hecht, M. H.; Grunthaner, F. J.; Johnson, N. M. *J. Appl. Phys.* **1987**, *61*, 629-638.
- (18) Keister, J. W.; Rowe, J. E.; Kolodziej, J. J.; Niimi, H.; Tas, H. S.; Madey, T. E.; Lucovsky, G. *J. Vac. Sci. Technol. A* **1999**, *17*, 1250.
- (19) Durbin, T. D.; Simpson, W. C.; Chakarian, V.; Shuh, D. K.; Varekamp, P. R.; Lo, C. W.; Yarmoff, J. A. *Surf. Sci.* **1994**, *316*, 257-266.
- (20) Yarmoff, J. A.; Shuh, D. K.; Durbin, T. D.; Lo, C. W.; Lapianosmith, D. A.; Mcfeely, F. R.; Himpsel, F. J. *J Vac Sci Technol A* **1992**, *10*, 2303-2307.
- (21) Schnell, R. D.; Rieger, D.; Bogen, A.; Himpsel, F. J.; Wandelt, K.; Steinmann, W. *Phys. Rev. B* **1985**, *32*, 8057-8065.
- (22) Terry, J.; Linford, M. R.; Wigren, C.; Cao, R. Y.; Pianetta, P.; Chidsey, C. E. D. *Journal of Applied Physics* **1999**, *85*, 213-221.
- (23) Buriak, J. M. *Chemical Communications* **1999**, 1051-1060.
- (24) Royea, W. J.; Juang, A.; Lewis, N. S. *Appl. Phys. Lett.* **2000**, *77*, 1988-1990.

- (25) Bansal, A.; Li, X. L.; Yi, S. I.; Weinberg, W. H.; Lewis, N. S. *J. Phys. Chem. B* **2001**, *105*, 10266-10277.
- (26) Seah, M. P. In *Practical Surface Analysis*; 2nd ed.; Briggs, D., Seah, M. P., Eds.; John Wiley & Sons: Chichester, 1990; Vol. 1, p 201-255.
- (27) Webb, L. J., California Institute of Technology, 2005.
- (28) Allen, L. C. *J. Am. Chem. Soc.* **1989**, *111*, 9003.
- (29) Webb, L. J.; Nemanick, E. J.; Biteen, J. S.; Knapp, D. W.; Michalak, D. J.; Traub, M. C.; Chan, A. S. Y.; Brunschwig, B. S.; Lewis, N. S. *J. Phys. Chem. B* **2005**, *109*, 3930-3937.
- (30) Niwano, M.; Takeda, Y.; Ishibashi, K.; Kurita, K.; Miyamoto, N. *J. Appl. Phys.* **1992**, *71*, 5646.
- (31) Thanh, V. L.; Bouchier, D.; Hincelin, G. *J. Appl. Phys.* **2000**, *87*, 3700.
- (32) Chabal, Y. J.; Higashi, G. S.; Ragahavchari, K.; Burrows, V. A. *J. Vac. Sci. Technol. A* **1989**, *A7*, 2104.

Chapter 4

Molecular Dynamics Calculations of Alkyl Monolayer Formation on Si (111) Surfaces Under Thermodynamic Control

4.1 Introduction

Interest in the formation of alkyl monolayers on single crystal and porous silicon surfaces has surged due to the utility of these modification techniques for possible applications for semiconductor devices. It has been shown that alkyl surface functionalization can stabilize porous silicon towards oxidation, prepare stable silicon electrodes in oxidizing media, and passivate surface electronic trap states (*vide supra*). These techniques employ the conversion of surficial Si-H bonds formed by wet fluoride etch techniques to covalent Si-C bonds. The first functionalization technique for the formation of Si-C bonds used the H-terminated Si(111) surface to react with unsaturated alkenes through a radical process catalyzed by a diacyl peroxide initiator.^{1,2} The reaction was further refined by use of UV³⁻⁵ or white⁶ light, thermal energy,^{7,8} transition metal complexes,⁹ and Lewis acids¹⁰⁻¹² to catalyze the reaction, and expanded to encompass the Si(100)^{7,8} surface as well as porous silicon.⁶ Functionalization of silicon surfaces has expanded to encompass the electrochemical functionalization,^{13,14} radical halogenation,¹⁵ and transmetalation with alkyl Grignard and lithium reactions.¹⁵⁻¹⁷ These surfaces have

been characterized to be well ordered, to show excellent chemical stability under a variety of conditions, and to inhibit the oxidation of the silicon surface.

Along with the varying techniques for the formation of different alkyl monolayers on silicon surfaces, there have been a number of attempts to quantify the actual as well as theoretical¹⁸⁻²¹ packing density for these surfaces. The most popular functionalization technique is the hydrosilylation reaction with alkene molecules, creating long chain alkyl groups on the surface, and previous computational studies have focused on long chain alkyl groups such as octadecyl groups. These studies have shown that the minimum energy for the packing density of alkyl chains on these surfaces was in agreement with experimental results which report that long chain alkyl groups formed by thermal hydrosilylation cover about 50% of the surface. However, these studies do not report the effect of a thermodynamic driving force on the production of these monolayers. Even though 50% surface packing may represent a minimum in energy for packed surfaces, if the formation of a more densely packed surface is still thermodynamically favorable over the reactants, then one would predict that the reaction would continue until the further alkylation of surface sites was thermodynamically (or kinetically) unfavorable. By adding a driving force for the reaction, it is possible to more accurately model surfaces formed by these reactions.

For the formation of alkyl monolayers using the two-step chlorination/alkylation procedure, H-terminated surfaces are first chlorinated using a radical chlorine source such as PCl_5 , and then reacted with alkyl Grignard or alkyl lithium reagents to form densely packed monolayers on the surface. This reaction can form monolayers on the surface of alkyl groups that are impossible with the hydrosilylation reaction, such as CH_3

functionalization, or are more difficult, such as C_2H_5 and C_3H_7 . While for dynamics simulations on long chain alkyl monolayers, the Van der Waals interactions of the chain tails would dominate the packing, for smaller groups it is predicted that electrostatics and bond formation would have a larger effect. Also, the use of non-alkenes allows for the reaction of more unusual alkyl groups, such as *iso*-propyl, *tert*-butyl, and phenyl (C_6H_5). The steric bulk of these groups should cause more sparse packing on the surface than for straight chain groups. Studies of alkyl monolayers formed through the chlorination/alkylation process have shown higher densities for the packing of alkyl groups on the surface than those formed by hydrosilylation, with unity coverage for CH_3 -terminated Si(111), and 90% for C_2H_5 -terminated surfaces. While the small Van der Waals diameter of a CH_3 group ($\sim 4 \text{ \AA}$) does not preclude tight packing, the much larger diameter for a C_2H_5 group, or any straight chain alkyl, with a Van der Waals diameter of over 5 \AA for the base two carbon unit, indicates that such highly packed surfaces must suffer large amounts of unfavorable Van der Waals interactions.

In this report we performed molecular dynamics modeling using Cerius² and quantum mechanical calculations to calculate the free energy of formation for packed alkyl groups on Si(111). The energy values were referenced relative to the energy of the reactants and products of the chlorination/alkyl reaction using alkyl Grignards. This thermodynamic approach will allow for the determination of the packing densities of alkyl monolayers formed by a strong driving force reaction. These surfaces represented the bulk of packed surfaces, as repeat unit cells are employed to remove any edge effects for the calculations. Surface packing structures were constructed using varying patterns to represent differing packing arrangements for single total packing densities. Chain

lengths investigated were CH₃, C₂H₅, and C₈H₁₇, as well as the bulkier groups *iso*-propyl, *tert*-butyl, and phenyl (C₆H₅).

4.2 Experimental

Molecular Dynamics simulations were conducted with Cerius² software (Accelrys, San Diego, CA), using previously reported force field parameters for silicon^{22,23} and hydrocarbons.²⁴

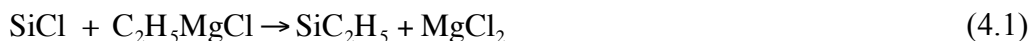
Charges for the atoms in the molecular dynamics calculations were calculated by performing Density Functional Theory (DFT) calculations [Jaguar 5.0 software (Schrodinger, Portland, OR) at the B3LYP level of theory with 631G**++ basis sets) on Si₁₀H₁₅R clusters, where R is the hydrocarbon chain of interest, H or Cl. After construction and application of calculated charges, the charges of the top four atomic layers of Si and the bound alkyl groups/H/Cl atoms were averaged to zero overall charge to maintain charge neutrality.

Surfaces were formed of stacks of bulk crystalline silicon, with the (111) face exposed 11 double layers deep, as repeating unit cells, with periodic boundary conditions to avoid edge effects. Surfaces were 5x5, 6x6, 8x8, or 10x10 terminal Si-X species in size, depending on the packing density used. Only the top four layers of silicon were free to move, and all other silicon atoms were fixed in place at their bulk parameters.

Surfaces were constructed H-terminated, and alkyl groups were bound to the surface, replacing H atoms with some packing density of R groups. Alkyl groups were arrayed on the surface to simulate various packing patterns for certain packing densities. Figure 4.1

shows the packing patterns used. To avoid influencing the individual conformation of alkyl groups, groups were bound and stretched to 10 Å away from the surface before energy minimization. To insure an energetic distribution of alkyl chain conformations, samples were given kinetic energy equivalent to 800 °C, under the constraint that no bonds were allowed to break to disorder the surface to avoid artificial crystallinity. Surface energy was then minimized using the Cerius² Smart Minimizer.

ΔG for the reaction:



was calculated using the Jaguar software within the Poisson-Boltzmann continuum solvation model, using THF as the solvent. For this calculation the silicon site was modeled as a Si₄H₉ cluster, to which either Cl or R were bonded. ΔG for this reaction was calculated to be -47.1 kcal/mol. This ΔG was used for all surfaces regardless of Grignard identity. ΔG for the reaction:



was calculated from ΔG from (4.1), subtracting ΔH for the formation of an Si-R bond (-84 kcal/mol²⁵) and forming a C-H bond (-98 kcal/mol^{26,27}), and adding the ΔH for forming an Si-H bond (-90 kcal/mol^{28,29}) and formation of a C-C bond (-88 kcal/mol³⁰). This reaction energy was used across all surfaces considered. ΔG_s for the formation of a particular surface of packing density d was calculated by:

$$\Delta G_s = \Delta G_a * d + \Delta G_H(1 - d) + H_{S,u} + H_{THFCl} * (1 - d) - H_G * d - H_{SiCl,u} - H_{THF} * (1 - d) \quad (4.3)$$

where ΔG_a was the driving force for the alkylation reaction, d was the fraction of a unit cell alkylated (i.e. 0.667 for a 66.7% packed surface), ΔG_H was the ΔG for (4.2), $H_{S,u}$ was

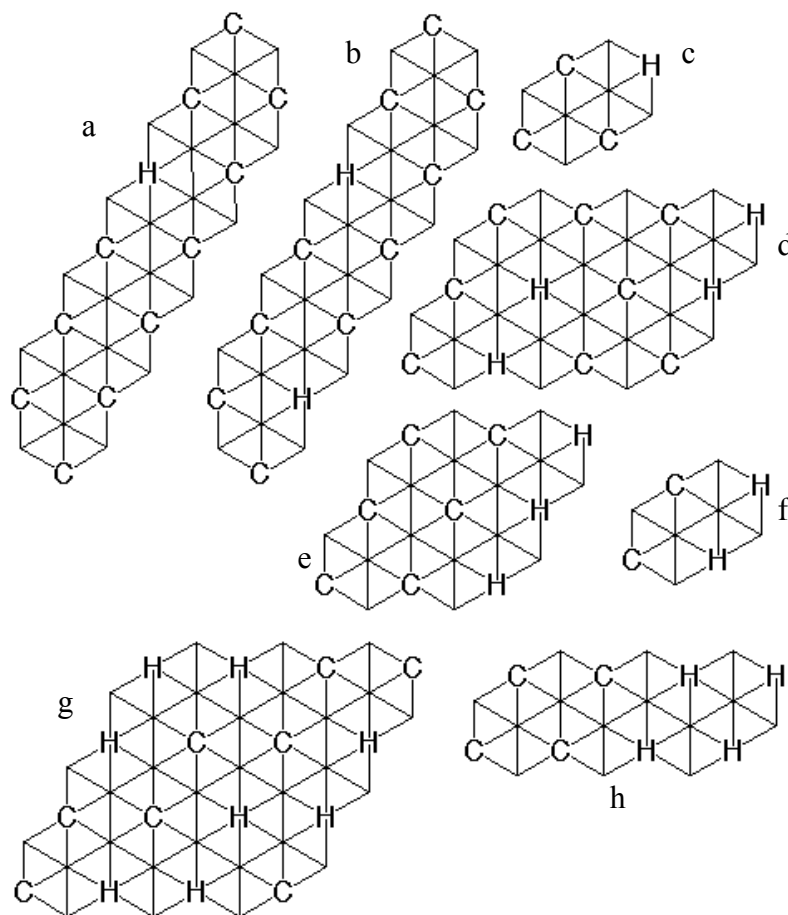


Figure 4.1: Packing patterns for alkyl groups on Si(111). The patterns are: a) 90%, b) 80%, c) 75%, d) 66% oval, e) 66% linear, f) 50% linear, g) 50% zig-zag, and h) 50% diagonal. Packing densities lower than 50% were the inverse of the higher packing densities.

the calculated force field enthalpy for the formation of a surface for a packing density d , per unit cell, $H_{\text{THF-Cl}}$ was the force field enthalpy for THF-Cl, H_G was the force field enthalpy for each Grignard, H_{SiCl_u} was the force field enthalpy per unit cell for a Cl-terminated Si(111) surface, and H_{THF} was the force field enthalpy for a THF molecule. Using this products minus reactants approach, a ΔG for the production of a surface of a packing density d , can be calculated.

4.3 Results and Discussion

4.3.1 Straight Chain Packing Energies

Alkyl monolayer formation can be treated as a sequential process whereby one Si-Cl bond is replaced by a Si-C bond, after which an adjacent bond can be reacted. The steric and energetic environment for subsequent alkylation is then strongly determined by previous alkylation. For initial alkylation, with no interfering neighboring alkyl groups bound, the two reactions for a Si-Cl bond, the alkylation of the Si atom versus the H-termination of the atom compete. The larger ΔG for the alkylation reaction of an unhindered site indicates that with no interfering neighbors, the Si site will be alkylated. After alkylation of the surface progresses, any given unreacted Si-Cl site will then have neighboring alkyl groups, and alkylation of that site versus H-termination will have different overall ΔG . From this, it can be seen that the competition to alkylate versus H-terminate any particular site will vary with the local packing density. For bulky alkyl groups, then, steric effects will cause H-termination to energetically outcompete

alkylation at higher packing densities, resulting in partial alkylation. The use of surfaces larger than the unit cell for each packing pattern allows for disordering the surface on a scale larger than that of the unit, to further minimize the surface energy.

Figure 4.2 shows the energy for the reaction of CH_3MgCl with the Cl-terminated Si(111) surface for all final surface packings. The energy for each packing outcome was an overall reaction energy starting with the reactants and ending with the surface packing given. The total energy of the reaction decreased for each surface as a larger fraction of the surface was CH_3 terminated rather than H-terminated. Replacing each chlorine atom and with a CH_3 group as opposed to an H atom leads to a decrease in overall energy for the reaction. From this, it can be seen that 100% methylation of the surface represents the thermodynamically predicted result of this reaction. For low alkylation percentages, the overall energy for the reaction trends towards the energy for the total conversion of the Si-Cl surface to Si-H, indicating that formation of Si-H bonds was unfavorable at all interim packing densities. Thus for any progressing reaction for Grignards with the chlorinated surface, to either form an Si-H bond or a Si- CH_3 bond, at all points, the alkylation of a surface site was preferred. For the CH_3 -terminated surface, the only divergent packing pattern for a given density was the 50% diagonal, higher in energy than the other 50% packing patterns, due likely to the slight increase in steric crowding by clustering of lines of CH_3 groups.

The results for the C_2H_5 surface packing were different from that of the CH_3 -terminated surface, as shown in Figure 4.3. The energy for the complete alkylation thermodynamically was lower than that of the reactants, or for the partial H-termination of the surface, mainly due to the energy from the used of the Grignard reagents.

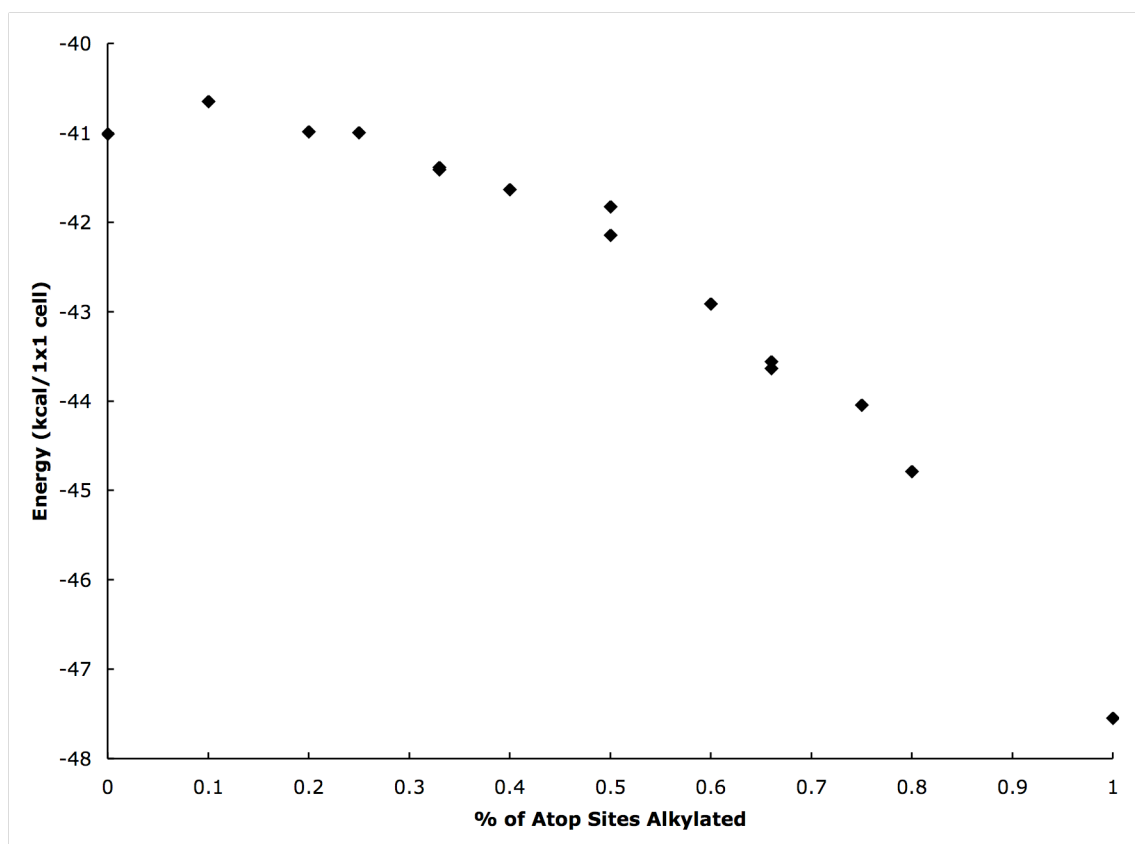


Figure 4.2: Packing energies for CH₃-terminated Si(111), per unit cell. Unalkylated sites are H-terminated. For 50% packing, the divergent data point was for 50% diagonal.

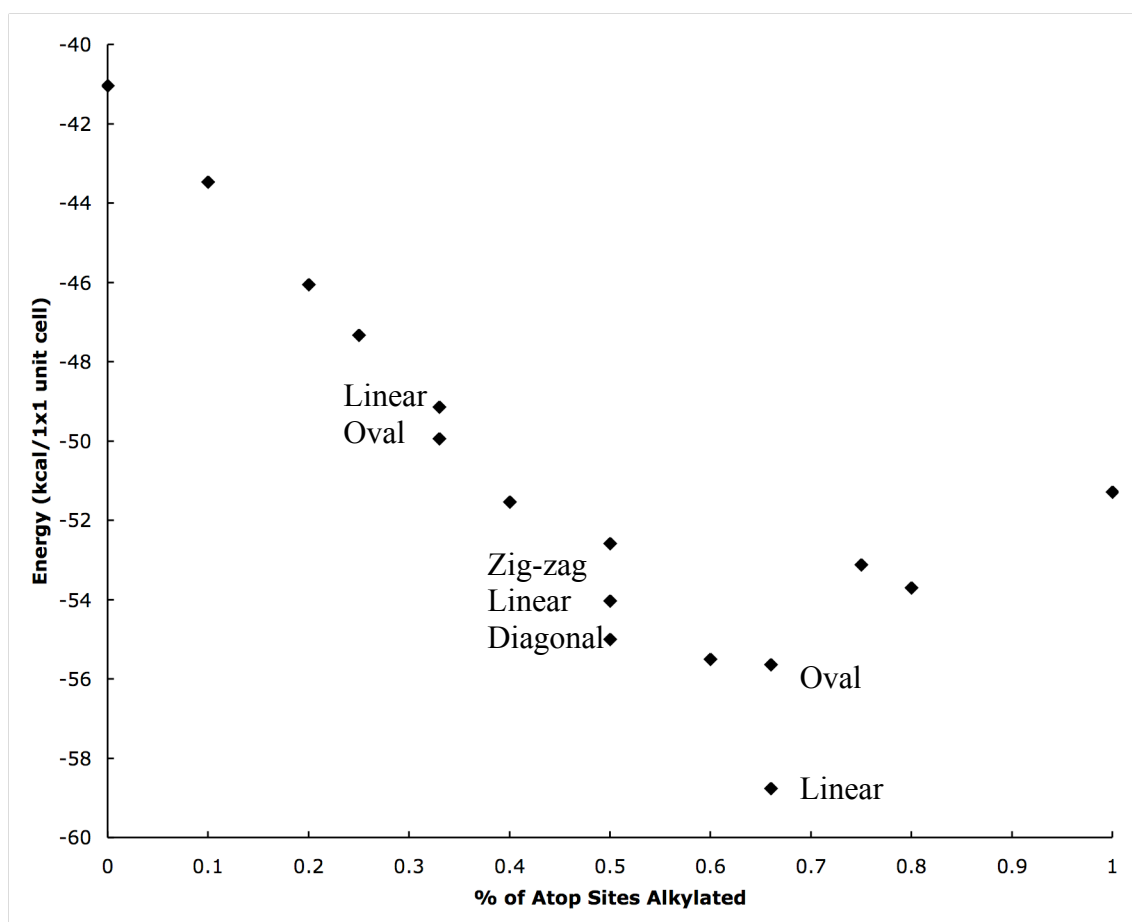


Figure 4.3: Packing energies for CH₃CH₂-terminated Si(111), per unit cell. Unalkylated sites are H-terminated.

However, despite the relative driving force to alkylate over H-termination, the steric crowding causes a shift in the curve towards the highest packing energies. The thermodynamically favored packing energies reach a minimum at 66.7% packing in a larger minima between 50-80% packing, and with only a small difference in energy, on the order of single kcal/mol to higher or lower packing energies. For these structures, the small differences in thermodynamic packing energies should cause kinetic effects to dominate over overall energetic effects. The extreme minimum represented by the 66.7% linear packing results from perfect crystalline packing, and small deviations from this pattern should move the surface energy closer to the more random arrangement of the 66.7% oval pattern.

Figure 4.4 shows the side on view of C_2H_5 groups bound to the Si(111) surface at 66.7% (linear) and 100% packing density. The bond strain which caused the 100% packing density to rise sharply over lower surface packings is evident. The C_2H_5 groups were distorted from the surface normal by $\sim 15^\circ$, caused by the interaction of the terminal CH_3 group with the CH_2 group for the neighboring C_2H_5 row. This distortion was not sufficient to halt the alkylation of the surface, however, as the total energy of the 100% packing density surface for C_2H_5 groups was overall negative. The Si-Cl to Si-H reaction, however, became more favorable as the steric interactions between C_2H_5 groups rose. For the 66.7% (linear) case, there was no bond distortion, and each C_2H_5 group is turned towards a vacant row, and suffer little comparable bond strain. This packing pattern represents an extreme minimum in the C_2H_5 packing scheme, but required a high degree of alkyl orientation as well as alkyl group placement.

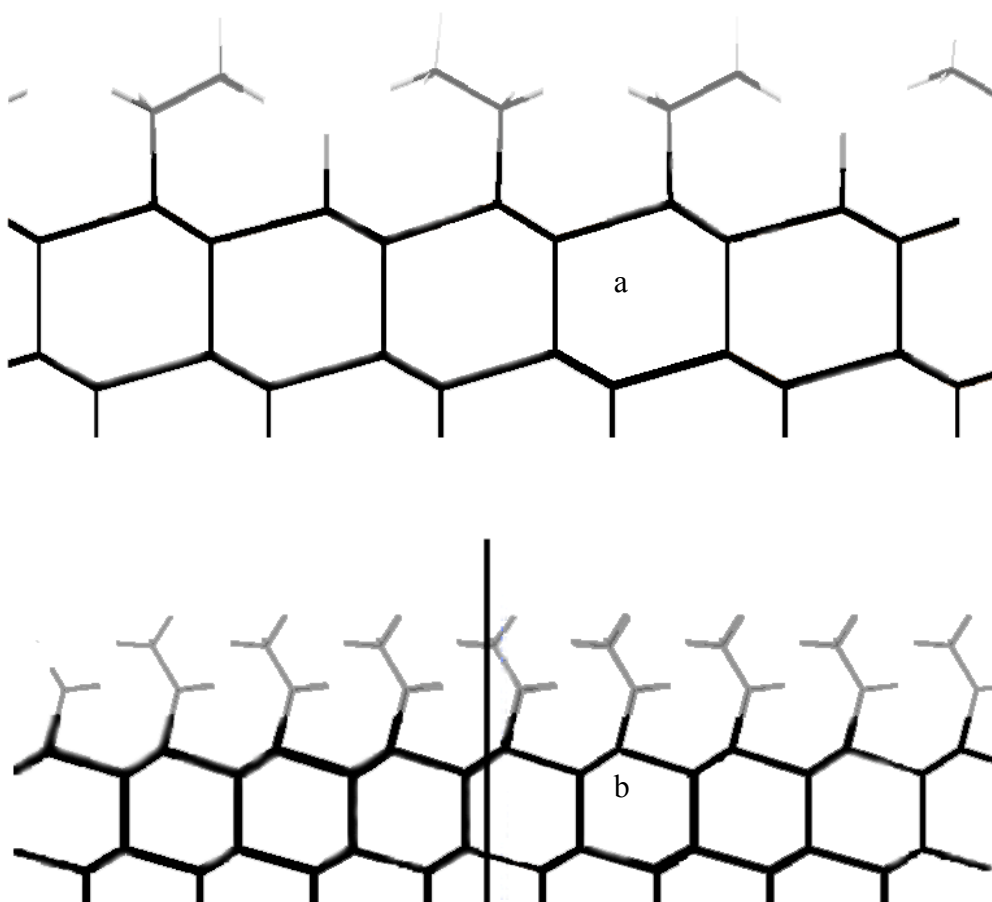


Figure 4.4: Side on view of CH_3CH_2 -terminated $\text{Si}(111)$, a) 66% linear packing, and b) 100% packing.

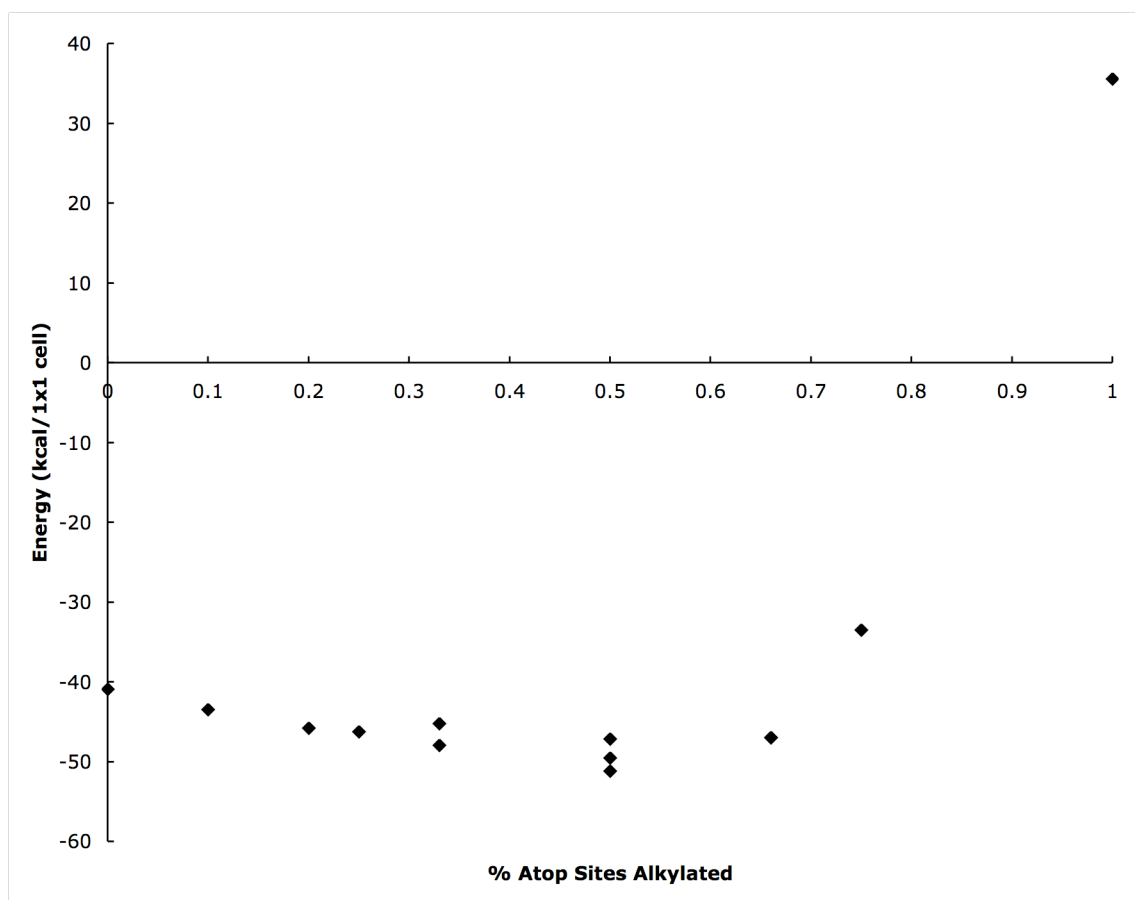


Figure 4.5: Packing energies for C₈H₁₇-terminated Si(111), per unit cell. Unalkylated sites are H-terminated.

With a longer chain length, however, the tail-tail Van der Waals interactions became more limiting. Figure 4.5 shows the relative energy of C_8H_{17} groups bound to the surface, with the surface energy rising much faster as the packing grows denser after 50% packing. While the minimum energy surface remained little changed by moving from C_2H_5 to C_8H_{17} , there was a substantial restriction on the denser packing, of 86.9 kcal/1x1 cell for 100% packing, shifting the energy minimum to lower packing densities than C_2H_5 . This rise in energy towards 100% was almost entirely due to sharp rises in the Van der Waals component of the calculated force field energy for the surface.

4.3.2 Bulky Alkyl Surface Groups

Figure 4.6 shows the packing energies for the branched alkyl groups *iso*-propyl and *tert*-butyl. These groups have, in addition to the chain-chain interactions of the straight chain alkyl groups, additional stresses as the packing density rose, from the extra steric interactions as the branching encroached on neighboring sites. The *iso*-propyl group, which has the same tip to tail length as the C_2H_5 , shows a striking increase in surface energy after 50% packing density. This rise was due to the interactions with neighboring bonded groups, which could no longer arrange to minimize the negative interactions between the tails, as the two tails for each group were confined to be $\sim 120^\circ$ apart, pointing at corresponding groups for adjacent bound groups. Each bond group, now, has more than twice the negative interactions as bifurcating the tail increases steric stresses, as well as limiting the contortion of the group to find more favorable interactions. These surfaces now would be projected to pack at between 33-50% due to

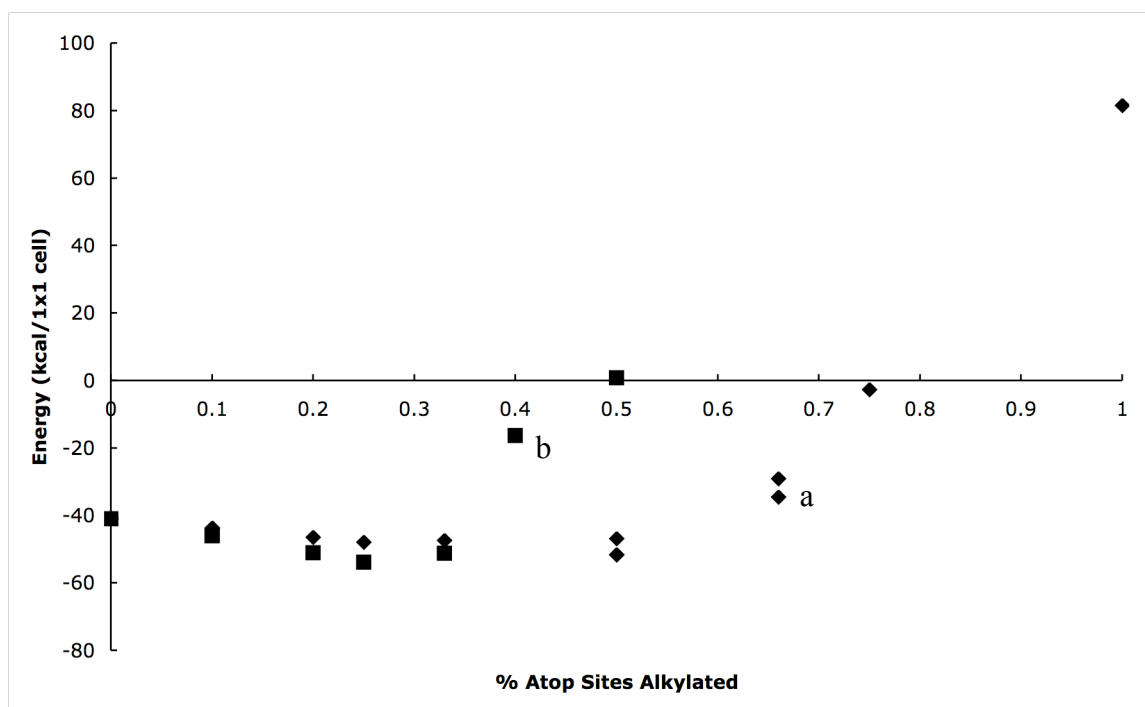


Figure 4.6: Packing energies for a) *iso*-propyl-terminated Si(111) and b) *tert*-butyl-terminated Si(111), per unit cell. Unalkylated sites are H-terminated.

these interactions. The *tert*-butyl group was far more hindered by its branching. Surface structures for packings higher than 50% could not be constructed, as this would have required interpenetration of the bonds between bound groups, for which Cerius² has no empirical data from which to calculate strain energy for the surface. However, for surfaces that were constructed, the sharp rise in energy after 33% packing density indicate that higher density *tert*-butylated surfaces would be extremely high in energy. Both the *iso*-propyl and *tert*-butyl groups tracked closely with similar energies for the low packing densities; the *tert*-butyl groups were lower in energy for the lowest packing densities due to the beneficial van der Waals interactions between the bulky groups and neighboring Si-H species.

For the larger phenyl group, there was increased steric bulk in two dimensions, in the plane of the group, as well as rigidity in the C-H groups in the *ortho* position on the ring. These bonds could no longer rotate away from the surface to avoid unfavorable interactions. Figure 4.7 shows the energy trend with respect to surface packing for phenyl groups, showing a similar trend to both *iso*-propyl groups, as well as octyl, with a broad minimum from 40-66.7% packing, with a minimum at 50%. The sharp rise towards 100% packing was the largest calculated, and groups at this high density showed extreme distortion with Si-H bond skewed out of the plane of the ring. For the 50% packing density, in the linear arrangement, the rings align face-to-face along the direction of the linear packing.

4.3.3 Comparisons

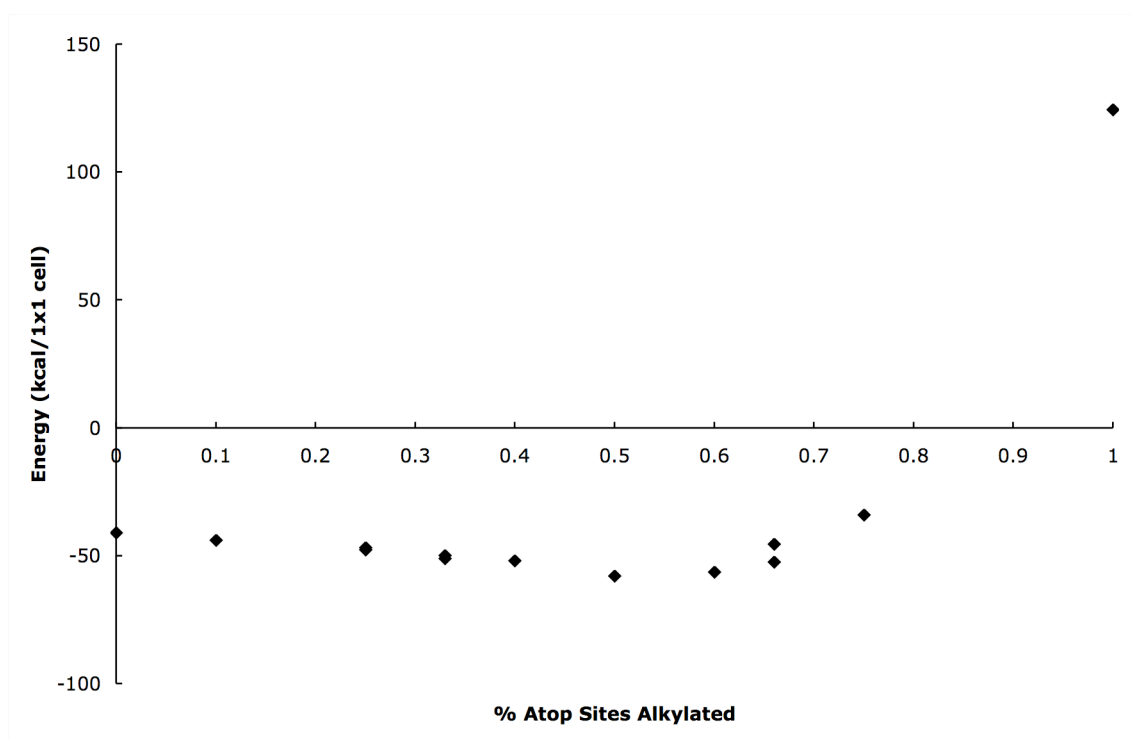


Figure 4.7: Packing energies for phenyl (C_6H_5)-terminated Si(111), per unit cell. Unalkylated sites are H-terminated.

The sharp rise in strain energy from the C1 to C8 terminated surface corresponds well with experimental results on these surfaces, indicating that C2 and C8 pack progressively less densely as the chain length extends.^{3,31} Previous measurements of the alkylated surface prepared in this manner, have shown comparable results for these straight chain groups. CH₃-terminated surfaces by transmission IR absorbance show no evidence of the Si-H stretch at $\sim 2080\text{ cm}^{-1}$, indicating that complete termination of the surface has occurred, consistent with these computational results. Both larger groups C₂H₅ and *tert*-butyl by IR show a return of the Si-H stretch after alkylation, indicating that incomplete termination of the surface has occurred, with partial replacement of the Si-Cl bond by Si-H bonds.

4.4 Conclusions

The use of a thermodynamic approach for referencing the surface energy has resulted in a more effective framework for the evaluation of this two-path reaction. Previous calculations of the packing density of alkyl groups on Si(111) focused on the formation of long chain groups such as octadecyl through the hydrosilylation reaction, starting from the assumption that the monolayers would pack with 50% efficiency. These studies reported only the minimum energy for the surfaces tested, relative to the unstrained surface ignoring the driving force for the surface formation, as well as the electrostatic components of the surface energy. The hydrosilylation reaction, triggered through the use of UV light or thermal energy, can be considered to have a strong driving force through the formation of surficial Si radical species. The surfaces can be expected

to react based on the overall thermodynamic and kinetic considerations for this reaction, rather than simply terminating when the surface reaches a minimum energy. The two-step chlorination/alkylation reaction studied herein also has a strong driving force for the completion of the alkylation reaction, and must start with every atop site reacting, forming either an Si-H bond, or a Si-C bond. The competing termination reactions for each site are driven by both the thermodynamic energy of the reaction, as well as the various kinetic and steric considerations for the reaction, which are not considered in this report. Thermodynamically, from these calculations, the CH₃ termination reaction was predicted to attain 100% coverage, in good agreement with experiment.³¹⁻³³ Larger groups were predicted to monolayers between 50-75% coverage, with broad energy minima. These reactions are most likely controlled within these minima by kinetic considerations, as the depth of these minima are only a few kcal/mol. Further studies are required to understand the mechanism of this reaction for resolution of the final predicted packing density.^{31,34}

4.5 Acknowledgements

These calculations were performed in collaboration with Santiago Solares and William Goddard, of the California Institute of Technology. We gratefully acknowledge the NSF, grant CHE-021358, and the California Institute of Technology for support of this work.

4.6 Bibliography

- (1) Linford, M. R.; Chidsey, C. E. D. *J. Am. Chem. Soc.* **1993**, *115*, 12631-12632.
- (2) Linford, M. R.; Fenter, P.; Eisenberger, P. M.; Chidsey, C. E. D. *J. Am. Chem. Soc.* **1995**, *117*, 3145-3155.
- (3) Terry, J.; Linford, M. R.; Wigren, C.; Cao, R. Y.; Pianetta, P.; Chidsey, C. E. D. *Appl. Phys. Lett.* **1997**, *71*, 1056-1058.
- (4) Terry, J.; Mo, R.; Wigren, C.; Cao, R. Y.; Mount, G.; Pianetta, P.; Linford, M. R.; Chidsey, C. E. D. *Nucl. Instrum. Meth. B* **1997**, *133*, 94-101.
- (5) Effenberger, F.; Gotz, G.; Bidlingmaier, B.; Wezstein, M. *Angew. Chem. Int. Ed.* **1998**, *37*, 2462-2464.
- (6) Stewart, M. P.; Buriak, J. M. *Angew. Chem. Int. Ed. Eng* **1998**, *23*, 3257.
- (7) Sieval, A. B.; Demirel, A. L.; Nissink, J. W. M.; Linford, M. R.; van der Maas, J. H.; de Jeu, W. H.; Zuilhof, H.; Sudholter, E. J. R. *Langmuir* **1998**, *14*, 1759-1768.
- (8) Sung, M. M.; Kluth, G. J.; Yauw, O. W.; Maboudian, R. *Langmuir* **1997**, *13*, 6164-6168.
- (9) Zazzera, L. A.; Evans, J. F.; Deruelle, M.; Tirrell, M.; Kessel, C. R.; Mckeown, P. J. *Electrochem. Soc.* **1997**, *144*, 2184-2189.
- (10) Buriak, J. M.; Allen, M. J. *J. Am. Chem. Soc.* **1998**, *120*, 1339-1340.
- (11) Buriak, J. M.; Allen, M. J. *J. Lumin.* **1998**, *80*, 29-35.

- (12) Holland, J. M.; Stewart, M. P.; Allen, M. J.; Buriak, J. M. *J. Solid State Chem.* **1999**, *147*, 251-258.
- (13) Henry de Villeneuve, C.; Pinson, J.; Ozanam, F.; Chazalviel, J. N.; Allongue, P. In *Mat. Res. Soc. Symp. Proc.* 1997; Vol. 451, p 185-195.
- (14) Vieillard, C.; Warntjes, M.; Ozanam, F.; Chazalviel, J.-N. *Proc. - Electrochem. Soc.* **1996**, *95*, 250.
- (15) Bansal, A.; Li, X.; Lauermann, I.; Lewis, N. S.; Yi, S. I.; Weinberg, W. H. *J. Am. Chem. Soc.* **1996**, *118*, 7225-7226.
- (16) Juang, A.; Scherman, O. A.; Grubbs, R. H.; Lewis, N. S. *Langmuir* **2001**, *17*, 1321-1323.
- (17) Royea, W. J.; Juang, A.; Lewis, N. S. *Appl. Phys. Lett.* **2000**, *77*, 1988-1990.
- (18) Sieval, A. B.; van der Hout, B.; Zuilhof, H.; Sudholter, E. J. R. *Langmuir* **2000**, *16*, 2987.
- (19) Sieval, A. B.; van der Hout, B.; Zuilhof, H.; Sudholter, E. J. R. *Langmuir* **2001**, *17*, 2172-2181.
- (20) Yuan, S.-L.; Cai, Z.-T.; Jiang, Y.-S. *New J. Chem.* **2003**, *27*, 626.
- (21) Zhang, L.; Wesley, K.; Jiang, S. *Langmuir* **2001**, *17*, 6275.
- (22) Shapiro, I. R.; Solares, S. D.; Esplandiu, M. J.; Wade, L. A.; Goddard III, W. A.; Collier, C. P. *J. Phys. Chem. B* **2004**, *108*, 13613-13618.
- (23) Solares, S. D.; Esplandiu, M. J.; Goddard III, W. A.; Collier, C. P. *J. Phys. Chem. B* **2005**, *109*, 11493-11500.
- (24) Mayo, S. L.; Olafson, B. D.; Goddard III, W. A. *J. Phys. Chem. B* **1990**, *94*, 8897-8909.

- (25) Walsh, R. *Acc. Chem. Res.* **1981**, *14*, 246.
- (26) Golden, D. M.; Benson, S. W. *Chem. Rev.* **1969**, *69*, 125.
- (27) Egger, K. W.; Cocks, A. T. *Helv. Chim. Acta* **1973**, *56*, 1516.
- (28) Wu, Y.-D.; Wong, C.-L. *J. Org. Chem.* **1995**, *60*, 821-828.
- (29) Kanabus-Kaminska, J. M.; Hawari, J. A.; Griller, D. *J. Am. Chem. Soc.* **1987**, *109*, 5267.
- (30) Benson, S. W. *Thermochemical Kinetics*; Wiley: New York, 1976.
- (31) Nemanick, E. J.; Hurley, P. T.; Brunschwig, B. S.; Lewis, N. S. *J. Phys. Chem. B* **2005**, *submitted for review*.
- (32) Terry, J.; Linford, M. R.; Wigren, C.; Cao, R. Y.; Pianetta, P.; Chidsey, C. E. D. *Journal of Applied Physics* **1999**, *85*, 213-221.
- (33) Webb, L. J.; Nemanick, E. J.; Biteen, J. S.; Knapp, D. W.; Michalak, D. J.; Traub, M. C.; Chan, A. S. Y.; Brunschwig, B. S.; Lewis, N. S. *J. Phys. Chem. B* **2005**, *109*, 3930-3937.
- (34) Solares, S. D.; Goddard III, W. A. *unpublished work*.

Chapter 5

Chemical and Electrical Passivation of Single Crystal Silicon(100) Surfaces Through a Two-step Chlorination/Alkylation Process

5.1 Introduction

Interest in silicon surface functionalization has stemmed from a need to passivate semiconductor surfaces towards oxidation in air or water, as well as to passivate surfaces towards charge carrier recombination at surface-localized electronic defect states. The semiconductor device industry, which predominantly uses the (100) face of silicon,¹ passivates the surface through the fabrication of a layer of high temperature annealed silicon dioxide to passivate the surface towards charge carrier recombination. The highly ordered Si/SiO₂ interface thus formed provides a bulk-terminating structure that is free from electronically active defects.² However, this oxide capping technique requires large thermal energy inputs, as well as the formation of a layer of at least a few nanometers in thickness. As the dimensions of silicon-based devices become smaller, this minimum thickness becomes an obstacle, suggesting that passivating layers of reduced thickness could have significant effects on the miniaturization of silicon based devices.

Interest in modifying silicon surfaces using covalently attached groups has surged in recent years, due to the utility of these functionalizations for surface passivation and

substrate modification.³⁻⁶ Silicon-carbon covalent bonds have shown exceptional utility both from the stability of the bond itself as compared to the silicon-hydrogen bond, as well as providing access to a wealth of reaction schemes for attachment of functional groups from organic literature. The first functionalization technique for the formation of Si-C bonds used the H-term Si(111) surface to react with unsaturated alkenes through a radical process catalyzed by a diacyl peroxide initiator.^{7,8} The reaction was further refined by use of UV⁹⁻¹¹ or white¹² light, thermal energy,^{13,14} transition metal complexes,¹⁵ and Lewis acids¹⁶⁻¹⁸ to catalyze the reaction, and expanded to encompass the Si(100)^{13,14} surface as well as porous silicon.¹² Functionalization of silicon surfaces has expanded to encompass the electrochemical functionalization,^{19,20} radical halogenation,²¹ and transmetallation with alkyl Grignard and lithium reactions.²¹⁻²³

To be an effective replacement for thermal oxide layers, Si-C monolayer functionalization must prevent the formation of charge carrier recombination sites with energies within the band gap of silicon.²⁴ Removal of the thermal oxide capping layer also requires that the growth of defect-rich native oxide must be suppressed as well. Silicon-carbon covalent bonds are an attractive alternative to the thermal oxide passivation layer, as the silicon-carbon bond is very stable, and greatly reduces the reactivity of an alkylated surface towards oxygen, both preventing the formation of oxide as well as retarding the subsequent formation of recombination sites at the bulk silicon/surface interface. It has been shown that Si(111) surfaces can be modified using a two step chlorination-alkylation process using Grignard reagents to give electrically and chemically stable surfaces.^{23,25,26} These surfaces have shown greatly reduced oxidation in air and decreased electrical surface recombination through the addition of small straight-

chain alkyl groups by removing the chemically active hydrogen-silicon bond, as well as physically blocking the surface from attack by oxidants. The H-terminated Si(111) surface prepared by etching in NH_4F (aq) presents well-ordered terraces of mono-hydride silicon atoms that span hundreds of nanometers, presenting only a single Si-H bond per Si atop site.^{27,28} The chemically etched Si(100) surface, however, cannot be prepared as cleanly. Fluoride etches of the Si(100) surface reveal several hydride species including SiH, SiH₂, as well as SiH₃, leaving the surface rough on the atomic scale.²⁷⁻²⁹ This rough, diverse surface presents a more significant challenge for passivation, due to the higher density of surface bonds for functionalization. On the Si(111) surface, where no more than one alkyl group can be bound to each surface silicon, steric crowding limits the number of atop sites that can be functionalized. For the Si(100) surface, the fraction of atop sites functionalized must be far less, due to both the higher Si-H_x bond density, and the non-perpendicular bond angle to the surface. However, since Si(111)-alkyl surfaces formed by the two step chlorination/alkylation procedure show exceptional electronic and oxidative passivation despite fractional surface alkyl coverage,³⁰ functionalization of the Si(100) surface using the same technique should allow for surface passivation.

In this study, single crystal Si(100) surfaces were chlorinated using PCl_5 in a radical reaction followed by reaction with alkyl Grignard reagents at temperatures above the boiling point of the Grignard solvent in sealed reaction chambers. Both short chain alkyl groups (CH_3 , C_2H_5 , and C_4H_9) were used as well as the bulkier group phenyl (C_6H_5). Surface recombination velocities for photogenerated charge carriers (S) were measured through rf conductivity decay to monitor electronic passivation. X-ray photoelectron spectra (XPS) of the samples using both soft (140 eV) and hard (1486.6

eV) X-rays was employed to characterize the surface after functionalization, as well as to measure oxidation of the surfaces after exposure to oxidizing conditions..

5.2 Experimental

5.2.1 Alkylation of Silicon

Silicon wafers used were from Virginia Semiconductor, n-type, phosphorus doped, with a resistivity of 1-6 $k\Omega \cdot \text{cm}$ and were $270 \pm 25 \mu\text{m}$ thick. The samples were high purity, float-zone grown, double-side polished for both oxidation studies as well as electrical passivation measurements to insure correlation between samples. Except as noted, all reagents used were stored in a nitrogen purged glove box, and were used as received. Nanopure 18 $M\Omega \cdot \text{cm}$ water was used for all rinses. Silicon samples were scribed into squares averaging 0.7 cm on a side and handled only with Teflon tweezers, only by the edges, never touching the face of the samples to prevent scratching. Native oxide covered samples were first cleaned by sequential sonication in methanol, acetone, dichloromethane, 1,1,1 trichloroethane, dichloromethane, acetone, and methanol (VWR Scientific Products, West Chester, PA) for three seconds at a time, with their faces never touching the sonication beaker to prevent scratches. Samples were then rinsed in water, and etched in buffered HF (pH 5, Transene Corp., Danvers, MA) for 30 s. Samples were then removed and rinsed in water, for less than 2 s per side to limit oxidation and were completely dried in flowing nitrogen for ten s. The samples were then passed into a nitrogen atmosphere glove box for functionalization.

To chlorinate the surfaces, the H-terminated Si(100) samples were immersed in septa-capped test tubes in hot (95 °C) chlorobenzene saturated with PCl_5 (99.998% Strem, Newburyport, MA) for 1 h. Benzoyl peroxide (97% Aldrich) was added (<1 mg) to initiate chlorination of the surface. Care was taken to insure that the polished surfaces of the silicon samples were never touched to avoid scratching and contamination of the surface which might influence surface reactivity. For XPS measurements of the chlorinated surface, samples were rinsed in THF and dried under flowing nitrogen and passed into a UHV load lock directly into the XPS without exposure to air. After chlorination, the samples were washed in anhydrous tetrahydrofuran (THF) (99.8%, inhibitor free, Aldrich) and were placed in Teflon screw-cap sealed glass reaction flasks that contained 10 mL of anhydrous THF and 10 mL of a 1 M Grignard reagent in THF. The Grignard reagents were either CH_3MgCl , $\text{CH}_3\text{CH}_2\text{MgCl}$, $\text{CH}_3(\text{CH}_2)_3\text{MgCl}$, or $\text{C}_6\text{H}_5\text{MgCl}$. The reaction solution was heated to 110-120 °C for 21 hr in a sealed reaction vessel. After reaction, samples were rinsed in THF followed by anhydrous methanol (99.8% Aldrich), removed from the glove box, and sonicated in a 5 mL solution of methanol and glacial acetic acid (10:1) (Aldrich) for 5 min to remove any adsorbed magnesium salts. Samples were then rinsed with 18 M Ω cm resistivity H_2O and either passed directly into the ultra-high vacuum (UHV) load lock for XPS analysis or placed in scintillation vials for SRV measurements.

5.2.2 X-ray Photoelectron Spectroscopy Measurements

XPS data were collected on a UHV system that has been described previously.³¹ The collection chamber was maintained at $\approx 5 \times 10^{-10}$ torr when not in use, whereas due to sample outgassing the pressure rose to $\approx 2 \times 10^{-8}$ torr during data collection. Due to the relatively low resistivity of the samples, charge compensation was not needed. All measurements were taken on the center of the sample to ensure reproducibility and to minimize the effects of scratches or contamination at the edges. The incident beam consisted of 1486.6 eV X-rays from an Al K α source, and ejected electrons were collected at 55° off of the surface normal. All energies are reported as binding energies in eV. The XPS system was periodically calibrated using the 4f peaks of a Au standard at 83 and 87 binding eV.

Data were collected using ESCA 2000 E Capture software, v. 102.04 (Service Physics). Samples were first scanned from 0 to 1000 binding eV to monitor signals for Cl as well as C and O. The Si 2p, Cl 2p and C 1s regions of 98-105, 198-204, and 282-287 binding eV, respectively, were investigated in detail. The Si 2p region was used to monitor the growth of Si oxides. Scan times of up to 4 h were employed for data collection. The spectrometer resolution was ≈ 0.5 eV.

Oxide coverages were determined by integration of the area under the broad oxygen-shifted Si 2p peak centered around 103 binding eV, which was comprised of SiO₂ and Si suboxides. This peak area was ratioed to the area of the bulk Si 2p_{3/2} and Si 2p_{1/2} peaks. Using ESCA 2000 A Analysis, v. 102.04 integration software, the peak shapes were fitted to Voigt functions fixed at 95% Gaussian and 5% Lorentzian lineshapes. The position of the Si 2p_{1/2} peak was fixed at 0.6 binding eV higher than the 2p_{3/2} peak and

the FWHM was constrained to be identical to that of the Si 2p_{3/2} peak, with the total integrated area ratio of the 2p_{1/2}/2p_{3/2} peaks fixed at 0.51.²⁵

The fractional monolayer coverage of oxide species on the surface was determined using the substrate-overlayer model:³²

$$\frac{d_o}{d_1} = \lambda_o \sin \theta \left\{ \ln \left[1 + \left(\frac{I_{Si}^o}{I_o^o} \right) \left(\frac{I_o}{I_{Si}} \right) \right] \right\} \quad (5.1)$$

where d_o is the overlayer thickness, d_1 is the thickness of one monolayer of oxide, (3.5 Å), and λ_o is the attenuation factor of the oxide layer (26 Å). θ is the take-off angle for the measurement (90°-55°, i.e., 35°), I_{Si}^o/I_o^o is a normalizing factor for the particular instrument used (1.3 for this instrument²⁵), and I_o/I_{Si} is the ratio of the peak area of the oxide-shifted silicon to the area of the unshifted silicon peak.

Data from the carbon 1s emission region were fitted to three peaks, representing silicon-bonded carbon at 283.9 eV, carbon-bonded carbon at 285.0 eV, and oxygen-bonded carbon at 286.8 eV. Peaks were fitted to Voigt functions having 70% Gaussian and 30% Lorentzian character. The peak centers were allowed to float, though the center to center distances were fixed at 1.1 eV between the silicon-bonded carbon and the carbon-bonded carbon emissions, and at 1.8 eV between the oxygen-bonded carbon and the carbon-bonded carbon emissions. The integrated area under each carbon peak was ratioed to the integrated area under the silicon 2p peaks for that sample, normalized for scan time. The ratio of the silicon-bonded carbon to the normalized area for the Si 2p peak (C_{Si}/Si) was then compared between alkylated surfaces. The methyl-terminated Si(100) surface was used as a reference surface for the other alkylated Si surfaces, so surface coverages for each alkyl group are reported as $(C_{Si}/Si)_{alkyl}/(C_{Si}/Si)_{methyl}$.

5.2.3 Soft X-ray Photoelectron Spectroscopy

Soft X-ray experiments were performed at Brookhaven National Laboratory at the National Synchrotron Light Source on the U4A beamline. Samples were pumped into a UHV analysis chamber, kept at a pressure of $<1 \times 10^{-9}$ torr between samples. The resolution of the spherical grating monochromator for the selected X-ray energies was 0.1 eV. All measurements were made relative the Si 2p bulk peak, as no internal reference was available for binding energy calibration in the scan energies available. Samples were probed by X-rays of 140 eV, and ejected electrons were collected at 35° and 70° off the sample normal by a VSW 100nm hemispherical analyzer at 45° from the incident X-ray beam. The escape depth for this energy on silicon surfaces was calculated to be 3.5\AA .³³ Samples were sufficiently conductive that no charging-induced peak shifts were observed. X-ray energies available were limited to 10-200 eV, preventing data acquisition for the high energy peaks C and O 1s, as well as Cl 2s and 2p peaks.

For data analysis, spectra were first fitted to a Shirley background, which was then subtracted to allow for peak fitting. The Si $2p_{1/2}$ component peaks were stripped from the spectra for each surface species present, to facilitate peak fitting.³³ The Si $2p_{1/2}$ was removed by fixing the peak-peak energy shift at 0.6 eV, and the $2p_{3/2}/2p_{1/2}$ peak area at 0.51. For each Si $2p_{3/2}$ peak, a peak 0.6 eV higher in energy and 0.51 the size was subtracted from the spectra. Residual spectra were fit to modified Voigt peaks with peak shapes that were 95% Gaussian and 5% Lorentzian. Using a substrate-overlayer model, the sum of all surface species present was assigned to one monolayer as a tool for

distinguishing between equivalent local minima on the peak fitting surface. This model gives the surface monolayer coverage of a species derived from the ratio of the surface to bulk Si 2p signal. The peak area ratio for the surface and bulk species (A_s/A_b) is equal to:

$$\frac{A_s}{A_b} = \frac{MD_s}{D_b d - D_s} \quad (5.2)$$

where M is the monolayers of surface atoms, D_s is the surface density of atoms for Si (100), 6.9×10^{14} atoms cm^{-2} ,¹ D_b is the bulk density for silicon, 5.0×10^{22} atoms cm^{-3} , and d is the escaped depth for the photoelectrons, 3.5 \AA .

5.2.4 Charge Carrier Lifetime Measurements

Surface recombination velocity measurements were collected using a contactless rf conductivity apparatus.²³ Samples were excited with 10 ns pulses at 1064 nm from a Nd:YAG laser operating at 10 Hz. The photogenerated electron-hole pairs diffused to either surface of the sample to recombine through surface-localized electronic states within the Si bandgap. The bulk charge-carrier lifetimes as reported by the manufacturer (~6 ms) were much longer than the observed lifetimes, indicating that charge-carrier recombination effectively only occurred at the silicon surfaces. Charge-carrier concentrations were monitored by measuring the reflected signal from a 450 MHz rf coil. The absorbed rf signal was recorded by averaging 128 traces and the data were fitted to a single exponential decay:

$$A = y_0 + ae^{-t/\tau} \quad (5.3)$$

where τ is the observed charge-carrier lifetime. The surface recombination velocity, S , is obtained from τ through:

$$\frac{1}{\tau} = \frac{1}{\tau_b} + \frac{2S}{d} \quad (5.4)$$

where τ_b is the bulk lifetime, and d is the sample thickness. For all measurements, $\tau_b \gg \tau$, so $S \approx d/2\tau$.

All τ values are reported after the first 24 h following alkylation. Initial measurements of τ for an individual sample showed a slight increase in charge-carrier lifetime over the first day, but stabilized thereafter. To monitor the stability of the alkylated surface towards oxidation, samples were stored in scintillation vials under laboratory air and normal laboratory illumination conditions for up to 11 months, and τ values were monitored periodically during this time interval.

5.3 Results

5.3.1 X-ray Photoelectron Spectroscopy

Figure 5.1 shows representative XPS for the two-step chlorination/alkylation of Si(100) surfaces. H-terminated surfaces exhibited peaks for elemental silicon 2s at 150 eV and 2p at 100 eV as well as the silicon phonon absorption bands at 17 eV and 36 eV above the 2s and 2p peaks, respectively. Trace amounts of C and O were observed at 284 and 532 eV on H-term Si(100). Cl 2s and 2p peaks, at 201 and 271 eV appeared after the chlorination reaction. After alkylation with CH_3MgCl , the Cl 2s and 2p peaks disappeared from the spectrum, and the C 1s peak increased in amplitude. No oxidized Si peak at 101-104 eV was detected in high-resolution scans of the Si 2p region for surfaces throughout the functionalization process, indicating that the oxygen 1s peak

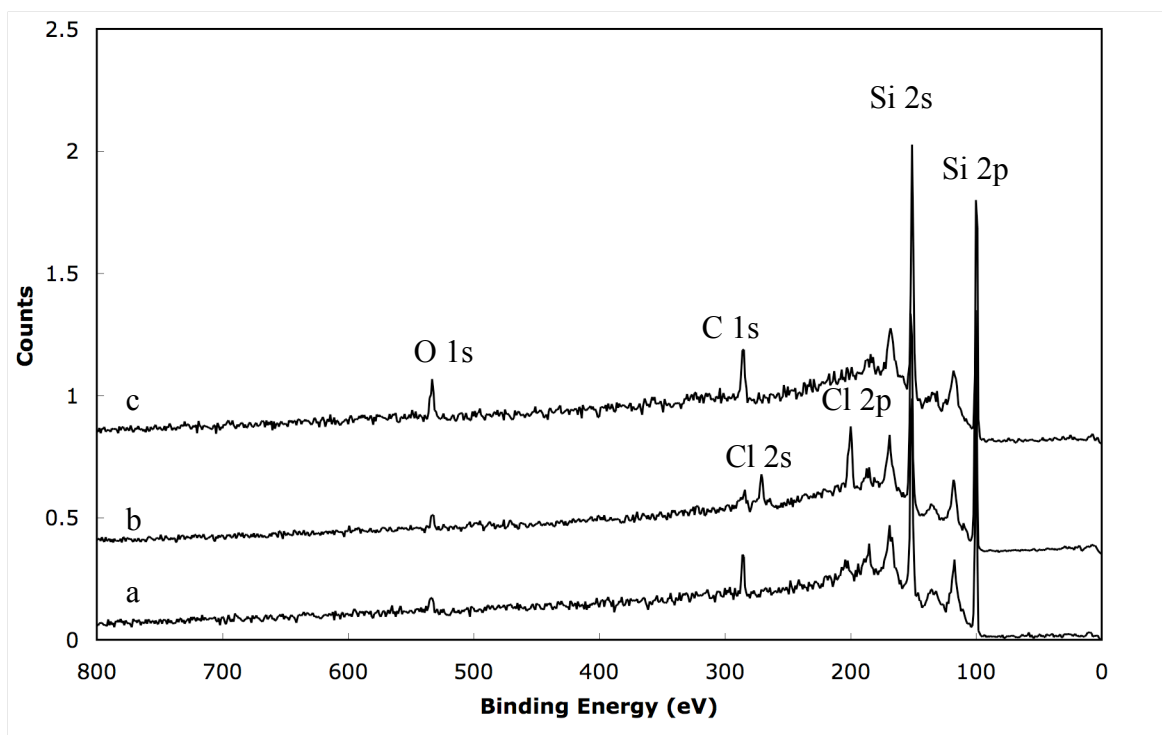


Figure 5.1: XPS spectra of the Si(100) surface a) H -terminated, b) Cl-terminated, and c) CH₃-terminated. O 1s peaks were due to oxidized adventitious carbonaceous materials, as no sign of oxygen-shifted Si 2p was observed.

observed was due to adventitious C sources resulting from the functionalization process and not from oxidation of the Si surface.

Figure 5.2 shows a high resolution XPS scan of the C 1s region of a C₂H₅-functionalized surface. Two main peaks were observed at 284.1 and 285.3 eV, with a third, small signal at 286.9 eV. The peaks located at 285.3 and 286.9 eV were common to alkylated as well H-terminated silicon surfaces, whereas the low binding energy peak at 284.1 eV was unique to alkylated Si surfaces. This peak then can be assigned to emission from core level electrons of C atoms covalently bonded to the relatively electropositive Si.^{9,34} The higher energy peak at 285.3 can be ascribed to carbon in a non-polar bond with either hydrogen or another carbon atom. This carbon peak was the sum of C 1s electrons from adventitious carbon sources as well as alkylating carbons that do not participate in the Si-C bond. The appearance of a third C 1s peak shifted to higher binding energy at 286.9 eV is ascribed to adventitious carbon bonded to oxygen from the THF solvent used in functionalization, or carbonaceous materials present in laboratory air or on surfaces.

The low binding energy peak at 284.1 eV for the 1s peak of silicon-shifted carbon (C_{Si}) represents a tool for the quantitative measurement of surficial Si-C bonds. Table 5.1 reports the peak area ratio of C 1s silicon-shifted carbon to the Si 2p signal (C_{Si}/Si) for each alkyl group measured. C_{Si}/Si peak ratios are reported relative to the C_{Si}/Si for the CH₃-terminated surface, as an internal standard for surface coverage. Each entry represents a single surface measured. Ethylated surfaces showed a C_{Si}/Si peak ratio of 60% relative to CH₃-terminated Si surfaces, indicating that ethyl groups pack relatively

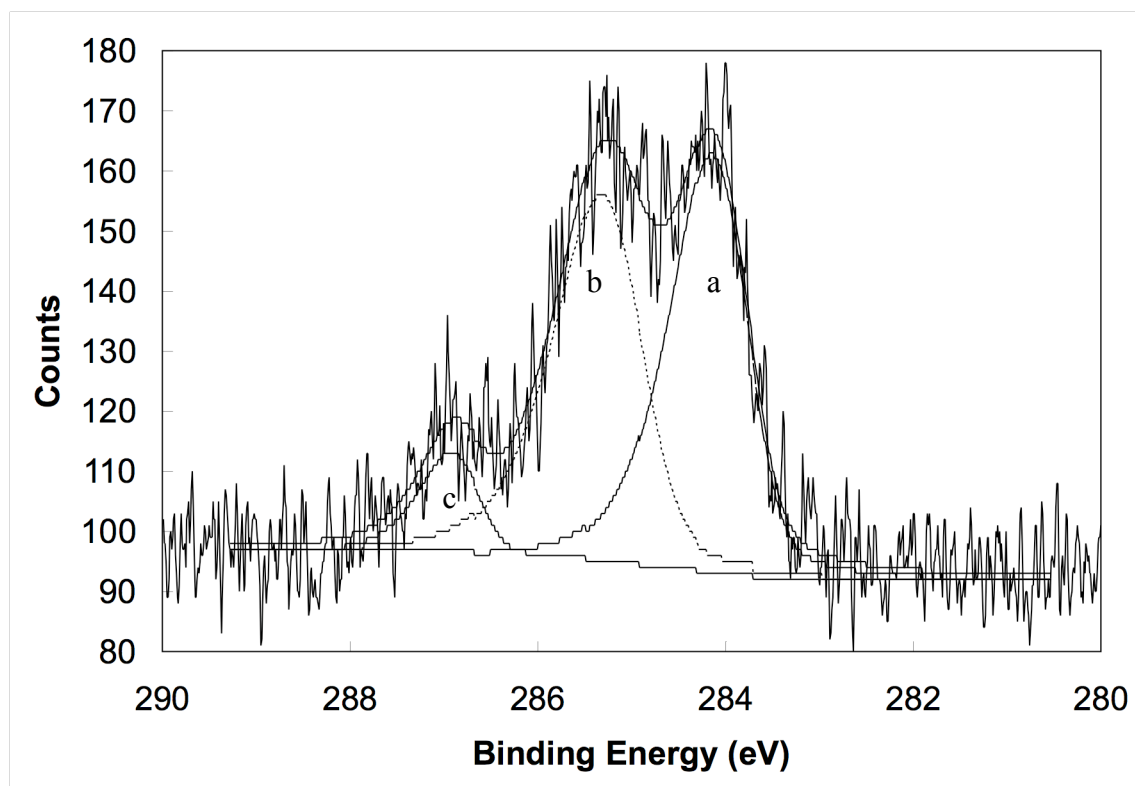


Figure 5.2: XPS spectrum of the C 1s region for a CH₃-terminated Si(100) surface, showing peak fits for the a) (dashed line) carbon atoms bonded to silicon atoms (C_{Si}), b) (dotted line) carbon atoms bonded to carbon (and hydrogen atoms), and c) (solid line) carbon atoms bonded to oxygen atoms (from adventitious sources).

	ratio C _{1s} /Si	% of methyl coverage
Methyl	0.14	--
Ethyl	0.09	0.6
<i>iso</i> -propyl	0.05	0.3
<i>tert</i> -butyl	0.04	0.3
Phenyl	0.06	0.4
Octyl	0.07	0.5

Table 5.1: The C_{1s}/Si XPS integrated area ratios of alkylated surfaces showing the relative amount of carbon bonded to silicon for each alkylated surface. Each sample was measured once.

well on the surface by this alkylation method. The larger alkyl groups phenyl and octyl suffered a larger decline in surface packing at 40% and 50% on the surface, while alkylation with *iso*-propyl and *tert*-butyl groups produced signals having 30% of the ratio exhibited by CH₃-terminated Si, indicating that these groups cannot pack with great efficiency on the surface.

Figure 5.3a represents the oxidation of cleaned and etched Si(100) exposed to laboratory air and illumination for 24 hours, showing the progressive oxidation of the surface. The broad oxygen-shifted silicon 2p peak at ~103.5 eV was assigned to a combination of Si⁴⁺ and Si³⁺ from SiO_x on the surface. The region from 101-102 eV showed little signal, indicating a paucity of lesser oxides such as Si¹⁺ or Si²⁺ from partial oxidation. The lack of these lesser oxides on the surface may be due to either the oxidation of Si⁰ directly to Si^{3/4+}, or that sequential oxidation of the surface has a rate limiting step with the conversion from Si⁰ to Si^{1/2+}, and subsequent oxidation to Si^{3/4+} is relatively swift. The H-terminated surface rapidly oxidized over the course of 24 hours, to an integrated peak area equivalent of 1.1 monolayers of oxide. Figure 5.3b shows the contrasting oxidation of a CH₃-terminated surface over 32 days, showing surface oxidation at a greatly reduced rate, reaching only 0.44 monolayers of oxide, representing a dramatic reduction in the rate of oxidation of the Si(100) surface by functionalization. Furthermore, a comparison of the grown-in oxides between these two samples shows that the oxide peak for the CH₃-terminated surface occurs at a lower binding energy, indicating a relatively higher fraction of lower order oxides such as Si¹⁺ and Si²⁺. Alkylation of the Si(100) surface then causes a reduction in the formation rate of higher

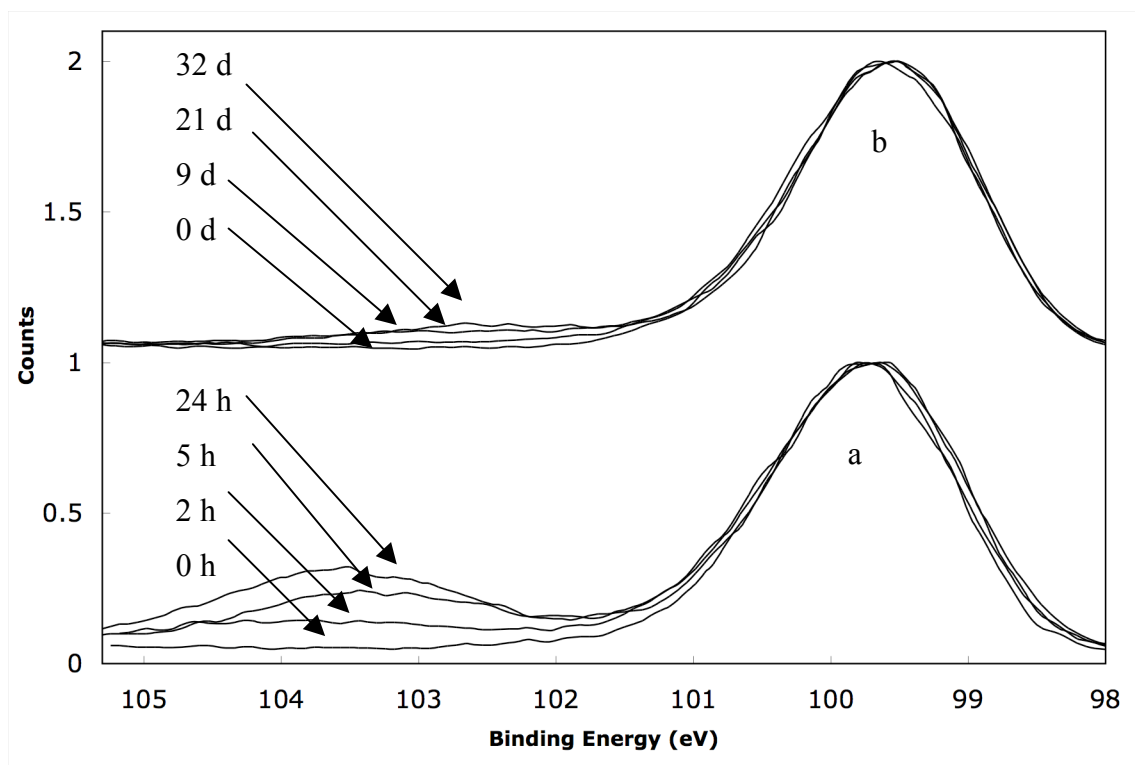


Figure 5.3: XPS spectra of the Si 2p region showing the relative oxidation of the surface for a) H-terminated Si (100) for 0, 2, 5, and 24 hours and b) CH₃-terminated Si (100) for 0, 9, 21, and 32 days.

order oxides either by shutting down their direct production or halting the conversion of the lower order oxides.

Si(100) surfaces functionalized with larger alkyl groups showed the same reduction in oxidation rate compared to the H-terminated surface as CH₃-terminated surfaces. Figure 5.4 gives the monolayers of SiO₂ formed on alkylated and H-terminated surfaces exposed to laboratory air and illumination at times exceeding one month. The H-terminated surface quickly oxidizes to 1.1 monolayers after 24 hours exposure, while surface oxidation for all functionalized surfaces was significantly reduced, reaching less than 0.5 monolayers of SiO₂ after one month. While the surface coverage for each alkyl group varies widely as shown above, there is no discernable trend surface oxidation between surface functionalization. Despite the CH₃-terminated surface having nearly twice the number of alkyl groups on the surface as compared to phenyl, the oxidation proceeds at a comparable rate. Since different alkyl functionalizations leave differing fractions of the surface H-terminated, the population of Si-H bonds on the surface must have no impact on the surface alkylation rate.

5.3.2 Charge Carrier Lifetime Measurements

Photogenerated charge carrier lifetimes as measured by rf conductivity decay for unfunctionalized (H-terminated) Si (100) surfaces were extremely low, < 10 μs. Assuming negligible recombination in the bulk, charge carrier lifetimes this low are dominated by diffusion of photogenerated charge carriers to the sample surface, and were

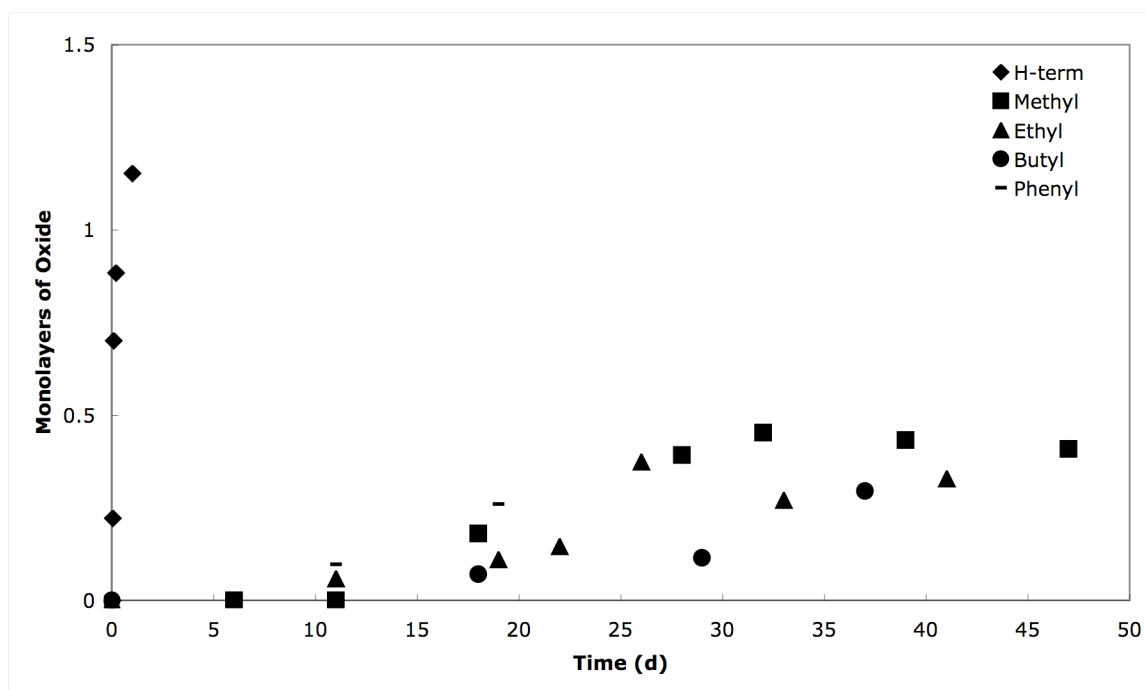


Figure 5.4: Surface oxide growth for H-terminated and alkylated Si(100) surfaces vs. time in air as measured by XPS, showing the rapid oxidation of the H-terminated surface compared to alkylated surfaces. Size of alkylating groups show no effect on oxidation rate.

indicative of all carriers recombining at the surface. Such high surface recombination velocities result from substantial populations of inter-bandgap electronic states, allowing for facile surface-based carrier recombination. These samples showed no measurable change in charge carrier lifetime after prolonged exposure to atmosphere.

Alkyl-functionalized surfaces showed substantial improvements in charge carrier lifetime over the H-terminated surface, indicating a dramatic reduction of recombination at the surface, and by inference, a sharp decrease in electronic states through which recombination occurs. Table 5.2 shows the charge carrier lifetimes measured for the alkylated samples prepared. Unlike surface oxidation trends, for where there were no discernable trends in surface oxidation for different surface alkylations, τ for CH₃-terminated surfaces was significantly higher than for other alkylations. CH₃-terminated surfaces showed substantially longer lifetimes, with charge carrier lifetimes of $(5 \pm 2) \times 10^2 \mu\text{s}$. While the surfaces alkylated with larger alkyl groups had lifetimes shorter than the CH₃-terminated surfaces, τ for these surfaces were still excellent, showing a dramatic reduction in charge carrier recombination as compared to H-terminated surfaces. Despite the lower surface coverage as compared to CH₃-, C₆H₆-terminated surfaces demonstrated excellent charge carrier lifetimes, even at times exceeding one month. The electronic passivation effect of alkylation must require relatively few Si-C bonds to be formed, ruling out removal of active Si-H bonds as the key component.

All samples showed extreme robustness in τ with charge carrier lifetimes remaining stable over extended periods of time. After 11 months in capped, air-filled vials on a laboratory bench top, samples were measured to have $\tau = (4 \pm 1) \times 10^2 \mu\text{s}$ for

	τ (μs)	S (cm s^{-1})
Methyl	$(5 \pm 2) \times 10^2$	$(3 \pm 1) \times 10^1$
Ethyl	$(2 \pm 1) \times 10^2$	$(6 \pm 2) \times 10^1$
Butyl	$(2 \pm 1) \times 10^2$	$(6 \pm 2) \times 10^1$
Phenyl	$(3 \pm 1) \times 10^2$	$(5 \pm 3) \times 10^1$
H-terminated	< 10	$> 10^3$

Table 5.2: Charge carrier lifetimes and surface recombination velocities as measured by rf photoconductivity decay. H-terminated Si(100) surfaces had lifetimes shorter than could be measured by rf conductivity apparatus.

CH₃-terminated samples, $(2 \pm 1) \times 10^2$ μ s for H₅C₂-terminated samples, and $(2 \pm 1) \times 10^2$ for H₉C₄-terminated samples. C₆H₅-terminated samples were lost in the interim and no long term exposure data was recorded.

Surface oxidation of functionalized Si(100) does not have a significant effect on charge carrier lifetime and surface recombination. Figure 5.5 shows the charge carrier lifetime for a CH₃-terminated surface vs. surface oxide formation. After alkylation, τ quickly rose to ~ 500 μ s while the surface remained relatively unoxidized. There was no noticeable change in charge carrier lifetime even as the surface began to oxidize. After one month's exposure to air, the surface had continued to oxidize at a low rate, but no change was seen in τ . Since even extremely low populations of inter-bandgap electronic states would cause a significant drop in charge carrier lifetime, the oxidation of the alkylated surface must create virtually no electronic states that are active towards charge carrier recombination. Well ordered thermally grown Si/SiO₂ interfaces are known to exhibit low charge carrier recombination, raising the possibility that the Si/SiO₂/SiR surface interface has a similar lack of active recombination states, either by highly ordered formation of oxide or inactivation by a local potential.

5.3.3 Soft X-Ray Spectroscopy

Figure 5.6 represents the soft X-ray photoelectron spectrum (SXPS) for the H-terminated Si(100) surface, allowing for the detection of surface species in much higher detail than with conventional XPS. This figure shows the Si 2p region after the removal of the Si 2p_{1/2} component of the spin-orbit doublet. Removal of the second peak of each

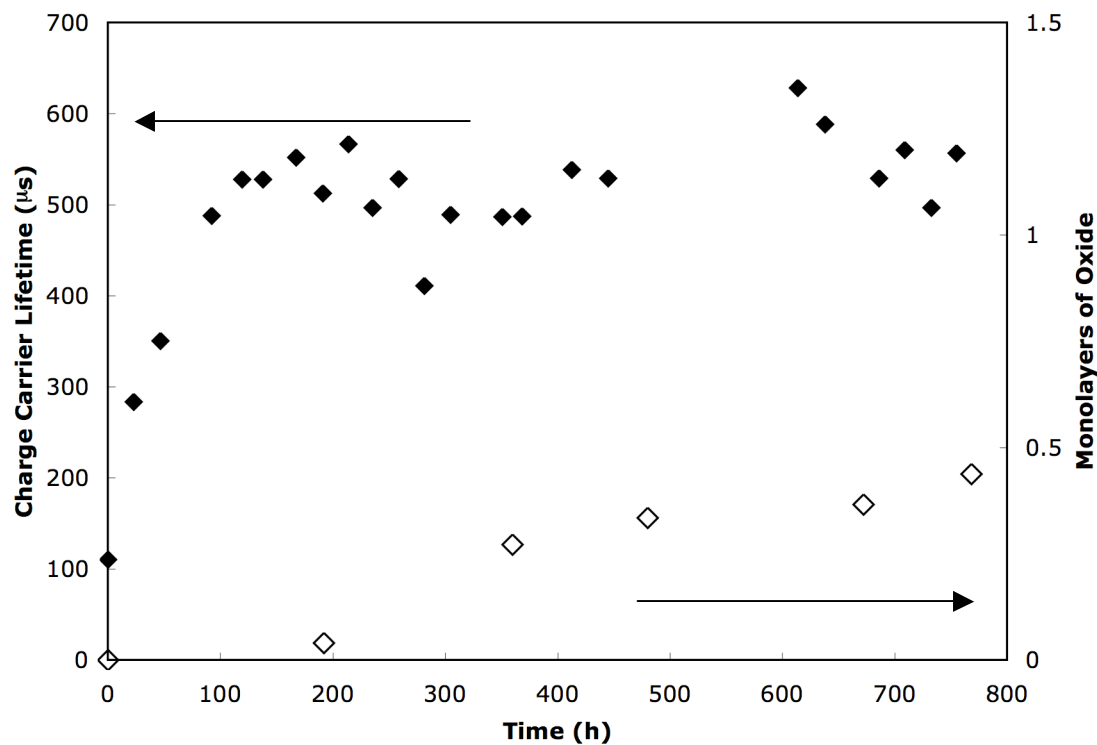


Figure 5.5: Charge carrier lifetime and surface oxidation vs. time for CH₃-terminated surfaces exposed to air. Gradual oxidation of the functionalized surface had no effect on surface electronic passivation.

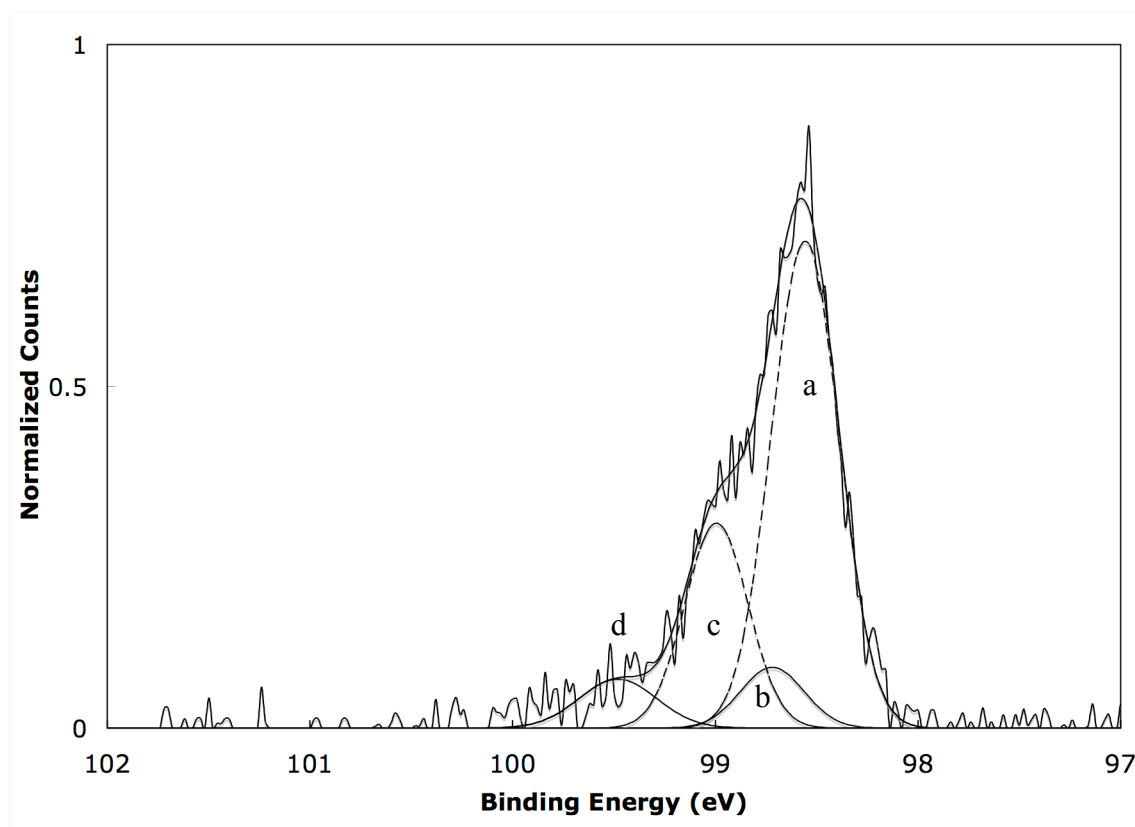


Figure 5.6: Si 2p region of H-terminated Si(100) surface studied by soft X-ray XPS. The data has been fit to four separate Voigt functions, after stripping of the spin-orbit doublets, and were assigned to a) bulk Si, b) H-Si, c) H₂Si, and d) H₃Si surface species.

doublet allows for simpler and more accurate fitting of the peaks for each of the distinct Si species present. The largest peak, at the lowest binding energy of 98.5 eV, was assigned to bulk silicon, bonded only to other silicon atoms in non-polar bonds. At higher binding energies were H-bonded Si atoms, the first at 0.2 eV higher than the bulk Si peak, representing SiH at 98.7 eV. The next, at 0.3 eV higher at 99.0 eV was assigned to SiH₂, the predominant surface species, and finally at 99.4 eV was a peak assigned to SiH₃. The wet-chemically prepared H-terminated surface shows populations of all three silicon-hydride species, as has been previously observed by IR absorbance studies.^{27,29} Table 5.3 shows the relative percentage of surface species for H-, Cl-, CH₃-, CH₃CH₂-, and C₆H₅CH₂- modified surfaces as determined by integration of peak fits for each species. While the raw data show no external need for a peak at 99.7 eV, the binding energy shift for singly H-terminated silicon atoms is known and a peak was inserted for the SiH surface species. The H-terminated Si(100) surface as measured showed that a large fraction (61%) of the surface was SiH₂, with 20% SiH and 19% SiH₃ for the two samples measured. Not all of these Si-H bonds could be replaced with Si-C bonds, however, as multiple hydrogens on the same surface silicon cannot be effectively replaced by the larger Cl atoms or the bulkier alkyl groups. The steric crowding of multiple alkyl groups, even the compact methyl, on the Si(100) surface severely limits the alkylation reaction, which then leaves some population of Si-H bonds behind.

Figure 5.7 shows the doublet stripped spectrum for the Cl-terminated Si(100) surface. A broad peak at ~102 eV appeared to be the oxidation peak associated with SiO_x. These samples were prepared in air and had to be transported across a facility to the beamline for measurement, requiring exposure to air for several minutes. A peak at

X	% bulk		% Surface		Surface %		Surface %		Surface %	
					SiX	SiX ₂	SiX ₃ (SiO ₂)	SiH ₂		
-H	0.61		0.39		0.20	0.61	0.19			
-Cl	0.56 ± 0.05		0.44 ± 0.06		0.34 ± 0.08	0.18 ± 0.08	0.41 ± 0.06	0.03 ± 0.02		
-CH ₃	0.63 ± 0.02		0.37 ± 0.02		0.82 ± 0.08	0.10 ± 0.05	0.08 ± 0.05			
-C ₂ H ₅	0.63		0.37		0.79	0.11	0.09			
-C ₆ H ₅ CH ₂	0.62		0.38		0.81	0.11	0.08			

Table 5.3: Relative integrated area for peak fits of SXPS data of functionalized Si(100) surfaces. SiH, SiC₂H₅, and SiC₆H₅CH₂ represent two averaged values for each column. SiCl entries are for six measurements, and SiCH₃ entries are for eight measurements. % bulk and % surface represent % of total signal resulting from bulk or surface species. SiX represents % of surface signal resulting from singly bonded -X. For SiCl, a SiH₂ peak was fitted to the spectra in addition to the SiCl peak.

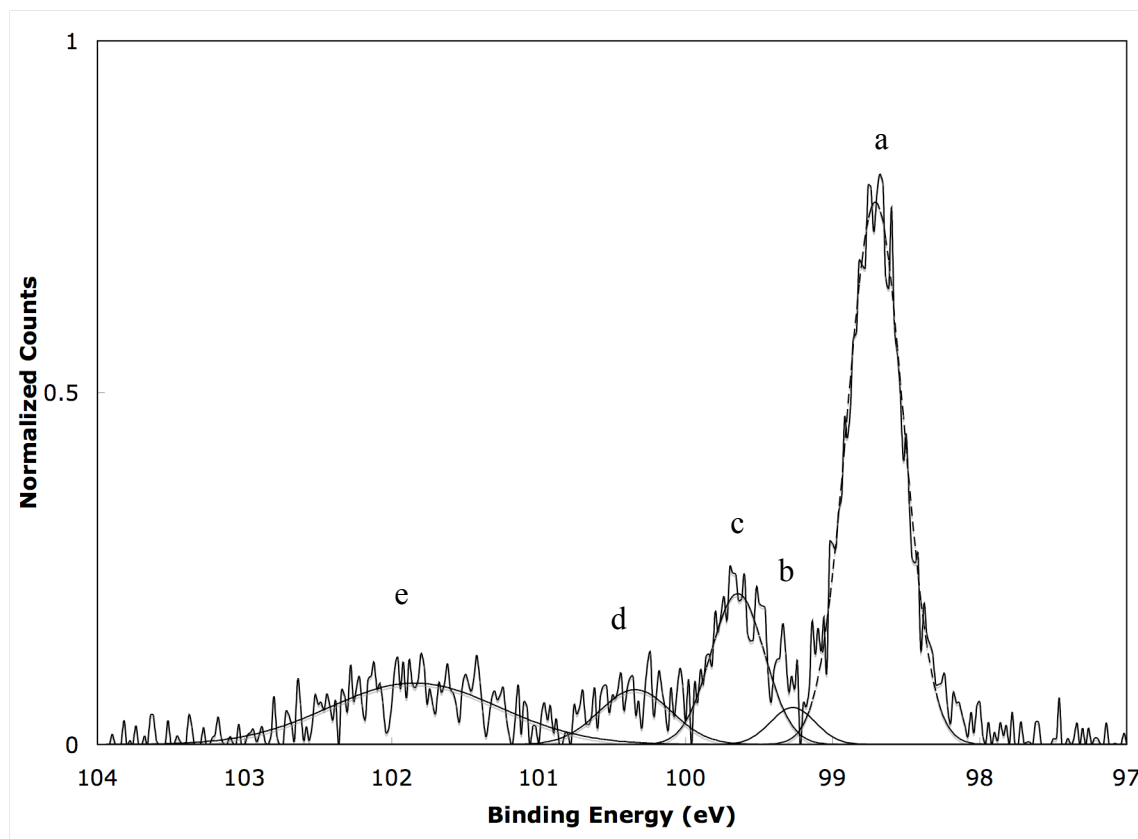


Figure 5.7: Si 2p region for Cl-terminated Si(100) using SXPS. The data was fit to Voigt peaks after subtraction of spin-orbit doublets, and assigned to a) bulk silicon, b) SiH_2 , c) ClSi , d) Cl_2Si , and e) SiO_x surface species.

98.7 eV was assigned to unshifted bulk silicon, and a peak shifted 0.9 eV higher was assigned to SiCl. A smaller peak at 0.4 eV higher than bulk silicon (99.1 eV) was added to account for SiH₂. The improvement in the overall fit of the spectra by adding this peak was small, but noticeable in the low-binding energy edge of the SiCl peak. Another peak 0.9 eV higher than the monochlorinated peak was assigned to SiCl₂ species, with the final broad peak at 101.9 eV for oxidized surface species. Table 5.3 shows that $34 \pm 8\%$ of the surface was SiCl, compared with $18 \pm 8\%$ which was SiCl₂. No significant population of SiCl₃ was expected, as the large size of Cl atoms would greatly hinder the production of SiCl₃. If there was any SiCl₃ on the surface, it was obscured by the oxide peak, which accounted for $41 \pm 6\%$ of the surface silicon atoms. Other than SiH₂, no minority population peaks such as HSiCl, SiH₃, or H₂SiCl were fit to peaks, as their populations were below the resolution of the fitting and had small expected peak shifts from larger population species. These minority species contribute to some of the integrated area of the assigned peaks, though in what quantity it cannot be known.

The alkylated surface shows similar features to the H-terminated surface by SXPS. Figure 5.8 shows the spin-orbit doublet stripped spectrum for a CH₃-terminated surface, fit to peaks assigned to CH₃-terminated silicon species. The broad peak at 99.8 eV was shifted 0.4 eV higher than bulk Si at 99.4 eV and was attributed to a number of surface species, with peak shifts too similar to distinguish or too small in population to reliably measure, including SiH, SiH₂, and SiCH₃. The center for this peak was shifted higher than bulk silicon by 0.4 BeV, similar to the 0.4 BeV shift in the doubly H-terminated silicon species. This peak shift value was also similar to the 0.4-0.5 eV shift seen in similar Si(111) studies on the same instrument for SiCH₃.³³ With no external tool

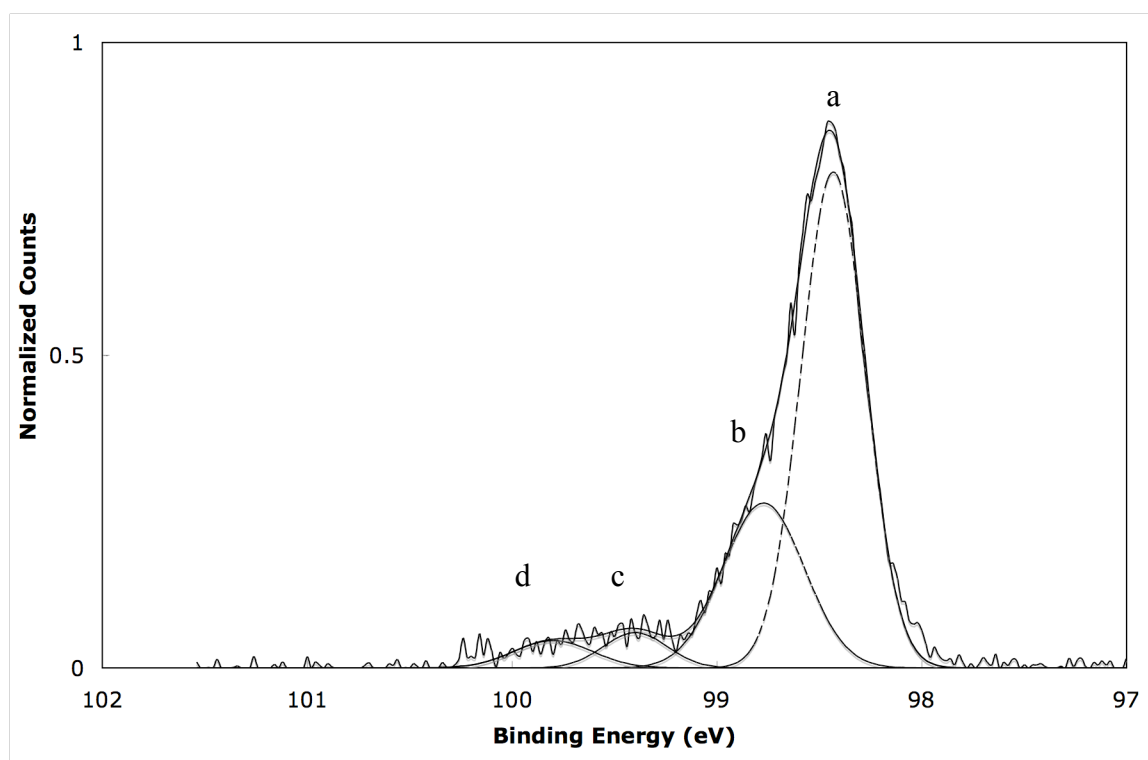


Figure 5.8: Si 2p region of soft X-ray spectrum of the CH₃-terminated Si(100) surface after subtraction of spin-orbit doublets, fit to Voigt peaks. The multiplicity of species present prevents assigning specific peak identity. Peaks are roughly assigned to a) bulk silicon; b) CH₃-Si plus CH₃-SiH and SiH and SiH₂; c) (CH₃)₂Si and SiH₃; and d) (CH₃)₃Si surface species.

for determination of the exact fraction of the surface covered by each subspecies, attempting to fit peaks for each subspecies was not possible. Two other peaks shifted higher in energy at 99.3 and 99.8 eV and were combinations of H_2SiCH_3 , $\text{Si}(\text{CH}_3)_2$, and $\text{H}_2\text{Si}(\text{CH}_3)_2$.

C_2H_5 -terminated Si(100) spectra were similar in character to those of the CH_3 -terminated surface, with a peak shifted 0.3 eV from the bulk Si peak that was a mix of singly C_2H_5 -terminated species, though the lower binding energy of the peak center for this peak may indicate that SiH/SiH_2 was a larger component of the surface than on CH_3 -terminated surfaces. $\text{C}_6\text{H}_6\text{CH}_2$ -terminated samples also showed similar SXPS spectra to C_2H_5 -terminated surfaces with the first surface peak only shifted by 0.3 eV from the Si bulk indicating that there was a component of SiH/SiH_2 within the first peak, reducing the aggregate peak shift.

5.4 Discussion

5.4.1 Surface Passivation of Si(100)

The alkyl groups used herein clearly did not bond to all sites on the Si(100) surface. The high resolution XPS data for the C 1s region indicated that as alkylating groups increased in size and steric bulk, the surface density of Si-C bonds decreased, leaving larger percentages of the surface unreacted. Previous transmission IR studies³⁰ on the Si(111) surface indicated that unreacted sites after chlorination/alkylation were H-terminated, removing excess chlorine from unalkylated sites and leaving these sites H-

terminated. The presence of H-termination of unalkylated Si surface sites offers an explanation for the low S values observed for such systems. Si(100) surfaces prepared in vacuum and hydrogen terminated have been observed to have low densities of surface localized electronic recombination centers, resulting in low surface recombination velocities for charge carriers. CH₃-terminated Si(111) surfaces prepared through chlorination/alkylation as well have shown low surface recombination velocities.^{25,31} A surface with mixed populations of SiH and SiC groups could be expected to show low surface recombination as a whole if other electronic defects are not generated in sample preparation. Further, it is possible that the Cl-terminated surface, which has been observed to have extremely low S values,²⁵ may indicate that chlorination of the H-term Si surface may remove surface defects generated by the wet etch technique, and no additional defects are generated by alkylation.

The relatively slow oxidation in air of the surface of Si(100) and analogous porous silicon surfaces alkylated with various alkylation procedures have been demonstrated. For the alkyl groups investigated herein, at least partial inhibition of the rate of surface oxidation might be expected due to steric crowding of surficial Si-H bonds by neighboring alkyl groups. A modest degree of oxidative protection has been observed by forming self-assembled monolayers with very long chain alkylthiols on Cu,³⁵ indicating that steric bulk may be the cause of the oxidative passivation rather than Si-C bond formation. This crowding should inhibit the oxidation of an initially unreacted site as well as the oxidation of adjacent surface silicon atoms, because oxygen or water would need to intercalate into the alkyl surface covering to react with the surface. The stark contrast in air oxidation rates of alkylated vs. H-terminated Si surfaces indicates that the

reaction mechanism may involve neighboring available Si-H sites or oxidation spreading outward on the surface from imperfect passivation from either H- or C- termination caused by surface defects left by surface preparation. If chlorination/alkylation generates a lower density of oxidatively active defect sites while forming both Si-C bonds as well as Si-H bonds than the wet etch, then mixed population surfaces may demonstrate both superior electrical and oxidative passivation. Thus even modest alkyl coverages on the surface are sufficient to significantly reduce the observed rate of oxidation by reduction of highly active imperfectly passivated sites.

5.4.2 Soft X-ray Photoelectron Spectra

H-terminated Si(100) surfaces measured by SXPS show relative populations of SiH, SiH₂, and SiH₃ that are consistent with IR and thermal desorption measurements.^{28,29,36} However, the peak fitting relies on constraining the fitting outcomes such that the relative peak separation is predefined using SXPS measurements of the H-Si(111) surface, as well as limiting the FWHM for SiH and SiH₂ to be within 20% of each other.

While the oxide seen on the Cl-terminated surface was unavoidable due to a lack of an inert atmosphere loading mechanism on the soft X-ray beamline, the peak fit could not be noticeably improved by adding a peak representing SiCl₃. The shape of the SiO_x peak does not appear to contain a significant size low energy subpeak, indicating that any missing peak would be extremely small. The steric bulk of chlorine atoms would make triply chlorination unlikely for most surface SiH₃ sites, and a large population of SiCl₃

was not expected. The inclusion of an SiH_2 peak in between bulk silicon and SiCl was due to the low binding energy asymmetry of the SiCl peak. This included peak composes less than 5% of the surface, and its removal from the peak fitting does not result in a significant change in the peak fit. However, its inclusion points to residual hydrogen on the surface, leaving the possibility that the SiCl peak may contain other species such as HSiCl and H_2SiCl , while the SiCl_2 peak may contain SiCl_2 , HSiCl_2 , and H_2SiCl_2 .

For alkylated surfaces, the SXPS peak fitting results in an unconvoluted peak containing an unknown number of surface species shifted 0.3-0.4 eV higher than the bulk Si. The first peak higher in energy than the bulk peak for an alkylated sample should contain SiH , SiR , SiH_2 , and HSiR , while peaks assigned to the minority species SiR_2 , HSiR_2 , and H_2SiR , SiH_3 , and SiR_3 can be assigned to total the two peaks of higher binding energy. Since the XPS survey scans showed no trace of the Cl 2s or 2p peaks after alkylation, there is not expected to be any contribution to these higher energy peaks for chlorinated species.

5.5 Conclusions

Alkylation of $\text{Si}(100)$ surfaces through a two-step chlorination/alkylation procedure provided both chemical and electrical passivation of Si surfaces even when only a fraction of the surface was functionalized. All of the Cl was removed by functionalization even with very bulky alkyl Grignard reagents, and other reports of this two step alkylation method have shown a return of hydrogen termination at unalkylated sites.³⁰ The intensity of a low binding energy C 1s XPS peak, ascribable to carbon

bonded to Si, provided a quantitative estimate of the coverage of alkyls on such surfaces relative to the coverage of methyl groups on CH₃-terminated Si(100) surfaces. C₂H₅ groups yielded coverages as high as 60% of the CH₃-terminated surface, whereas bulkier and longer groups produced lower coverages, as expected. Even C₆H₅ groups, which were measured by XPS to bond at only 40% of the CH₃-terminated surface, showed excellent surface passivation, with less than half a monolayer of Si oxide formed on the surface after three weeks exposure to air, and surface recombination velocities <60 cm s⁻¹ after that same time period.

Soft X-ray photoelectron spectra of the Si(100) surface have shown that while the wet chemically etched Si(100) surface was predominantly SiH₂, after chlorination the most dominant surface species is singly chlorinated, indicating that the surface became mostly SiCl and HSiCl. Surfaces after alkylation by SXPS were largely indistinguishable as the number of surface species with similar binding energy shifts precluded separation in the soft X-ray spectra. These surfaces showed no large populations of doubly alkylated species, meaning that substantial amounts of Si-H bonds remained on the surface, despite which these surfaces demonstrate robust charge carrier lifetimes for periods of time approaching one year's exposure to air.

5.6 Acknowledgements

We gratefully acknowledge the NSF, grant CHE-021358, and the California Institute of Technology for support of this work. Soft X-ray spectra collected were in collaboration with Dr. Lauren Webb, David Michalak, David Knapp, and Julie Biteen.

This work was carried out in part at the National Synchrotron Light Source, Brookhaven National Laboratory, which is supported by the U.S. Department of Energy, Division of Materials Sciences and Division of Chemical Sciences, under contract DE-AC02-98CH10866.

5.7 Bibliography

- (1) Dabrowski, J.; Mussig, H. J. *Silicon Surfaces and Formation of Interfaces*; World Scientific Publishing Co. Pte. Ltd.: London, 2000.
- (2) Yablonovitch, E.; Swanson, R. M.; Eades, W. E.; Weinberger, B. R. *Appl. Phys. Lett.* **1986**, *48*, 245.
- (3) Buriak, J. M. *Chem. Rev.* **2002**, *102*, 1271.
- (4) Buriak, J. *Chem. Comm.* **1999**, 1051-1060.
- (5) Haber, J. A.; Lauermann, I.; Michalak, D.; Vaid, T. P.; Lewis, N. S. *J. Phys. Chem. B* **2000**, *104*, 9947-9950.
- (6) Stewart, M. P.; Robins, E. G.; Geders, T. W.; Allen, M. J.; Choi, H. C.; Buriak, J. M. *Physica Status Solidi a-Applied Research* **2000**, *182*, 109-115.
- (7) Linford, M. R.; Chidsey, C. E. D. *J. Am. Chem. Soc.* **1993**, *115*, 12631-12632.
- (8) Linford, M. R.; Fenter, P.; Eisenberger, P. M.; Chidsey, C. E. D. *J. Am. Chem. Soc.* **1995**, *117*, 3145-3155.
- (9) Terry, J.; Linford, M. R.; Wigren, C.; Cao, R. Y.; Pianetta, P.; Chidsey, C. E. D. *Appl. Phys. Lett.* **1997**, *71*, 1056-1058.
- (10) Terry, J.; Mo, R.; Wigren, C.; Cao, R. Y.; Mount, G.; Pianetta, P.; Linford, M. R.; Chidsey, C. E. D. *Nucl. Instrum. Meth. B* **1997**, *133*, 94-101.
- (11) Effenberger, F.; Gotz, G.; Bidlingmaier, B.; Wezstein, M. *Angew. Chem. Int. Ed.* **1998**, *37*, 2462-2464.
- (12) Stewart, M. P.; Buriak, J. M. *Angew. Chem. Int. Ed. Eng* **1998**, *23*, 3257.
- (13) Sieval, A. B.; Demirel, A. L.; Nissink, J. W. M.; Linford, M. R.; van der Maas, J. H.; de Jeu, W. H.; Zuilhof, H.; Sudholter, E. J. R. *Langmuir* **1998**, *14*, 1759-1768.

- (14) Sung, M. M.; Kluth, G. J.; Yauw, O. W.; Maboudian, R. *Langmuir* **1997**, *13*, 6164-6168.
- (15) Zazzera, L. A.; Evans, J. F.; Deruelle, M.; Tirrell, M.; Kessel, C. R.; Mckeown, P. *J. Electrochem. Soc.* **1997**, *144*, 2184-2189.
- (16) Buriak, J. M.; Allen, M. J. *J. Am. Chem. Soc.* **1998**, *120*, 1339-1340.
- (17) Buriak, J. M.; Allen, M. J. *J. Lumin.* **1998**, *80*, 29-35.
- (18) Holland, J. M.; Stewart, M. P.; Allen, M. J.; Buriak, J. M. *J. Solid State Chem.* **1999**, *147*, 251-258.
- (19) Henry de Villeneuve, C.; Pinson, J.; Ozanam, F.; Chazalviel, J. N.; Allongue, P. In *Mat. Res. Soc. Symp. Proc.* 1997; Vol. 451, p 185-195.
- (20) Vieillard, C.; Warntjes, M.; Ozanam, F.; Chazalviel, J.-N. *Proc. - Electrochem. Soc.* **1996**, *95*, 250.
- (21) Bansal, A.; Li, X.; Lauermann, I.; Lewis, N. S.; Yi, S. I.; Weinberg, W. H. *J. Am. Chem. Soc.* **1996**, *118*, 7225-7226.
- (22) Juang, A.; Scherman, O. A.; Grubbs, R. H.; Lewis, N. S. *Langmuir* **2001**, *17*, 1321-1323.
- (23) Royea, W. J.; Juang, A.; Lewis, N. S. *Appl. Phys. Lett.* **2000**, *77*, 1988-1990.
- (24) Hall, R. N. *Physical Review* **1952**, *87*, 387.
- (25) Webb, L. J.; Lewis, N. S. *J. Phys. Chem. B* **2003**, *107*, 5404-5412.
- (26) Bansal, a.; Lewis, N. S. *J. Phys. Chem. B* **1998**, *102*, 1067-1070.
- (27) Chabal, Y. J.; Higashi, G. S.; Ragahavchari, K.; Burrows, V. A. *J. Vac. Sci. Technol. A* **1989**, *A7*, 2104.
- (28) Niwano, M.; Takeda, Y.; Ishibashi, K.; Kurita, K.; Miyamoto, N. *J. Appl. Phys.* **1992**, *71*, 5646.
- (29) Chyan, O. M. R.; Wu, J.; Chen, J.-J. *Appl. Spectrosc.* **1997**, *51*, 1905.

- (30) Nemanick, E. J.; Hurley, P. T.; Brunschwig, B. S.; Lewis, N. S. *J. Phys. Chem. B* **2005**, *submitted for review*.
- (31) Bansal, A.; Li, X. L.; Yi, S. I.; Weinberg, W. H.; Lewis, N. S. *J. Phys. Chem. B* **2001**, *105*, 10266-10277.
- (32) Seah, M. P. In *Practical Surface Analysis*; 2nd ed.; Briggs, D., Seah, M. P., Eds.; John Wiley & Sons: Chichester, 1990; Vol. 1, p 201-255.
- (33) Webb, L. J.; Nemanick, E. J.; Biteen, J. S.; Knapp, D. W.; Michalak, D. J.; Traub, M. C.; Chan, A. S. Y.; Brunschwig, B. S.; Lewis, N. S. *J. Phys. Chem. B* **2005**, *109*, 3930-3937.
- (34) Hunger, R.; Fritsche, R.; Jaeckel, B.; Jaegermann, W.; Webb, L. J.; Lewis, N. S. *Phys. Rev. B* **2005**, *72*.
- (35) Laibinis, P. E.; Whitesides, G. M. *J. Am. Chem. Soc.* **1992**, *114*, 1990-1995.
- (36) Thanh, V. L.; Bouchier, D.; Hincelin, G. *J. Appl. Phys.* **2000**, *87*, 3700.

